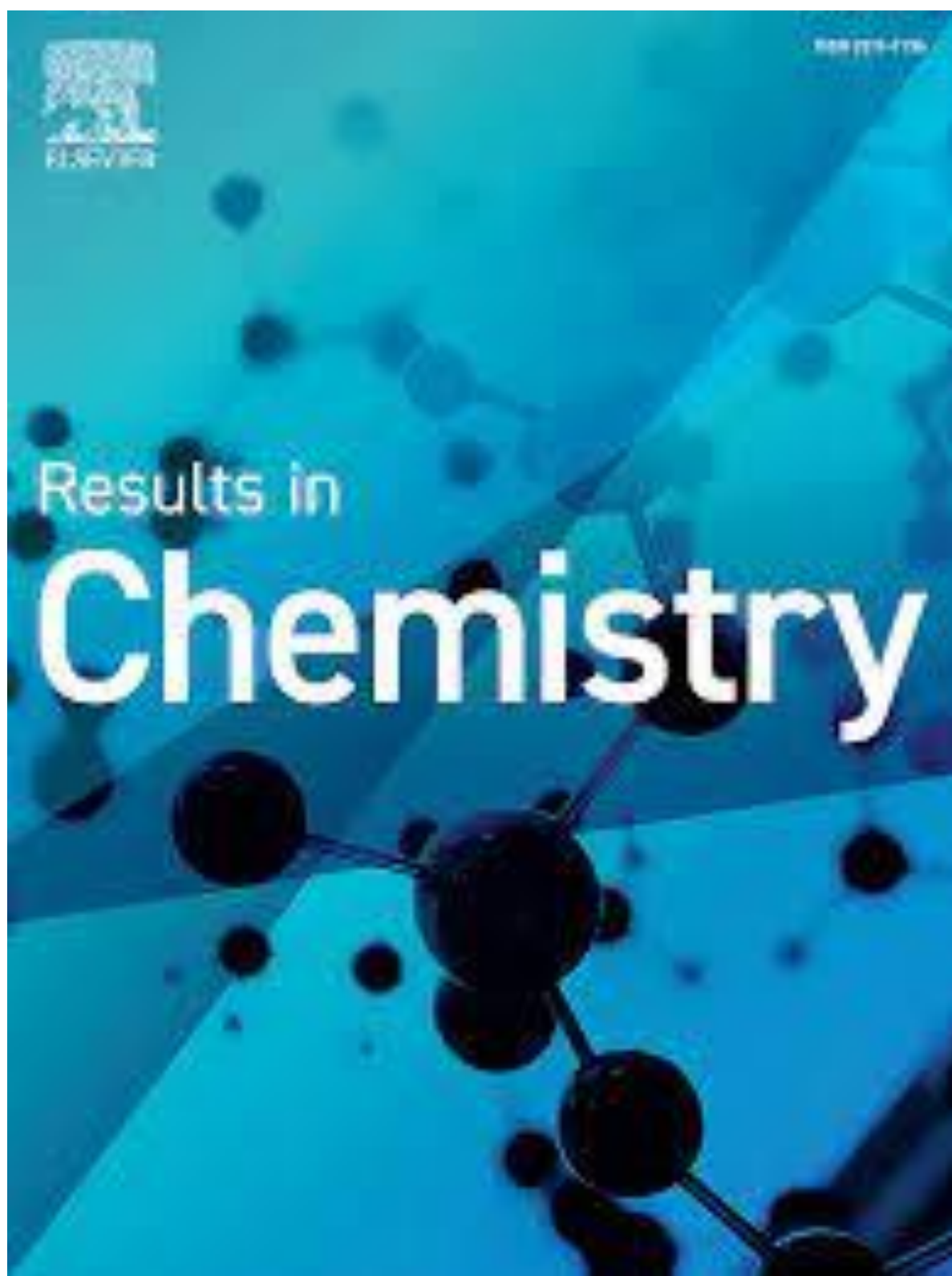




ISSN 0950-4230

Results in

Chemistry





ScienceDirect®

[Submit your article](#)

[Guide for autho](#)

[Menu](#)



[Search in this journal](#)

Volume 3

January 2021

[< Previous vol/issue](#)

[Next vol/issue >](#)

Receive an update when the latest issues in this journal are published

[Sign in to set up alerts](#)

[FEEDBACK](#)

Results in Chemistry

Open access

Submit your article

Guide for autho

Menu

Search in this journal

VSI:Dyes, probes and Results

Research article *Open access*

One-step condensation synthesis and characterizations of indocyanine green

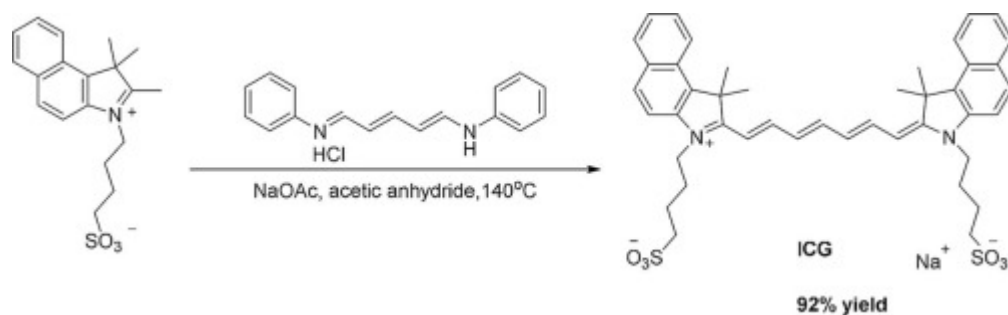
Xiangning Fang, Wenjuan Liu, Xia Wu, Wei Zhou, ... Zhaochao Xu

Article 100092

[Download PDF](#) [Article preview](#)

Abstract **Graphical abstract**

Graphical abstract



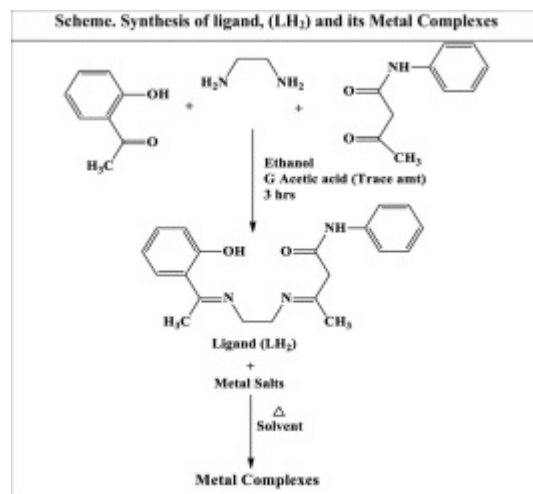
FEEDBACK

[Submit your article](#)[Guide for autho](#)[Menu](#)[Search in this journal](#)

ligand, (E)-3-((2-((E)-(1-(2-hydroxyphenyl)ethylidene)amino)ethyl)imino)-N-phenylbutanamide

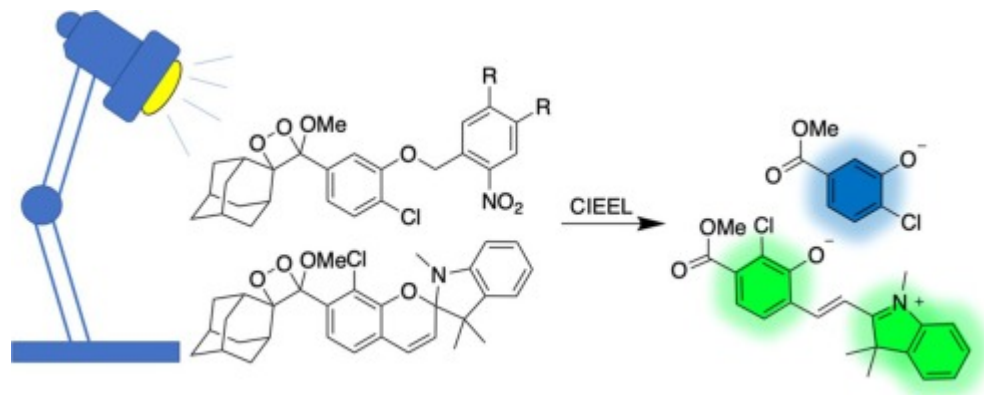
K. Subin Kumar, K.K. Aravindakshan

Article 100129

[Download PDF](#) [Article preview](#)[Abstract](#)[Graphical abstract](#)[Graphical abstract](#)[FEEDBACK](#)

[Submit your article](#)[Guide for autho](#)[Menu](#)[Search in this journal](#)[Abstract](#)[Graphical abstract](#)

Graphical abstract

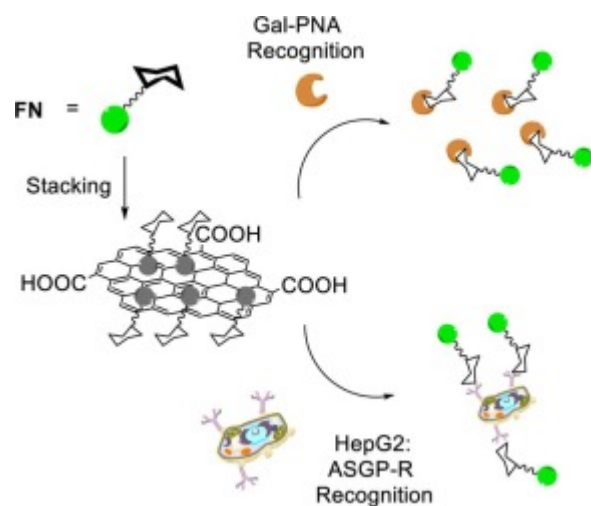


Analytical Chemistry

[Research article](#)[Open access](#)[FEEDBACK](#)

[Submit your article](#)[Guide for autho](#)[Menu](#)[Search in this journal](#)[Abstract](#)[Graphical abstract](#)

Graphical abstract

Research article [Open access](#)

Naphthalimide-based probe with strong two-photon excited fluorescence and high specificity to cell membranes

Xiaoli Zhang, Huizi Man, Yi Xiao

Article 100100

[FEEDBACK](#)

Results in Chemistry

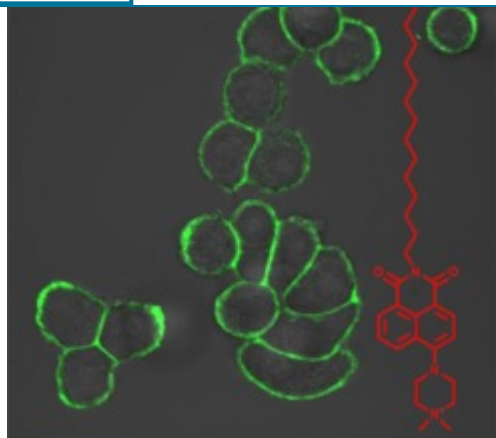
Open access

Submit your article

Guide for autho

Menu

🔍 Search in this journal



Research article *Open access*

Environment-insensitive two-photon ratiometric probe for *in cellulo* quantitative measurement of hydrogen peroxide

Seo Won Cho, Yong Woong Jun, Ye Jin Reo, Sourav Sarkar, Kyo Han Ahn

Article 100117

📄 Download PDF Article preview ⤴

Abstract

Graphical abstract

Graphical abstract

FEEDBACK 

Results in Chemistry

Open access

Submit your article

Guide for autho

Menu



Search in this journal

Wavelength (nm)

analysis

Physical Chemistry and Chemical Physics

Research article *Open access*

Detection of benzo[a]pyrene with silver nanorod substrate in river water and soil based on surface-enhanced raman scattering

Wenxi Cao, Ying Luo, Jingwen Li, Anyi Qian, ... Caiqin Han

Article 100126

[Download PDF](#) [Article preview](#)

Abstract

Abstract

Benzo[a]pyrene (BaP) widely presents in soot, tar, cigarette smoke, and has a strong carcinogenic effect. It is stable in the environment and accumulates through the biological chain. Therefore, it is of vital importance to develop a simple and rapid

FEEDBACK

Results in Chemistry

Open access

Submit your article

Guide for autho

Menu



Search in this journal

Theoretical and Computational Chemistry

Research article *Open access*

Theoretical studies on triplet formations in nitrobenzoxadiazole (NBD) derivatives: The impact of donor group and heteroatom substitution

Chao Wang, Hui Juan Koh, Zhaochao Xu, Xiaogang Liu

Article 100116

[Download PDF](#) [Article preview](#)

Abstract

Graphical abstract

Graphical abstract

FEEDBACK

[Submit your article](#)[Guide for autho](#)[Menu](#)[Search in this journal](#)

Medicinal Chemistry and Chemical Biology

Review article [Open access](#)

Triazole, imidazole, and thiazole-based compounds as potential agents against coronavirus

Insa Seck, Filomain Nguemo

Article 100132

[Download PDF](#) [Article preview](#)

Abstract

Abstract

The expansion of the novel coronavirus known as SARS-CoV-2 (severe acute respiratory syndrome coronavirus 2), COVID-19 (coronavirus disease 2019), or 2019-nCoV (2019 novel coronavirus) is a global concern over its pandemic potential. The need for therapeutic alternatives to stop this new pandemic is urgent. Nowadays, no efficacious therapy is available, and vaccines and drugs are underdeveloped to cure or prevent SARS-CoV-2 infections in many countries. Some vaccines candidates have been approved; however, a number of people are still skeptical of this coronavirus vaccines. Probably because of issues related to the quantity of the vaccine and a possible long-term side effects which are still being studied. The previous pandemics of infections caused by

[FEEDBACK](#)

Results in Chemistry

Open access

Submit your article

Guide for autho

Menu



Search in this journal

Lan Wang, Wenjing Qin, Ding Chen, Nanxiang Wang, ... Lin Li

Article 100103

[Download PDF](#) Article preview

Abstract

Abstract

Fluorescence-based in vitro assays are highly sensitive, selective and convenient to use, which is suitable for qualitative and quantitative detection of various types of biological samples. Herein, we designed and synthesized a novel fluorogenic probe **TPAN-Asn** for in vitro L-asparaginase detection. **TPAN-Asn** exhibited selective and robust response to L-asparaginase over various anions, cations and amino acids. More importantly, we have demonstrated that **TPAN-Asn** is able to accurately quantify the amount of L-asparaginase in patient serum samples. These results suggest that **TPAN-Asn** holds great potential in the benchmarking and analysis of L-asparaginase-based cancer therapy.

Research article Open access

Fluorogenic probes for thioredoxin reductase activity

Tendai J. Mafireyi, Jorge O. Escobedo, Robert M. Strongin

FEEDBACK

Results in Chemistry

Open access

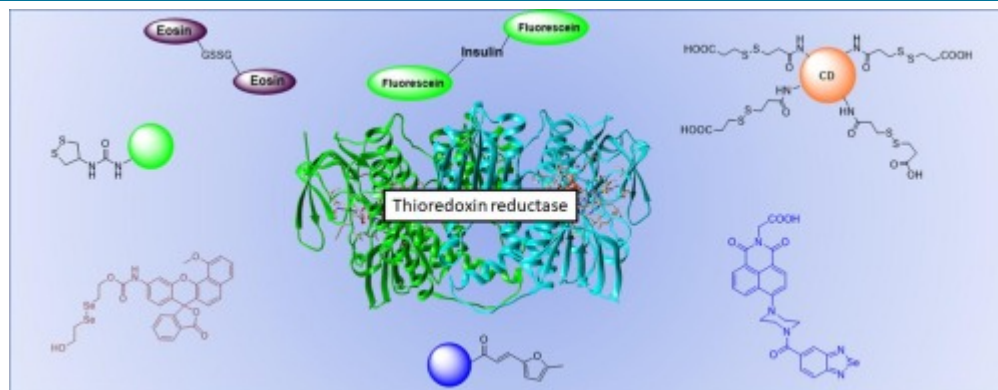
Submit your article

Guide for autho

Menu



Search in this journal



Others

Research article Open access

Fluorescent 4-amino-1,8-naphthalimide Tröger's bases possessing conjugated 4-amino-1,8-naphthalimide moieties and their potential fullerenes Host-Guest complexes

Samantha A. Murphy, Oxana Kotova, Steve Comby, Thorfinnur Gunnlaugsson

Article 100128

[Download PDF](#) Article preview

FEEDBACK

Results in Chemistry

Open access

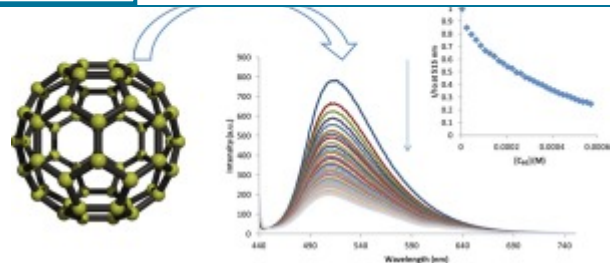
Submit your article

Guide for autho

Menu



Search in this journal



Full Length Article

Organic Chemistry

Research article *Open access*

Unanticipated ionic ferrocenyl compounds based on 5,5'-bis(1-hydroxytetrazole). Molecular structures, anti-migration and burning rate catalytic performances

Fangfang Xing, Xiaoling Shi, Fuqiang Bi, Jizhen Li, Guofang Zhang

Article 100090

[Download PDF](#) [Article preview](#)

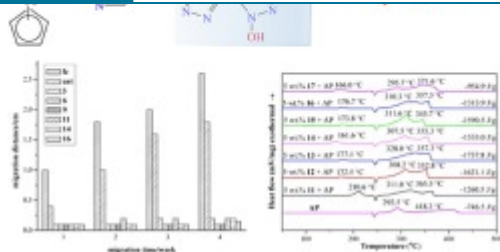
FEEDBACK

[Submit your article](#)[Guide for autho](#)

Menu



Search in this journal

Research article *Open access*

NMR spectroscopic investigation of benzothiazolylacetonitrile azo dyes: CR7 substitution effect and semiempirical study

H.M. Alsoghier, M. Abdellah, H.M. Rageh, H.M.A. Salman, ... S.A. Ibrahim

Article 100088

[Download PDF](#) [Article preview](#)

Abstract

Abstract

FEEDBACK

Results in Chemistry

Open access

Submit your article

Guide for autho

Menu



Search in this journal

wavelengths of benzothiazole azo dyes. Also, the relative photoluminescence quantum yields (PL QY) of these dyes (1–6) were

Research article *Open access*

Synthesis of novel coumarin-thiazolidine-2,4-dione derivatives: An approach to computational studies and biological evaluation

Sumitra N. Mangasuli

Article 100105

[Download PDF](#) [Article preview](#)

Abstract

Graphical abstract

Graphical abstract

FEEDBACK

Results in Chemistry

Open access

[Submit your article](#)[Guide for autho](#)[Menu](#)[Search in this journal](#)

Determination of SADT and TMR_{ad} of 3-bromo-1-(3,5-dichloropyridin-2-yl)-4,5-dihydro-1H-pyrazole-5-carboxylic acid: Applying thermal decomposition kinetics

Yun-Bo Cong, Zhen-Yun Wei, Xiao-Hua Ma, Zi-Liang Li, ... Chun-Sheng Cheng

Article 100112

[Download PDF](#) [Article preview](#)

Abstract

Abstract

The aim of this study was the evaluation of the safety parameters: Time to Maximum Rate under adiabatic conditions (TMR_{ad}) and self-accelerating decomposition temperature (SADT) for 3-bromo-1-(3,5-dichloropyridin-2-yl)-4,5-dihydro-1H-pyrazole-5-carboxylic acid (BDPCA) using evaluated kinetic parameters. The required decomposition kinetics was determined from the results of differential scanning calorimetry (DSC), microcalorimetry (C600), and adiabatic accelerating calorimeter (ARC). AKTS Thermokinetics (TK) and Thermal Safety (TS) Software were used for evaluation of the kinetic parameters of a decomposition reaction. The kinetic analysis was based on the isoconversional Friedman method. The values of TMR_{ad} amount to 110.2 °C, 107.3 °C, and 104.9 °C when calculated from the data collected by DSC, C600, and ARC, respectively. The simulated values of SADT for a 50 kg package of BDPCA amount to 101 °C and 96 °C when elaborating the DSC and C600 signals, respectively. Obtained results indicate that the application of kinetic parameters evaluated from the experiments carried out by three different

[FEEDBACK](#)

[Submit your article](#)[Guide for autho](#)[Menu](#)[Search in this journal](#)[Download PDF](#) [Article preview](#)[Abstract](#)[Graphical abstract](#)

Graphical abstract

Research article [Open access](#)

Aerobic oxidative cleavage of C=C bond to carbonyl compound

Long-Fei Jia, Huai-Zhu Li, Zhi-Hao Li, Rui-Jun Li, Guan-yu Yang

Article 100137

[Download PDF](#) [Article preview](#)[FEEDBACK](#)

Results in Chemistry

Open access

Submit your article

Guide for autho

Menu



Search in this journal

acids and its esters, 2-substituted 5-phenylacrylic acids and its esters, chalcones, 1-phenyl-5-buten-2-one and bis(2-phenylvinyl) ketone, 5-benzylidene-1,3-dimethyl-pyrimidine-2,4,6-triones, could be effectively oxidized into the corresponding aryl carbonyl compounds, and the yield was up to 99%. A suitable mechanism was proposed. Gram-level synthesis further illustrated the practicality of our method.

Research article *Open access*

A simple method to obtain ursolic acid

Michael Azael Ludeña Huaman, Ana Luz Tupa Quispe, Renéé Isabel Huamán Quispe, Carlos Alberto Serrano Flores, Juana Robles Caycho
Article 100144

[Download PDF](#) [Article preview](#)

Abstract

Abstract

A simple method has been developed to obtain ursolic acid (UA) by crystallization and recrystallization of the ethanol extract of *Clinopodium revolutum*. Its structure was confirmed by 1D (^1H -, ^{13}C -, DEPT 45, 90 and 135) and 2D (COSY, HMBC and HSQC) nuclear

FEEDBACK

Results in Chemistry

Open access

Submit your article

Guide for autho

Menu

Search in this journal

12-Phosphomolybdic acid $[H_3PMO_{12}O_{40}]$ over natural bentonite as a heterogeneous catalyst for the synthesis of 3,4-dihydropyrimidin-2-(1H)-ones

Lakha V. Chopda, Pragnesh N. Dave

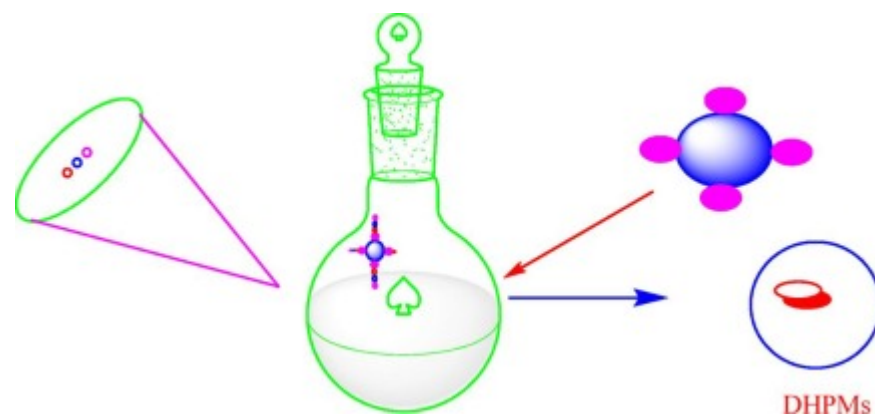
Article 100169

[Download PDF](#) Article preview 

Abstract

Graphical abstract

Graphical abstract



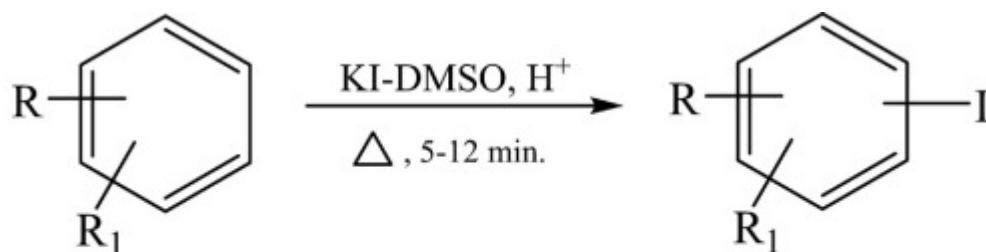
FEEDBACK 

Results in Chemistry

Open access

[Submit your article](#)[Guide for autho](#)[Menu](#)[Abstract](#)[Graphical abstract](#)

Graphical abstract

Regioselective iodination of aromatics using KI-DMSO, H⁺.R = COCH₃, NH₂, OH, OCH₃, CHOR₁ = H, Cl, Br, OCH₃, NO₂.Research article [Open access](#)

Synthesis, Spectral analysis and Anti-microbial properties of Cu, Ag, Au complexes of 2, 5-dihydroxy-1, 4-benzoquinone and 3, 6-dichloro-2, 6-dihydroxy-1, 4-benzoquinone

M. Amin Mir, Anuj Kumar, Shailendra P. Madwal, M.M.S. Jassal

FEEDBACK

Results in Chemistry

Open access

Submit your article

Guide for autho

Menu



Search in this journal

Many complexes of Cu, Ag, Au in combination with dianions derived from 2, 5-dihydroxy-1, 4-benzoquinone and 3, 6-dichloro-2, 6-dihydroxy-1, 4-benzoquinones have been synthesized and analysed for their antimicrobial activity. The I.R, ^1H and ^{13}C NMR data reveals that 2, 5-dihydroxy-1, 4-benzoquinone, coordinates as an O, O donor of the o-quinone type in *cis*- $\text{Na}_2[\text{Cu}_2\text{O}_5(\text{HBQ})_2] \cdot 5\text{H}_2\text{O}$, *cis*-(PPh_4) $_2[\text{Cu}_2\text{O}_5(\text{HBQ})_2]$, *cis*- $\text{Na}_2[\text{Ag}_2\text{O}_5(\text{HBQ})_2] \cdot 4\text{H}_2\text{O}$, *trans*- $\text{AuO}_2(\text{HBQ}) \cdot \text{H}_2\text{O}$ and chloranilate di-anion functions as an O, O ligand in *cis*- $\text{Na}_2[\text{Cu}_2\text{O}_5(\text{DDB})_2] \cdot 6\text{H}_2\text{O}$, *cis*-(PPh_4) $_2[\text{Cu}_2\text{O}_5(\text{DDB})_2] \cdot 4\text{H}_2\text{O}$, *cis*- $\text{Na}_2[\text{AgO}_2(\text{DDB})_2]$, *cis*-(PPh_4) $_2[\text{AgO}_2(\text{DDB})_2] \cdot 5\text{H}_2\text{O}$, *trans*-($n\text{-Bu}_4\text{N}$) $_2[\text{AuO}_2(\text{DDB})_2] \cdot 3\text{H}_2\text{O}$. The complexes synthesized showed a good response as antimicrobial agents against the bacterial strains, viz, *Bacillus subtilis*, *Staphylococcus aureus*, *Xanthomonas malvacearum*, *E. coli*, *Rhodococcus sp*, *Pseudomonas putida*.

Research article [Open access](#)

Novel method for the synthesis of Sulfonamide Urea's from *p*-toluene sulfonyl isocyanate using Amberlite IRA-400 Cl resin: Application towards the synthesis of Gliclazide

Ravi Kumar Sadineni, Rajesh Kumar Rapolu, V.V.N.K.V. Prasada Raju, Srinivasu Navuluri, ... Naveen Mulakayala
Article 100217

[Download PDF](#) [Article preview](#)

Abstract

Graphical abstract

FEEDBACK

Results in Chemistry

Open access

Submit your article

Guide for autho

Menu



Search in this journal

Gliclazide

Research article *Open access*

Preparation of adamantylidene enol ethers by Wittig-Horner reaction

Xinxin Huang, Chun Cai

Article 100238

[Download PDF](#) [Article preview](#)

Abstract

Abstract

A practical synthetic pathway of adamantylidene enol ethers by Wittig-Horner reaction has been developed. In this route, acetals were obtained by reaction of trimethyl orthoformate and benzaldehyde derivatives with tetrabutylammonium tribromide in methanol at room temperature. Trimethyl phosphite was converted into phosphonates with acetals in the presence of titanium (IV) tetrachloride in dichloromethane, followed by utilization of 2-adamantanone and lithium diisopropylamide (LDA) in anhydrous tetrahydrofuran under argon atmosphere at $-78\text{ }^{\circ}\text{C}$ to form adamantylidene enol ethers. Total yields are up to 66%.

FEEDBACK

Results in Chemistry

Open access

[Submit your article](#)[Guide for autho](#)[Menu](#)[Search in this journal](#)

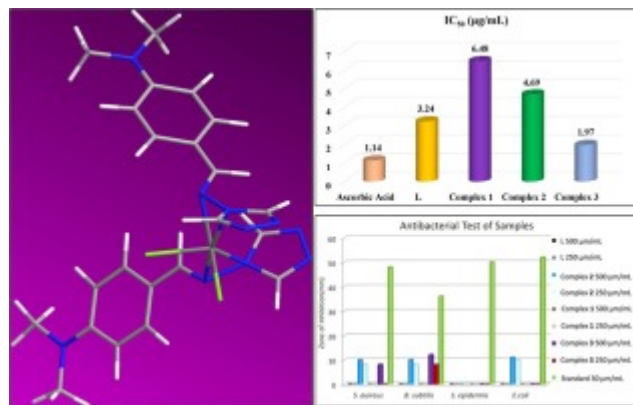
amine ligand and its transition metal complexes

Md. Mahadi Hasan, Habib Md. Ahsan, Prianka Saha, Jannatul Naime, ... A.B.M. Nazmul Islam

Article 100115

[Download PDF](#) [Article preview](#)[Abstract](#)[Graphical abstract](#)

Graphical abstract

[Research article](#) [Open access](#)[FEEDBACK](#)

Results in Chemistry

Open access

Submit your article

Guide for autho

Menu



Search in this journal

Abstract

Abstract

In this study, we have prepared an imine-based ligand, 2-methoxy-5-((6-methoxypyridin-3-ylimino)methyl)phenol (MIMP) and its Cu(II), Ni(II) and Zn(II) complexes in 2:1 stoichiometric ratio (2MIMP : Metal). The structure of obtained ligand and its metal complexes were elucidated with the aid of FT-IR, UV-Visible, NMR (^1H and ^{13}C) and mass spectra. Further, all the structures were analyzed via density functional theory (DFT) approach at B3LYP/LanL2DZ/6-311++G(2d,p) level, with HOMO-LUMO energies, geometric parameters, reactivity properties and electronic excitations obtained through TD-DFT calculations. Antibacterial activity of MIMP ligand and metal complexes have been evaluated via *in vitro* assays. In addition, the inhibition of the protein DNA gyrase-DNA complex was evaluated using molecular docking calculations, and the results revealed that biological accessibility of the metal complexes was better than ligand.

Research article *Open access*

Influence of the redox conditions on the crystallization behavior of anosovite in Ti-bearing titanomagnetite smelting slag

Zhen Wang, Qingshan Zhu, Han Wang, Haoyan Sun

Article 100136

FEEDBACK

Results in Chemistry

Open access

Submit your article

Guide for autho

Menu



Search in this journal

smelting slag. Under non-reducing conditions, besides anosovite, a part of Ti element was concentrated into rutile. Due to the much smaller particle size (within 10 μm) of rutile than anosovite, anosovite was the better choice for selective liberation and separation, indicating that non-reducing conditions were not adequate. Under reducing condition, anosovite was the only Ti-rich phase and its liberation was excellent as the reduction degree ($n(\text{Ti}^{3+})/n(\text{Ti}^{4+}+\text{Ti}^{3+})$) was about 0.25. But when the reduction degree increased to 0.51, the liberation of the anosovite was poor because of the jagged grain boundary of anosovite particle. So from the liberation and separation perspective, reducing condition within a suitable degree was indispensable. In addition, as the redox conditions changed from oxidizing to reducing, the Ti level in the anosovite phase increased from 65.9% to more than 85%. Reducing condition is particularly favorable to increasing the content of TiO_2 in anosovite phase. Above all, a moderate reducing

Research article Open access

Relative reactivity of the dinuclear ruthenium complex $[\text{CpRu}(\text{CO})_2]_2$ with diphenylselenyl sulphide and diphenyl disulphide

Wei Xiang Koh, Andrea Paris Gomez, Jiawen Lee, Jasmaadiyah Binte Habib Mohameed, Weng Kee Leong
Article 100159

[Download PDF](#) Article preview

Abstract

Graphical abstract

FEEDBACK

[Submit your article](#)[Guide for autho](#)[Menu](#)Research article *Open access*

Newly synthesized triazole-based Schiff base ligands and their Co(II) complexes as antimicrobial and anticancer agents: Chemical synthesis, structure and biological investigations

Sachin A. Deodware, Umesh B. Barache, Umakant B. Chanshetti, D.J. Sathe, ... Shiva Prasad Kollur

Article 100162

[Download PDF](#) [Article preview](#)

Abstract

Abstract

The new Schiff base ligands 4-(2'/3'/4'-nitrobenzylideneimino)-3-methyl/ethyl-5-mercapto-1,2,4-triazole and their Co(II) metal complexes were synthesized and characterized by elemental analysis, magnetic moment measurements, thermal studies, electronic absorption and NMR spectroscopy. The ligands were synthesized by condensation of 4-amino-5-mercapto-3-

[FEEDBACK](#)

Results in Chemistry

Open access

Submit your article

Guide for autho

Menu



Search in this journal

Research article *Open access*

Synthesis and the formation analysis of Ni (II), Zn (II) and L-glutamine binary complexes in dimethylformamide-aqueous mixture

M. Amin Mir, Mohammad Waqar Ashraf, Kim Andrews

Article 100188

[Download PDF](#) [Article preview](#)

Abstract

Abstract

The convergence analysis of Ni (II) and Zn (II) and L- Glutamine complexes were studied using (0–50% v/v) dimethylformamide (DMF)-water mixtures potentiometrically at temperature 301.0 K, having an ionic strength of 0.15 mol L⁻¹. The complex species models were analysed by a well-defined computer Programme MINIQUAD75. Exhaustive modeling have been carried out on a number of complex species. The main complex species formed have been found of NiL₂, NiL₂H, NiL₂H₂, ZnL₂, ZnL₂H and ZnL₂H₂ type. On the basis of the statistical parameters the best fit chemical modelling have been applied. The statistical data analysis validated the complex species. The occurrence of columbic interactions over non-columbic interactions have been

FEEDBACK

Results in Chemistry

Open access

Submit your article

Guide for autho

Menu



Search in this journal

Ariane Dasque, Marie Gressier, Pierre-Louis Taberna, Marie-Joëlle Menu

Article 100207

Download PDF

Article preview

Abstract

Abstract

Since the 2017 REACH restrictions on hexavalent chromium, the aeronautics industries have been seeking substitute processes for chromium plating. So far, use of trivalent chromium-based precursors seems to be the best solution in terms of process adaptation. The development of such processes requires a better understanding of plating bath solution chemistry. More specifically, there is a need to characterize the complexation mechanisms occurring with the chromium (III), since they are responsible for higher electrodeposition efficiency. Chromium (III) complexation occurs under specific conditions, such as in an acidic solution, where chromium hydrolysis takes place, leading to a stable aqua chromium complex, which is suspected to be detrimental to an even deposit. To tackle this issue, a complexing agent is added to destabilize hexaaquachromium complex. It is reported that ligands such as glycine allow the formation of chromium-ligand complexes under specific pH and chromium-ligand ratios. In order to identify and understand the formation of the various complexes, two characterization methods have

Research article *Open access*

FEEDBACK



Abstract

Dithiocarbamate compounds have interesting biological features, and have been considered as an alternative to conventional antibiotics in order to mitigate the spread of antimicrobial resistance. This accounts for the growing interest in the investigation of the antimicrobial potency of different dithiocarbamate compounds. In this study, the antimicrobial activities of Cu(II), In(III), and Sb(III) complexes of *N*-methyl-*N*-phenyl dithiocarbamate complexes were evaluated against ten bacteria species, comprising of both Gram positive [*Bacillus cereus* (ATCC 10876), *Enterococcus faecalis* (ATCC 29212), *Enterococcus gallinurium* (ATCC 700425), *Listeria monocytogenes* (ATCC 19115), *Listeria monocytogenes*, *Staphylococcus aureus* (ATCC 25923)] and Gram negative [*Escherichia coli* O177, *Klebsiella pneumoniae*, *Salmonella enterica* and *Salmonella Typhimurium*]. Three techniques; disc, well diffusion, and microdilution were explored to assess antimicrobial activity of dithiocarbamate compounds. The results showed good antimicrobial activities for both the ligand (ammonium *N*-methyl-*N*-phenyl dithiocarbamate) and complexes against Gram

Analytical Chemistry

Research article Open access

A simple and economical ultrasound-assisted method for Cd and Pb extraction from fruits and vegetables for food safety assurance

Results in Chemistry

Open access

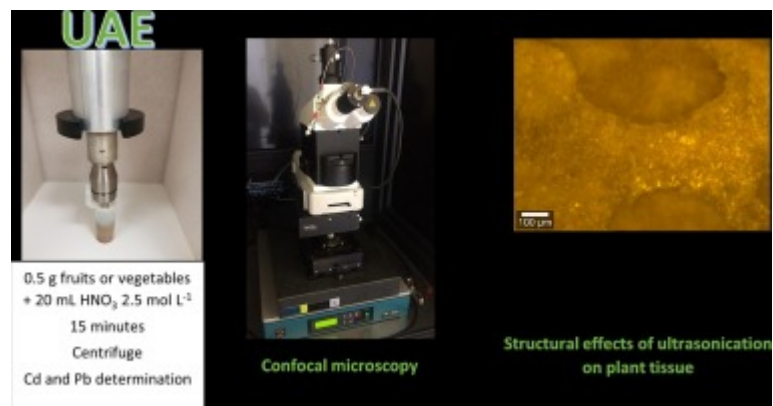
Submit your article

Guide for autho

Menu

Search in this journal

Graphical abstract



Research article *Open access*

Trace determination and speciation of elements in green tea

A. Hamza, S.O. Bahaffi, T.N. Abduljabbar, M.S. El-Shahawi

Article 100081

[Download PDF](#) [Article preview](#)

Abstract

FEEDBACK

Results in Chemistry

Open access

Submit your article

Guide for autho

Menu



Search in this journal

estimated. At 95% confidence level ($P > 0.50$), the student t -test values as calculated for essential and toxic metals were smaller than the critical value indicating no significant differences between element concentrations in the tested samples. The average daily dietary intake (ADDIs) for selected elements and the average daily intake (ADI) and the chronic reference dose (RFD) for Cd ($\mu\text{g kg}^{-1} \text{BW day}^{-1}$) were critically determined. Evaluation of inorganic composition allows quantification of the leaching percentage

Research article *Open access*

Application of response surface methodology to optimize removal efficiency of water turbidity by low-cost natural coagulant (Odaracha soil) from Saketa District, Ethiopia

Yohanis Birhanu, Seyoum Leta

Article 100108

[Download PDF](#) [Article preview](#)

Abstract

Abstract

Turbidity removal is a meaningful activity in the water treatment system, and it is an indicator of water quality. With this, natural coagulants are desirable and economical ways of removing water turbidity. The purpose of this study was to investigate the

FEEDBACK

[Submit your article](#)[Guide for autho](#)[Menu](#)[Search in this journal](#)Research article *Open access*

Spectral analysis of total phosphorus in soils based on its diagnostic reflectance spectra

Pingping Fan, Xueying Li, Huimin Qiu, Guang-Li Hou

Article 100145

[Download PDF](#) [Article preview](#)

Abstract

Abstract

Visible and near infrared spectroscopy (VNIR) has been successfully used to determine many soil parameters rapidly. However, total phosphorous (P) cannot be well quantified by VNIR, mainly because its absorption spectrum or reflectance spectrum was too weak to be studied. Here, we explored a new way to reveal the reflectance spectrum of total P in soils. Firstly, six types of soil residues were prepared after the original soil was sequentially extracted Ca₂-P, Ca₈-P, Al-P, Fe-P, O-P, and Ca₁₀-P, respectively. Secondly, the reflectance spectra of these P fractions were obtained using these soil residues by QE65000 spectrometer (Ocean Optics). Specifically, if we intended to get the spectrum of a certain P fraction, we would measure the reflectance spectrum of the soil residues without its neighboring former P fraction, using the soil residues after extracting this P fraction as the reference

[FEEDBACK](#)

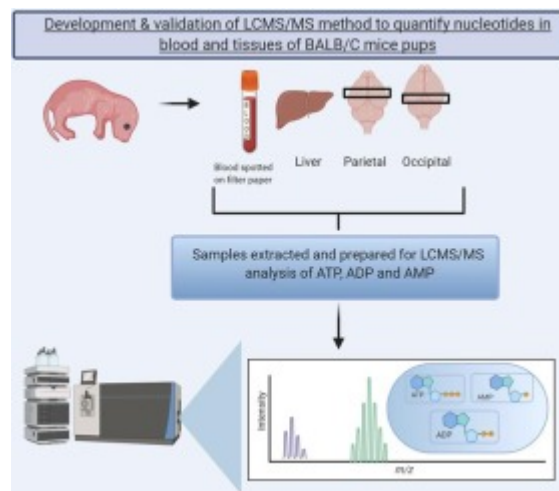
[Submit your article](#)[Guide for autho](#)[Menu](#)[Search in this journal](#)

Richard L. Jayaraj, Hassib Narchi, Radhakrishnan Subramanian, Priya Yuvaraju

Article 100172

[Download PDF](#) [Article preview](#)[Abstract](#)[Graphical abstract](#)

Graphical abstract

[Research article](#) [Open access](#)[FEEDBACK](#)

[Submit your article](#)[Guide for autho](#)[Menu](#)[Abstract](#)

Abstract

A new and sensitive (TLC) assay has been estimated for quantitation of synthetic binary mixtures of antipsychotic drug Amisulpride (AMS) with antimigraine drug Zolmitriptan (ZOL). These medications co-administered with each other for treatment of chronic migraine headache associated with psychosis. The synthetic mixture has been separated on precoated silica TLC plates G60 F254 by using mobile phase which consist of mixture of **Chloroform: Ethyl acetate: Methanol: Ammonia** in ratio (30:30:73:3 v/v/v/v). The mixture has been determined at λ_{\max} 231 nm. Retardation factor (RF) values for AMS and ZOL have been 0.6 and 0.43 respectively. Calibration graphs have been linear in range 50–500 ng/spot for all studied drugs. The detection limits have been 6.04 & 10.5 ng/spot and the quantitation limits have been 18.3 & 31.834 ng/spot for AMS and ZOL respectively. The described assay has been utilized for quantitation of synthetic mixture in pharmaceutical tablet & biological fluids.

Research article [Open access](#)

Evaluating bioavailability of elements in municipal wastewater sludge (Biosolids) from three rural wastewater treatment plants in East Texas (USA) by a sequential extraction procedure

Kefa K. Onchoke, Oluwadamilola Olasumbo Fateru

Article 100211

[FEEDBACK](#)

Results in Chemistry

Open access

Submit your article

Guide for autho

Menu



Search in this journal

protocol was utilized for speciation and bioavailability of metals in samples from Nacogdoches and Lufkin wastewater sludges (NWWWS, LWWS) and the Neches Compost sludge (NCS). Application of five steps (adsorbed, exchangeable, organically bound, carbonate and residual/sulfide) was performed to fractionate 26 elements (macroelements: Ca, Fe, K, Mg, Na, P, S, Li, Cs; microelements: As, B, Ba, Cd, Co, Cu, Hg, Mn, Mo, Pb, Se, V, Zn, Ni, Al, Cr, Sr) in samples via inductively coupled plasma optical emission spectrometry (ICPOES). The proximate amounts for most elements were predominant in the sulfide/residual fractions. Among macroelements 88.62–92.23% of K was found bioavailable vis-à-vis the organically-bound or sulfide fractions. About 100% of Li exists in the sulfide fractions vis-a-vis Group 2A elements. In contrast to microelements and transition metals, about 19–32 % Mo was found readily bioavailable. Additionally Mo occurred in relatively lesser percent in sulfide/residual fractions vis-à-vis

Research article *Open access*

Development of a robust method for the determination of fluorine in liquid petroleum products

María Fernanda Gazulla, Marta Rodrigo, María Jesús Ventura, Cristina Andreu, Mónica Orduña

Article 100235

[Download PDF](#) [Article preview](#)

Abstract

Abstract

FEEDBACK

Results in Chemistry

Open access

Submit your article

Guide for autho

Menu



Search in this journal

fluorine over organic materials from the refining industry of different matrices such as fuel oil, acid soluble oil, etc., containing from very low to high fluorine concentrations in a relatively short time, which makes the methodology suitable to be used as a

Research article *Open access*

Separating the true from the false: A rapid HPTLC-ESI-MS method for the determination of cannabinoids in different oils

Theresa Schmidt, Jacqueline Stommel, Tim Kohlmann, Annemarie E. Kramell, René Csuk

Article 100234

[Download PDF](#) [Article preview](#)

Abstract

Graphical abstract

Graphical abstract

FEEDBACK

[Submit your article](#)[Guide for autho](#)[Menu](#)[Search in this journal](#)

Electrochemistry

Research article [Open access](#)

N, O self-doped hierarchical porous carbon materials for high-performance super-capacitors

Liu Yang, Hong Zheng, Lian Liu, Wenjie Wu, Shuya Wang

Article 100109

[Download PDF](#) [Article preview](#)

Abstract

Abstract

Biomass carbon materials have been widely used as electrode materials for super-capacitors (SC) due to their economic, environmental, and sustainable characteristics. In this work, we proposed that the Sapindus Mukorossi Peel (SMP) was used as a precursor to prepare a Sapindus Mukorossi Peel-based activated carbon material (SMPC) through carbonization and KOH activation. The morphology and structure of SMPC were characterized by various test methods. Cyclic voltammetry (CV), galvanostatic charge–discharge (GCD) and electrochemical impedance spectroscopy (EIS) were used to characterize its electrochemical performance. The results show that SMPC has suitable pore size distribution, a large number of heteroatom

[FEEDBACK](#)

Results in Chemistry

Open access

Submit your article

Guide for autho

Menu



Search in this journal

polymerization method

Ling Li, Zhiqiang Wei, Jiahao Liang, Jinhuan Ma, Shangpan Huang

Article 100205

[Download PDF](#) Article preview

Abstract

Abstract

MoS₂/PPY nanocomposites with different mass ratios were successfully synthesized the *in-situ* oxidative polymerization method. The microstructure, morphology, element content of the samples was characterized by field emission scanning electron microscopy (FESEM), X-ray diffraction (XRD), energy-dispersive X-ray spectrum (EDX), high-resolution transmission electron microscopy (HRTEM), X-ray photoelectron spectrometer (XPS). And the influence of the composite ratio on the electrochemical properties was evaluated by galvanizing charge–discharge (GCD), cyclic voltammetry (CV), electrochemical impedance spectra (EIS) and cycle stability. The experimental results show that all samples exhibit hexagonal systems with great crystallization. The morphologies are uniform structures with an obvious cladding layer. The CV curve is rectangular and the redox peak is evident. MoS₂ nanocomposites have excellent specific capacitance and good cyclic stability. The Nyquist spectrum of the sample shows that the electrical resistance of the MoS₂ nanocomposite is low and the electronic conductivity is excellent. When the current

FEEDBACK

Results in Chemistry

Open access

Submit your article

Guide for autho

Menu



Search in this journal

Tanjuan You, Lingxin Kong, Junjie Xu, Baoqiang Xu, ... Bin Tang

Article 100143

[Download PDF](#) Article preview

Abstract

Abstract

In this study, the activities of binary alloys (Sn-Ag, Sn-Cu, Sn-Zn, Ag-Cu, Ag-Zn, Cu-Zn) and ternary alloys (Sn-Ag-Cu, Sn-Ag-Zn, Sn-Cu-Zn) were predicted using molecular interaction volume model (MIVM), modified MIVM (M-MIVM), Wilson equation, and nonrandom two-liquid model. The prediction deviations of the M-MIVM were the smallest among the four thermodynamic models, indicating that the M-MIVM is reliable for predicting the activity of these multicomponent lead-free solders. On this premise, the activities of all components in ternary Sn-Ag-Cu solders at 1300 K were predicted using the M-MIVM. We found that the activities of Sn, Ag and Cu exhibit negative deviations from Raoult's law and that these deviations eventually transform into positive deviations. The activities of all components in quaternary Sn-Ag-Cu-Zn solders at 1000 K were also predicted using the M-MIVM when Zn contents were 0.1 and 0.2. This study provides a complete thermodynamic description of Sn-Ag-Cu ternary and Sn-Ag-Cu-Zn quaternary alloys.

Research article Open access

FEEDBACK

Results in Chemistry

Open access

Submit your article

Guide for autho

Menu



Search in this journal

Abstract

Abstract

Photophysical studies of resorcinol-based family of acridinedione (ADR) dyes with a glycoprotein, ovalbumin (OVA) were carried out in water. Addition of OVA to photoinduced electron transfer (PET) based dye (ADR1) resulted in a considerable red shift of emission maxima with a slight increase in the fluorescence intensity, whereas no significant variation in the fluorescence intensity or shift of emission maxima results in the case of a non-PET dye. Fluorescence lifetime studies illustrates that the PET lifetime component enhances by several fold on the introduction of OVA which is accompanied with the formation of multi lifetime components in the aqueous phase of varying distribution as observed in well-known globular protein, bovine serum albumin (BSA). Interestingly, a decrease in the fluorescence lifetime of non-PET dye (ADR2) with the evolution of more than one distinct lifetime species results with OVA. This behaviour ascertains the presence of at least two different micro environment of dye residing in aqueous phase on the addition of OVA. The introduction of OVA induces the formation of several distinguishable

Polymer Chemistry and materials science

Research article Open access

Adsorption of ammonium and phosphates by biochar produced from oil palm shells: Effects of production conditions

FEEDBACK

Results in Chemistry

Open access

Submit your article

Guide for autho

Menu



Search in this journal

This study investigated the effects of production conditions on the ammonium and phosphate adsorption capacity of oil-palm-shell-biochar. Biochar was prepared at three pyrolysis temperatures (350, 650, and 750 °C), under three activation conditions (no oxidation, partial oxidation at 250 °C, and chemical activation with K_2CO_3), and using three washing methods (no washing, acid washing, and hot water). Physicochemical properties of certain biochar samples were characterized by SEM, CHON-S, XRF, FTIR, and area BET. The highest ammonium adsorption capacity (1.49 mg/g) was observed for chemically activated biochar pyrolyzed at 650 °C without washing. The best phosphate adsorption capacity (0.89 mg/g) was observed for partially oxidized biochar pyrolyzed at 650 °C with acid washing. The BET surface area ranged from 4 to 253 m^2/g . The biochar produced at 350 °C without washing had more surface functional groups than that produced at higher temperatures. The chemical activation process promoted the development of numerous functional groups on the biochar surface

Research article *Open access*

MHD heat and mass transport of Maxwell Arrhenius kinetic nanofluid flow over stretching surface with nonlinear variable properties

S.O. Salawu, E.O. Fatunmbi, S.S. Okoya

Article 100125

[Download PDF](#) [Article preview](#)

FEEDBACK

Results in Chemistry

Open access

Submit your article

Guide for autho

Menu



Search in this journal

molecular mixture is inspired by the Arrhenius pre-exponential kinetics. Reaction mixture occurs in a boundless slippery plate subject to a considerable quantity of tension that can prevent material deformity. With appropriate similarity variables, the flow model reduces to quasilinear coupled system of derivatives. A numerical simulation of the flow characteristics is carried out, and the results presented in tables and graphs for various thermodynamic phenomena. The results show that the flow momentum is damped by the material term, but augmented by nonlinear heat convection and radiation. The heat transfer rate is significantly propelled by temperature ratio and viscous heating, while the Lewis number, molecular Brownian motion and the chemical reaction term encourage species mass transfer. As such, the study involving activation energy plays a critical part in the diffusion

Research article *Open access*

Characterization and biological activities of synthesized citrus pectin-MgO nanocomposite

R. Supreetha, S. Bindya, P. Deepika, H.M. Vinusha, B.P. Hema

Article 100156

[Download PDF](#) [Article preview](#)

Abstract

Abstract

FEEDBACK

Results in Chemistry

Open access

Submit your article

Guide for autho

Menu



Search in this journal

studied on clinical pathogens *Bacillus subtilis* and *Lactobacillus*. Antifungal activity was also studied against pathogenic organisms; ▼

Research article Open access

Synthesis of a Divinyl-functionalized Diamantane-Analogue from naturally occurring *myo*-Inositol and its application to polymer synthesis via the Thiol-ene reaction

Kimikatsu Ikeya, Shusuke Okamoto, Atsushi Sudo

Article 100167

Download PDF Article preview

Abstract

Graphical abstract

Graphical abstract

FEEDBACK

[Submit your article](#)[Guide for autho](#)[Menu](#)Research article *Open access*

FT-IR, FT-Raman, UV–Visible, NMR, DFT and molecular docking investigation of 1-(phenyl (piperidin-1-yl) methyl) naphthalene-2-ol

P. Rajamani, V. Vijayakumar, N. Sundaraganesan, Mani Jeeva, Maria Susai Boobalan

Article 100096

[Download PDF](#) [Article preview](#)

Abstract

Abstract

1-(Phenyl(piperidin-1-yl)methyl)naphthalene-2-ol was synthesized and characterized utilizing spectroscopic techniques (FT-IR, FT-Raman, UV–Visible, NMR, Mass and CHNS analysis). The synthesized compound chemical structure was optimized using the Density Functional Theory (DFT) B3LYP/6-311G (d,p) basis set. The computational studies including NMR chemical shift value, vibrational frequencies, natural bond orbital (NBO), frontier molecular orbital (FMO), molecular electrostatic potential (MEP), HOMO-LUMO, NLO, dipole moment, Mulliken charge analysis, thermal studies and potential energy surface (PES) analysis. Molecular docking studies were also carried out for Haemophilus influenza protein with target molecule using Autodock 4.2 versions and showed potential inhibitor activity against Haemophilus influenzae diseases.

[FEEDBACK](#)

Results in Chemistry

Open access

Submit your article

Guide for autho

Menu



Search in this journal

Article 100099

Download PDF

Article preview

Abstract

Abstract

Nitrated benzo[a]pyrenes are known to be mutagenic, carcinogenic and teratogenic to bacterial and animal cells. For differentiation of isomers and environmental analytical trace studies, spectroscopic information is necessary. The present studies report the ^{13}C NMR spectra of 1-, 3- and 6-nitrobenzo[a]pyrene measured in CDCl_3 . Complete ^{13}C NMR assignments based on 2D NMR spectroscopy (HMQC and HMBC) were carried out. Further, the computation of fifty ^{13}C chemical shifts of 1-, 3-, and 6-nitrobenzo[a]pyrenes by using GIAO B3LYP/6-311+G(d,p)//B3LYP/6-31+G(d), 6-31+G(d,p), 6-311+G(d), 6-311+G(d,p), 6-311G(d,p) levels of theory was investigated. For 1-, 3- and 6-NBaP the calculated chemical shifts δ_{calc} versus δ_{expt} plots of chemical shifts fall on a linear correlation line with $r^2 > 0.90$. The GIAO B3LYP/6-311+G(d,p)//B3LYP/6-311G(d,p) level of theory was found to yield chemical shifts in good agreement with experiment with $r^2 > 0.90$. The most expensive method (larger basis set) has provided the best agreement with the experiment. It is therefore important to continue to seek computational methods that can predict precise

Research article [Open access](#)

FEEDBACK

Results in Chemistry

Open access

Submit your article

Guide for autho

Menu



Search in this journal

Abstract

A full-length three-dimensional structure of the tetrameric potassium ion channel (hERG Kv11.1) including the N- and C-terminal domains was built, with a diameter of 6 Å and 12 Å between the K⁺ selectivity filter and the pore cavity residue Tyr⁶⁵² of opposite subunits. Further docking studies with a set of 233 structurally known blockers have shown that compounds bind near the inner vestibule of the pore channel, as well as the helix-IV region of the voltage sensor domain (VSD) in the alpha subunit. The residues of hERG, Gly⁶²⁶, Phe⁶²⁷, Gly⁶²⁸, Tyr⁶⁵² and Phe⁶⁵⁶ of the pore channel and Arg⁴⁸⁸ of VSD plays an important role in ligand binding and hERG blockage. The conducted QuaSAR model is statistically significant, with R² of 0.72 in predicting the hERG blocking activity. Furthermore, QuaSAR descriptors employing computer-assisted multiple regression procedure reveal that increase in hydrophobicity with higher number of aromatic rings are favorable for the binding affinity of hERG blockers. Additionally the pIC₅₀ values of 25 commercial compounds screened using structure-based pharmacophore model also show

Catalysis

Research article *Open access*

Selective oxidation of benzyl alcohols with molecular oxygen as the oxidant using Ag-Cu catalysts supported on polyoxometalates

FEEDBACK

Results in Chemistry

Open access

[Submit your article](#)[Guide for autho](#)[Menu](#)[Search in this journal](#)

We report an efficient process for the oxidation of benzyl alcohols using molecular oxygen as the oxidant catalyzed by Ag-Cu catalysts supported on polyoxometalates (Ag-Cu/POM). The Ag-Cu/POM catalyst was prepared by galvanic displacement in the presence of polyvinyl pyrrolidone and polyethylene glycol. The catalysts were characterized using Fourier transform infrared spectroscopy (FTIR), ultraviolet-visible spectroscopy (UV-Vis), powder X-ray diffraction (PXRD), X-ray fluorescence (XRF), Brunauer-Emmett-Teller (BET) surface analysis, transmission electron microscopy (TEM), energy dispersive spectroscopy (EDS) and thermogravimetric analysis (TGA). The oxidation reaction was carried out using a Schlenk-line setup, under ambient atmospheric pressure. Reaction products were identified by GC-MS and quantified with GC using an internal standard method. The Ag-Cu/POM catalyst gave close to 100% benzyl alcohol conversion in 5 h with >99% selectivity to benzaldehyde. When tested on various benzyl alcohol derivatives the Ag-Cu catalysts showed good conversions and >99% selectivity to the corresponding

Research article [Open access](#)A novel heterogenized Ni/ β -diimine/SBA-15 complex applied for catalytic ethylene oligomerization

Adriano Martinez Basso, Bruna Pes Nicola, Katiúscia Machado Nobre Borba, Sibeles B.C. Pergher, Katia Bernardo-Gusmão

Article 100182

[Download PDF](#) [Article preview](#)[Abstract](#)[Graphical abstract](#)[FEEDBACK](#)

Results in Chemistry

Open access

Submit your article

Guide for autho

Menu



Search in this journal

SBA-15

Ethylene

Green and Sustainable Chemistry

Research article *Open access*

Sulfated TiO₂/SnO₂ nanocomposite as a green heterogeneous catalyst for direct amide formation reaction

S.M. Patil, S.A. Vanalakar, S.A. Sankpal, S.P. Deshmukh, S.D. Delekar

Article 100102

[Download PDF](#) [Article preview](#)

Abstract

Abstract

Heterogeneous binary TiO₂/SnO₂ nanocomposite (with 4:1 wt% of TiO₂ and SnO₂, respectively) catalyst was prepared by a sol-gel method, and further sulfated by chlorosulfonic acid. X-ray diffraction technique revealed the structure of the nanoc

FEEDBACK

Results in Chemistry

Open access

Submit your article

Guide for autho

Menu



Search in this journal

Research article *Open access*

Purification of xylooligosaccharides from bamboo with non-organic solvent to prepare food grade functional sugars

Yetao Jiang, Xiaoyu Wang, Zhen Wu, Jiaying Xu, ... Lu Lin

Article 100153

[Download PDF](#) [Article preview](#)

Abstract

Abstract

Food grade xylooligosaccharides (XOS) have a high application value, but most of the reported purification methods of XOS use organic solvents, which has significant problems such as large amount of solvent, residual solvent, and difficulty in solvent recovery. In addition, although there are many reported methods of separation and purification, quantitative analysis is lacking for each specific treatment step, such as sugar loss rate, decolorization rate, protein removal rate, and desalination rate. Therefore, purification of XOS from bamboo with non-organic solvent to prepare food grade functional sugars was presented by this study. What's more, quantitative analysis and optimization was made for each step of separation, which was of great significance for guiding the actual production. Overall, through activated carbon adsorption, ion exchange and membrane filtration

FEEDBACK

Results in Chemistry

Open access

Submit your article

Guide for autho

Menu



Search in this journal

D.J. Manasa, K.R. Chandrashekar, M.A. Pavan Kumar, D. Suresh, ... H.C. Ananda Murthy

Article 100178

[Download PDF](#)

Article preview

Abstract

Abstract

The zinc oxide nanoparticles (*T*-ZnO NPs) were synthesized successfully by the application of leaf, stem and callus extracts of *Tabernaemontana heyneana* Wall. via the green combustion method. The structural, bonding and morphological features of *T. heyneana* mediated ZnO NPs (*T*-ZnO NPs) were explored using XRD (X-ray powder diffraction), UV–Vis (Ultra-violet visible spectroscopy), FESEM-EDS (Field Emission-SEM and energy-dispersive X-ray spectra), DLS (Dynamic light scattering) and FTIR (Fourier transform infrared) techniques. UV–Vis spectra revealed the presence of a band in the region between 370 and 376 nm approving the presence of *T*-ZnO NPs. XRD, FESEM-EDS, TEM and DLS analysis confirmed the formation of nanosized, spherical shaped, highly stable and pure crystalline wurtzite *T*-ZnO NPs. FTIR spectra revealed the presence of most probable phytochemicals from plant extracts involved in the processes of reduction and stabilization of *T*-ZnO NPs. The *T*-ZnO NPs could effectively inhibit the activity of DPPH (1,1-Diphenyl-2-picrylhydrazyl) radical (IC_{50} value between 467.7 and 752.3 $\mu\text{g/ml}$)

Research article [Open access](#)

FEEDBACK

Results in Chemistry

Open access

Submit your article

Guide for autho

Menu



Search in this journal

Abstract

An expeditious protocol for the synthesis of structurally diversified β -carboline derivatives has been reported using a readily available natural surfactant medium. The synthesis of β -carboline derivatives in good yields under optimized conditions was carried out by the reaction of tryptamine with aldehydes in an aqueous extract of *Acacia Concinna* pods. The use of an aqueous medium, ease of purification, good yield and cost-effective reaction suggest for bulk scale production β -carboline derivatives.

Supramolecular Chemistry

Research article Open access

Enhanced multifunctionality of CuO nanoparticles synthesized using aqueous leaf extract of *Vernonia amygdalina* plant

H.C. Ananda Murthy, Tegene Desalegn Zeleke, K.B. Tan, Suresh Ghotekar, ... C.R. Ravikumar

Article 100141

[Download PDF](#) Article preview

Abstract

FEEDBACK

Results in Chemistry

Open access

Submit your article

Guide for autho

Menu



Search in this journal

high crystallinity of CuO. The purity of the NPs was corroborated by SEM-EDX analysis. The average particle size of the NPs was found to be 19.68 nm. In addition, the combined TEM, HRTEM and SAED analysis substantiated the presence of CuO with a d-spacing value of 0.2854 nm, which conformed to CuO (1 1 1). The antibacterial assay revealed that VeA-CuO NPs were synergistic in their influence versus bacterial strains, *S. aureus*, *E. coli*, *P. aeruginosa*, and *E. aerogenes*. The uppermost zone of inhibition of 15 mm was observed for *E. aerogenes*. The bioactive compounds capped around the CuO NPs served the effective role in

Medicinal Chemistry and Chemical Biology

Research article [Open access](#)

In-silico drug repurposing study: Amprenavir, enalaprilat, and plerixafor, potential drugs for destabilizing the SARS-CoV-2 S-protein-angiotensin-converting enzyme 2 complex

Ivonne Buitrón-González, Giovanny Aguilera-Durán, Antonio Romo-Mancillas

Article 100094

[Download PDF](#) [Article preview](#)

Abstract

Graphical abstract

Graphical abstract

FEEDBACK

Results in Chemistry

Open access

Submit your article

Guide for autho

Menu



Search in this journal

Research article *Open access*

Click chemistry: In vitro evaluation of glycosyl hybrid phosphorylated/thiophosphorylated 1,2,3-triazole derivatives as irreversible acetyl cholinesterase (AChE) inhibitors

B. Anjaneyulu, G.B. Dharma Rao, Tanima Bajaj

Article 100093

[Download PDF](#) [Article preview](#)

Abstract

Abstract

A novel series of phosphorylated/ thiophosphorylated glucosyl-1,2,3-triazole derivatives have been synthesized in three step process. The synthetic approach was progressed from the reaction of propargyl alcohol with dialkoxychlorophosphate/thiophosphate derivatives to give propargylphosphate/thiophosphate derivatives. Then, the reaction of above synthesized compounds with acetylated glucosyl azides through azide-alkyne [2 + 3]-cycloaddition reaction (click reaction) led to the formation of the title

FEEDBACK

[Submit your article](#)[Guide for autho](#)[Menu](#)[Search in this journal](#)

Synthesis, characterization of novel sesamol substituted with thiazolidin-4-one derivatives and their evaluation for anti-oxidant and anti-cancer activities

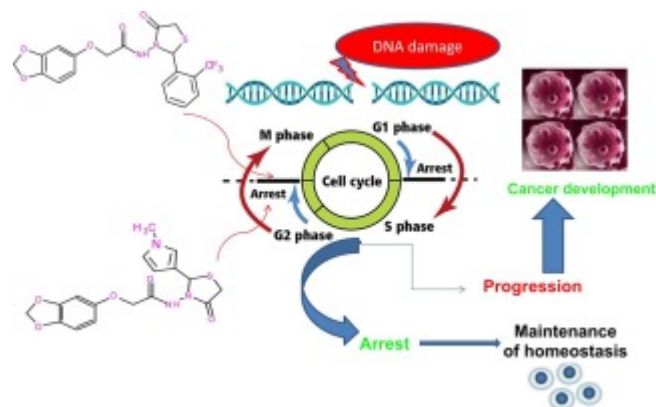
N.L. Yaswanatha Kumar,, Kumar K.N. Bharathi, Jayesh Mudgal, S.G. VasanthaRaju, S.A. Manohara Reddy

Article 100095

[Download PDF](#) [Article preview](#)

[Abstract](#) [Graphical abstract](#)

Graphical abstract

[FEEDBACK](#)

Results in Chemistry

Open access

Submit your article

Guide for autho

Menu



Search in this journal

Download PDF Article preview

Abstract

Abstract

The antioxidant activities of the aqueous extracts of seven wild plants were investigated, using both *in vitro* and *in vivo* assays. The former relied on the use of 2,2-diphenyl-1-picrylhydrazyl (DPPH) and the latter, on the sensibility towards hydrogen peroxide of the yeast *sod1* mutant. The studied plants were all wild, collected at the Ccamarrara hill (4000 m.a.s.l. Cusco, Peru), and of the following species: *Plantago australis*, *Baccharis latifolia*, *Ageratina sternbergiana*, *Stevia macbridei*, *Ageratina cuzcoensis*, *Calceolaria myriophylla*, and *Adiantum orbignyana*. The DPPH assay demonstrated high antioxidant contents in the dry leaves of all tested plants, with AAEAC values (ascorbic acid equivalent antioxidant capacity) ranging from 20.6 to 72.7 mg/g dry leaves. The antioxidant activities were also evident in the yeast assay, which also allowed distinction between the intracellular and extracellular effects. These *in vitro* and *in vivo* studies demonstrate the need to further investigate native wild plants from the Andes as important sources for water-soluble antioxidant compounds

Research article Open access

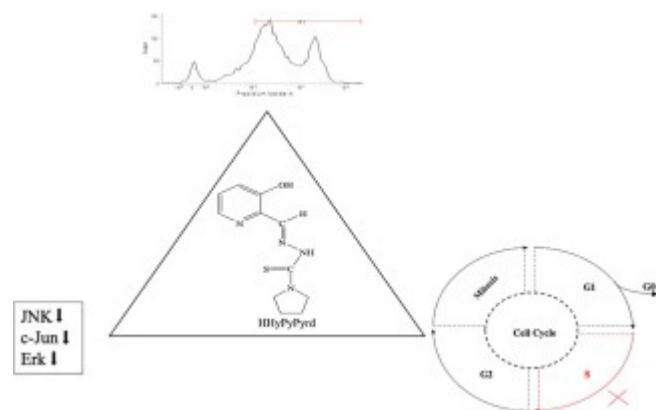
Anticancer potential of 3-hydroxypyridine-2-carboxaldehyde N(4)-methyl and pyrrolidinylthiosemicarbazones and their Zn(II) complexes in different cancers via targeting MAPK superfamily signaling pathway

FEEDBACK

[Submit your article](#)[Guide for autho](#)[Menu](#)[Search in this journal](#)

Graphical abstract

Schematic representation of mechanism of action of HHyPyPyrd on cancer cell proliferation.

Research article [Open access](#)

Cell cell death communication by signals passing through non-aqueous environments

Alla Potapovich, Vladimir Kostyuk

Article 100107

[Download PDF](#) [Article preview](#)

Abstract

FEEDBACK

[Submit your article](#)[Guide for autho](#)[Menu](#)[Search in this journal](#)

However, along with studies showing the existence of intercellular electromagnetic communication related to various responses of detector cells there have been numerous unsuccessful attempts to confirm the biological significance of MGR. Here we reported strong evidence for non-chemical intercellular signaling leading to biological cellular response. We found the ability of various cell types under conditions of oxidative stress induced by p-benzoquinones to generate death signals, which can affect target cells over long distances through non-aquatic environments resulting in morphological alterations and viability loss. We

Research article [Open access](#)

An integrated virtual screening of compounds from *Carica papaya* leaves against multiple protein targets of SARS-Coronavirus-2

Pandu Hariyono, Christine Patramurti, Damiana S. Candrasari, Maywan Hariono

Article 100113

[Download PDF](#) [Article preview](#)

Abstract

Abstract

The pandemic of SARS-Coronavirus-2 (Coronavirus-19) has been progressing by the increasing trend of the cases as well as deaths with neither vaccine nor drug is rationally used to stop the viral spread over. This study aims to perform an integrated virtual

[FEEDBACK](#)

Results in Chemistry

Open access

Submit your article

Guide for autho

Menu



Search in this journal

Research article *Open access*

Design and synthesis of novel estrogen receptor antagonists with acetal containing biphenylmethane skeleton

Materu Yuyama, Takashi Misawa, Yosuke Demizu, Takayuki Kanaya, Masaaki Kurihara

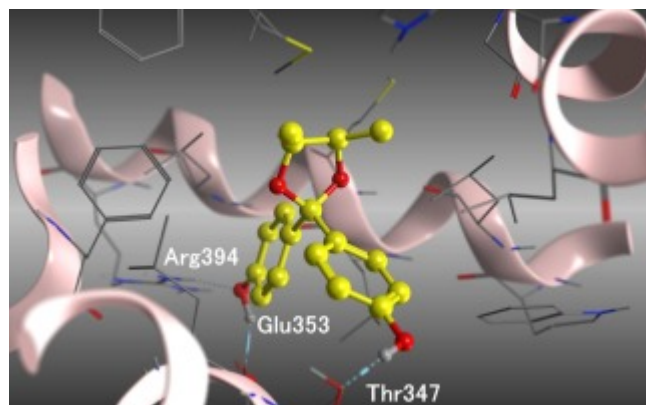
Article 100124

[Download PDF](#) [Article preview](#)

Abstract

Graphical abstract

Graphical abstract



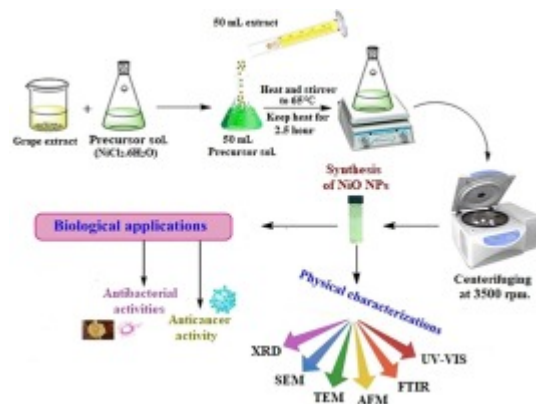
FEEDBACK

[Submit your article](#)[Guide for autho](#)[Menu](#)[Search in this journal](#)

Article 100142

[Download PDF](#) [Article preview](#)[Abstract](#)[Graphical abstract](#)

Graphical abstract

[Research article](#) [Open access](#)[FEEDBACK](#)

Results in Chemistry

Open access

Submit your article

Guide for autho

Menu



Search in this journal

Abstract

Abstract

A novel Schiff base ligand, 3-((2-((1-(4-hydroxyphenyl)ethylidene)amino)ethyl)imino)-N-(p-tolyl)butanamide (**H₂L**) and its some metal, Mn(II), Fe(III), Co(II), Ni(II) and Zn(II) complexes have been synthesized. Schiff base ligand was characterized by analytically and HRMS, IR-, ¹H NMR, ¹³C NMR- and UV-Vis spectral techniques. In addition to this molar conductance and magnetic moment calculations were used to characterize metal complexes. The ligand and its complexes have been evaluated for their *in vitro* cytotoxicity against Dalton's Lymphoma Ascites (DLA) cell lines by Trypan Blue Exclusion method. Zn(II) complex was selected to evaluate its efficiency against EAC (Earlich Ascites Carcinoma) induced ascites tumor and DLA induced solid tumor in Swiss Albino female mice. The results are expressed with an IC₅₀ value, 48 µg/ml, which indicated that Zn(II) complex showed as a potential anticancer agent. Metal complexes of Mn(II), Fe(III), Co(II), Ni(II) and Zn(II) are taken to examine for their larvicidal activity against larvae of *Cx. quinquefasciatus*. The statistically analyzed results showed that the sample of Zn(II) complex exhibited

Research article Open access

Use of molecular homology model to identify inhibitors of *Staphylococcus pseudintermedius* sortase A

Manasi Balachandran, Jerome Baudry, Stephen A. Kania

Article 100185

FEEDBACK

Results in Chemistry

Open access

Submit your article

Guide for autho

Menu



Search in this journal

recent years due to the increased prevalence of methicillin resistance and multidrug resistance. Therefore, development of alternate therapeutic strategies is a high priority. Treatments based on sortase inhibition hold potential to address this shortcoming. Sortase A (SrtA) is a transpeptidase, commonly produced by Gram positive bacteria, that interacts with proteins bearing a C-terminal Leu-Pro-X-Thr-Gly (LPXTG) motif, anchoring them on the peptidoglycan cell wall. SrtA substrates include numerous virulence factors that may overcome the host immune response including protein A, fibrinogen binding proteins and fibronectin binding proteins. In the present study, the *srtA* gene from *S. pseudintermedius* was identified and its conservation and level of transcription determined in isolates representing major clonal complexes. The gene was synthesized and then expressed in *Escherichia coli* and the recombinant enzyme's activity measured using a synthetic substrate. A three dimensional homology

Research article [Open access](#)

Potential SARS-CoV-2 3CLpro inhibitors from chromene, flavonoid and hydroxamic acid compound based on FRET assay, docking and pharmacophore studies

Maywan Hariono, Pandu Hariyono, Rini Dwiastuti, Wahyuning Setyani, ... Habibah Wahab

Article 100195

[Download PDF](#) [Article preview](#)

Abstract

FEEDBACK

Results in Chemistry

Open access

Submit your article

Guide for autho

Menu



Search in this journal

250 $\mu\text{g}/\text{mL}$ (925 μM) as well as hydroxamic acid compound, *N*-isobutyl-*N*-(4-methoxyphenylsulfonyl)glycyl hydroxamic acid (NNGH), which shows 69% inhibition at 100 μM . The *in vitro* results are supported by the docking studies revealing that the binding mode of both compounds is mainly by interacting with GLU166 residue in the hydrophobic pocket of the 3CLpro. Pharmacophore mapping further supported the results by confirming that the *in vitro* activities of both compounds are due to

Research article Open access

A *N*-(4-chlorophenyl)- γ -amino acid derivatives exerts *in vitro* anticancer activity on non-small cell lung carcinoma cells and enhances cytosine arabinoside (AraC)-induced cell death via mitochondria-targeted pathway

Povilas Kavaliauskas, Šarūnas Žukauskas, Kazimieras Anusevičius, Benas Balandis, ... Vytautas Mickevičius

Article 100193

[Download PDF](#) Article preview

Abstract

Graphical abstract

Graphical abstract

FEEDBACK

[Submit your article](#)[Guide for autho](#)[Menu](#)[Search in this journal](#)Research article [Open access](#)

High-valued pyrazinoindole analogues: Synthesis, antibacterial activity, structure activity relationship and molecular dynamics analyses

Aarushi Singh, Neeraj Kumar, Snigdha Singh, Shubham Sewariya, ... Ramesh Chandra

Article 100194

[Download PDF](#) [Article preview](#)

Abstract

Abstract

The constant emergence of drug-resistant strains of bacteria places a sustained burden on mankind as most antibiotics commonly used for treating bacterial infections are no longer efficient. This poses an urgent need for a new and effective class of antibacterial agents. Nitrogen-containing heterocycles have been found to have the most comprehensive spectrum of biological activities. Herein, we propose the route to access pyrazinoindole derivatives and evaluated them for *in-vitro* antibacterial activity. Synthesized analogs were tested for their antimicrobial activity against two gram-negative and two gram-positive bacteria. The range of minimum inhibitory concentration (MIC) was found in between 3.75 and 60 $\mu\text{g}/\text{mL}$ where gentamycin was used as a standard drug. The structure-activity relationship studies also depicted the correlation of the electronic parameters

[FEEDBACK](#)

Results in Chemistry

Open access

Submit your article

Guide for autho

Menu



Search in this journal

Others

Research article *Open access*

Solvent-free one pot synthesis of 1,2-dihydroquinolines from anilines and acetone catalysed by MOF-199

Vrushali Raut, Rucha R. Wani, Hemchandra K. Chaudhari, Dipanwita Das

Article 100097

[Download PDF](#) [Article preview](#)

Abstract

Graphical abstract

Graphical abstract

FEEDBACK

Results in Chemistry

Open access

Submit your article

Guide for autho

Menu

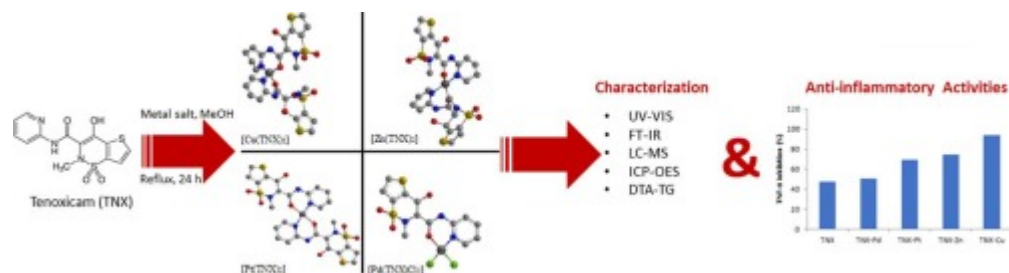
 Search in this journal

Harun Muslu, Zeynep Kalaycıoğlu, Taner Erdoğan, Ayşegül Gölcü, F. Bedia Erim
Article 100111

 [Download PDF](#) Article preview 

Abstract **Graphical abstract**

Graphical abstract

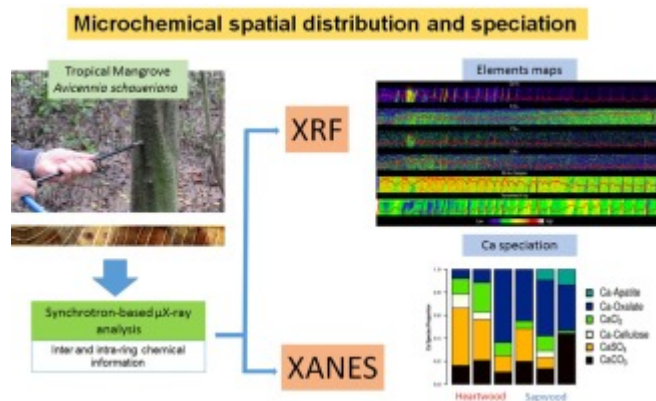


Research article Open access

Synchrotron-based X-ray microscopy for assessing elements distribution and speciation in mangrove tree-rings

Elton Eduardo Novais Alves, Daigard Ricardo Ortega Rodriguez, Pablo de Azevedo Rocha, Leonardus Vergütz, ... Liovando Marciano da Costa

FEEDBACK 

[Submit your article](#)[Guide for autho](#)[Menu](#)Research article *Open access*

HPLC-PDA combined with chemometrics for chemical markers of *Paeoniae Radix Alba* before and after sulfur-fumigated

Xiaozhou Jia, Yueyi Liang, Fang Chen, Xiaoxia Liu, ... Mei Wei

Article 100155

[Download PDF](#) [Article preview](#)[Abstract](#)

FEEDBACK

Results in Chemistry

Open access

Submit your article

Guide for autho

Menu



Search in this journal

analysis of several components, differential compounds were identified by GC-MS. The contents of gallic acid, catechins, albiflorin, paeoniflorin, 1,2,3,4,6-pentagalloyl glucose and benzoylpaeoniflorin before and after sulfur-fumigation Paeoniae Radix Alba were determined, and there were 6 common peaks in the HPLC fingerprints of Paeoniae Radix Alba before and after sulfur-fumigated. There were 6 common peaks in Paeoniae Radix Alba without sulfur-fumigated, and 7 peaks after sulfur-fumigated. The differential compound (peak 7) was proven to be paeoniflorin sulfite. The differential compound was proven to be

Organic Chemistry

Open access

Synthesis, spectral characterizations and biological applications of novel 3-[(E)-(4, 6-dihydroxy pyrimidin-5-yl)diazenyl]-4-methylbenzoic acid azo Dye and their derivatives

A.G. Prashantha, J. Keshavayya, R.A. Shoukat Ali

Article 100110

[Download PDF](#) Article preview

Abstract

Abstract

FEEDBACK

Results in Chemistry

Open access

Submit your article

Guide for autho

Menu



Search in this journal

Open access

Direct determination of absolute stereochemistry of α -methylselenocysteine using the Mosher method

Robert J. Wehrle, Douglas R. Powell, Douglas S. Masterson

Article 100114

[Download PDF](#) Article preview

Abstract

Abstract

Mosher amides of α -methylselenocysteine were synthesized to determine the absolute stereochemistry of the sterically hindered α -carbon utilizing ^1H , ^{13}C , ^{19}F , and ^{77}Se NMR spectroscopies. After analysis of these spectra using the established Mosher method, the stereochemistry of the α -carbon was determined to be (*R*), which was subsequently confirmed using x-ray crystallography.

Open access

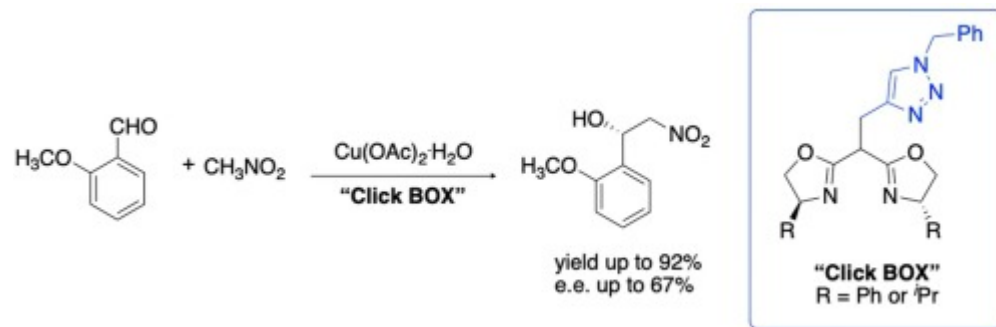
FEEDBACK

Results in Chemistry

Open access

[Submit your article](#)[Guide for autho](#)[Menu](#)[Search in this journal](#)[Abstract](#)[Graphical abstract](#)

Graphical abstract



Open access

A convenient method for preparing the ionic Nickel (bis-dithiolene) complexes

Y.L. Wang, J.Y. Jia, D. Zhang, A.H. Han

Article 100130

[Download PDF](#) [Article preview](#)

FEEDBACK

Results in Chemistry

Open access

Submit your article

Guide for autho

Menu



Search in this journal

Open access

Quick synthesis of isatin-derived knoevenagel adducts using only eco-friendly solvent

João Marcos Gomes de Oliveira Ferreira, Girlyanderson Araújo da Silva, Maísa Cavalcanti Coelho, Claudio Gabriel Lima Junior, Juliana Alves Vale

Article 100135

[Download PDF](#) [Article preview](#)

Abstract

Abstract

A variety of knoevenagel compounds from isatin were synthesized using an eco-friendly methodology. It was used only the binary solvent ethanol: water (3:7 v/v) without the presence of metal catalyst what enabled the reaction between different isatins with malononitrile in a quick reaction time of 2–5 min and isolated yields 80–96%. When cyanoesters were used as methylene actives, the reactions were longer and the knoevenagel products were obtained 79–92% isolated yields.

FEEDBACK

Results in Chemistry

Open access

Submit your article

Guide for autho

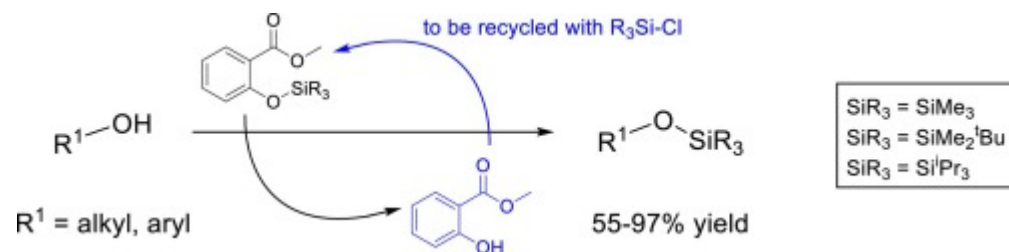
Menu

 Search in this journal

Abstract

Graphical abstract

Graphical abstract



Open access

Synthesis, characterisation and DFT studies of [3,5-bis(2-hydroxyphenyl)-1H-1,2,4-triazol-1-yl](phenyl)methanone derivatives

Louis-Charl C. Coetzee, Alfred J. Muller, Adedapo S. Adeyinka, Molahlehi S. Sonopo, D. Bradley G. Williams

Article 100165

[Download PDF](#)
[Article preview](#)

Abstract

Graphical abstract

 FEEDBACK 

Results in Chemistry

Open access

Submit your article

Guide for autho

Menu



Search in this journal

HO



OH

HO

Open access

Phenolic compounds with anti-inflammatory effects from *Knema furfuracea*

Chao-Fan Wang, Fang Kuang, Wen-Jiang Wang, Lei Luo, ... Rui Zhan

Article 100175

[Download PDF](#) Article preview

Abstract

Graphical abstract

Graphical abstract

FEEDBACK

Results in Chemistry

Open access

Submit your article

Guide for autho

Menu



Search in this journal

Open access

Steps toward enhancing the fluorescence of small-molecule-based protein labels using supramolecular hosts

Pragati K. Prasad, Leila Motiei, David Margulies

Article 100134

[Download PDF](#) Article preview

Abstract

Abstract

Labeling of proteins with small-molecule-based fluorescent probes provides a powerful tool to determine their expression level and localization in living cells. We propose a method for increasing and stabilizing the emission of such probes using supramolecular hosts such as β -cyclodextrin (β -CD). Although the emission of a His-tag binding probe was enhanced in the presence of β -CD, binding of the probe- β -CD complex to a His-tagged protein led to partial β -CD displacement and consequently, a reduction in the emission signal.

FEEDBACK

Results in Chemistry

Open access

Submit your article

Guide for autho

Menu



Search in this journal

Download PDF

Article preview

Abstract

Abstract

We report a one-step method for the synthesis of alkoxy substituted pyrazine derivatives. The process makes use of an improved acid-mediated coupling reaction to afford the products in good yields (70–90%). This method expands the scope to alkoxy substituted pyrazine structures that are poorly represented in literature.

Review article *Open access*

CoFe₂O₄/Cu(OH)₂ Nanocomposite: Expeditious and magnetically recoverable heterogeneous catalyst for the four component Biginelli/transesterification reaction and their DFT studies

Anjaneyulu Bendi, G.B. Dharma Rao, Nutan Sharma, Manoj.P. Singh

Article 100202

Download PDF

Article preview

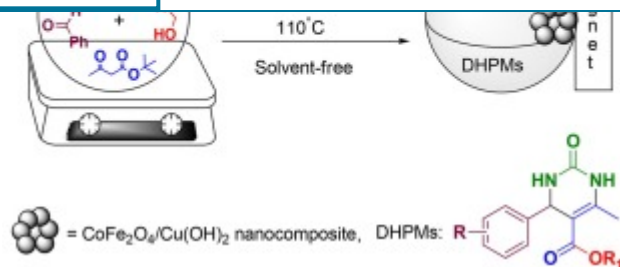
FEEDBACK

Results in Chemistry

Open access

[Submit your article](#)[Guide for autho](#)[Menu](#)

Search in this journal



Organic Chemistry

Review article [Open access](#)

Easy access to both enantiomers of 5-hydroxyequol and 3-(4-hydroxyphenyl)chroman-8-ol

Takahito Uemura, Motohiro Sonoda, Shinji Tanimori

Article 100252

[Download PDF](#) [Article preview](#)[Abstract](#)[Graphical abstract](#)

Graphical abstract

FEEDBACK

Results in Chemistry

Open access

Submit your article

Guide for autho

Menu



Search in this journal

Inorganic Chemistry

Review article *Open access*

Bismuth sulfide based compounds: Properties, synthesis and applications

Timothy O. Ajiboye, Damian C. Onwudiwe

Article 100151

[Download PDF](#) [Article preview](#)

Abstract

Abstract

Bismuth sulfide is one of the important compounds of bismuth that has garnered much attention due to its interesting properties and numerous applications. The structural orientation of bismuth sulfide and the characterization techniques have been highlighted. An in depth discussion were made on the various methods of synthesizing bismuth sulfide including chemical, sol-gel, deposition, pyrolysis, mechanical milling, microwave, microemulsion, Bridgman and successive ionic layer and reaction metho

FEEDBACK

[Submit your article](#)[Guide for autho](#)[Menu](#)[Search in this journal](#)*Analytical Chemistry*Review article *Open access*

A concise discussion on the potential spectral tools for the rapid COVID-19 detection

Abhijeet Mohanty, Adarsh P. Fatrekar, Saravanan Krishnan, Amit A. Vernekar

Article 100138

[Download PDF](#) [Article preview](#)

Abstract

Abstract

Developing robust methods to detect the severe acute respiratory syndrome coronavirus-2 (SARS-CoV-2), a causative agent for the current global health pandemic, is an exciting area of research. Nevertheless, the currently used conventional reverse transcription-polymerase chain reaction (RT-PCR) technique in COVID-19 detection endures with some inevitable limitations. Consequently, the establishment of rapid diagnostic tools and quick isolation of infected patients is highly essential. Furthermore, the requirement of point-of-care testing is the need of the hour. Considering this, we have provided a brief review of the use of very recently reported robust spectral tools for rapid COVID-19 detection. The spectral tools include, colorimetric reverse transcription loop-mediated isothermal amplification (RT-LAMP) and matrix-assisted laser desorption/ionization mass

[FEEDBACK](#)

[Submit your article](#)[Guide for autho](#)[Menu](#)[Search in this journal](#)

Biflavonoid as potential 3-chymotrypsin-like protease (3CLpro) inhibitor of SARS-Coronavirus

Yustina Hartini, Bakti Saputra, Bryan Wahono, Zerlinda Auw, ... Maywan Hariono

Article 100087

[Download PDF](#) [Article preview](#)

Abstract

Abstract

3CL protease is one of the key proteins expressed by SARS-Coronavirus-2 cell, the potential to be targeted in the discovery of antivirus during this COVID-19 pandemic. This protein regulates the proteolysis of viral polypeptide essential in forming RNA virus. 3CL protease (3CLpro) was commonly targeted in the previous SARS-Coronavirus including bat and MERS, hence, by blocking this protein activity, the coronavirus should be eradicated. This study aims to review the potency of biflavonoid as the SARS-Coronavirus-2 3CLpro inhibitor. The review was initiated by describing the chemical structure of biflavonoid and followed by listing its natural source. Instead, the synthetic pathway of biflavonoid was also elaborated. The 3CLpro structure and its function were also illustrated followed by the list of its 3D-crystal structure available in a protein data bank. Lastly, the pharmacophores of biflavonoid have been identified as a protease inhibitor, was also discussed. This review hopefully will help researchers to obtain packed information about biflavonoid which could lead to the study in designing and discovering a novel

[FEEDBACK](#)

Results in Chemistry

Open access

Submit your article

Guide for author

Menu

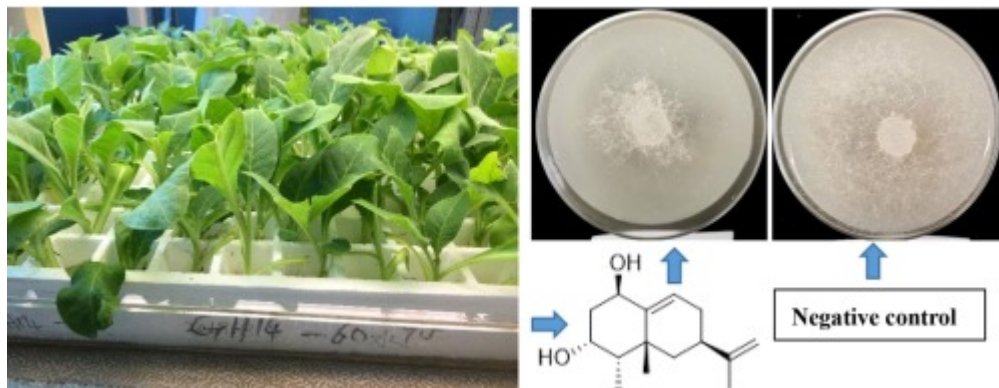


Search in this journal

Abstract

Graphical abstract

Graphical abstract



Others

Review article *Open access*

Graphene-supported nanomaterials as electrochemical sensors: A mini review

H.C. Ananda Murthy, Kiflom Gebremedhn Kelele, C.R. Ravikumar, H.P. Nagaswarupa, ... Tegene Desalegn

FEEDBACK

Results in Chemistry

Open access

Submit your article

Guide for autho

Menu



Search in this journal

Graphene has been a prominent choice as a base material for supporting varieties of inorganic and organic materials in scientific research and innovation due to its superior physico-chemical properties. Electrochemical sensors have been prepared by the use of a variety of nanoparticles and based on graphene which effectively supported on the surface of glassy carbon electrode through different methods. Graphene supported sensors have been utilized to detect and determine different electroactive species in samples. Many characterization techniques such as Powder X-ray diffraction (XRD), Energy dispersion spectroscopy (EDS), X-ray photoelectron spectroscopy (XPS), UV-Vis spectroscopy, Fourier transform infrared (FTIR) spectroscopy, Raman spectroscopy, High-resolution transmission electron microscopy (HRTEM), Scanning electron microscopy (SEM), transmission electron microscopy (TEM), and atomic force microscopy (AFM) have been successfully applied to explore the properties of graphene supported nanomaterials. Applications of the sensors have been assessed using signals from electrochemical measurements such

VSI:Inorg Bio Palaniandavar

Research article *Open access*

Molecular basis of quercetin as a plausible common denominator of macrophage-cholesterol-fenofibrate dependent potential COVID-19 treatment axis

Anil Pawar, Amit Pal, Kalyan Goswami, Rosanna Squitti, Mauro Rongioletti

Article 100148

FEEDBACK

Results in Chemistry

Open access

Submit your article

Guide for autho

Menu



Search in this journal

appeared to have little or no effect on hospitalized COVID-19 patients. This has again led to search for alternate re-purposed drugs and/or effective “add-on” nutritional supplementation, which can complement or enhance the therapeutic effect of re-purposed drug. Focus has been shifted to therapeutic targets of severe acute respiratory syndrome coronavirus (SARS-CoV-2), which includes specific enzymes and regulators of lipid metabolism. Very recently, fenofibrate (cholesterol-lowering drug), suppressed the SARS-CoV-2 replication and pathogenesis by affecting the pathways of lipid metabolism in lung cells of COVID-19 patients. A preclinical study has shown synergistic effect of quercetin (a flavonoid) and fenofibrate in reducing the cholesterol content, which might be useful in COVID-19 treatment. Based on the scientific literature, use of quercetin and fenofibrate in COVID-19 seems meaningful in pharmaceutical and biomedical research and warrants basic experimental and clinical studies. In this article we have

Inorganic Chemistry

Research article *Open access*

Spectroscopic, anticancer and antioxidant studies of fluxional *trans*-[PdCl₂(S-acylthiourea)₂] complexes

Dorothy Priyanka Dorairaj, Jebiti Haribabu, Vadivalagan Chithravel, Kailasam N. Vennila, ... Ramasamy Karvembu

Article 100157

[Download PDF](#) [Article preview](#)

FEEDBACK

Results in Chemistry

Open access

Submit your article

Guide for autho

Menu



Search in this journal

... NMR and ESI mass spectroscopy, and elemental analysis. Single crystal X-ray structure of complex 1 revealed the monodentate coordination of acylthiourea ligand through sulphur atom to the palladium ion in a *trans* fashion. In addition, variable-temperature (VT) NMR studies were performed to analyze the fluxional nature of complexes. The interaction of complexes with calf thymus (CT) DNA and BSA (bovine serum albumin) was analyzed by spectroscopic and molecular docking studies. The results inferred intercalation binding mode of the complexes with DNA. All the complexes exhibited good binding with BSA as well. Further, the complexes were found to act as good scavengers of DPPH as deduced from the antioxidant assay. *In vitro* cytotoxicity of the compounds against A549 (lung) cancer and HEK293 (human embryonic kidney) normal cell lines was

Physical Chemistry and Chemical Physics

Review article [Open access](#)

Graphene synthesis, characterization and its applications: A review

Vestince B. Mbayachi, Euphrem Ndayiragije, Thirasara Sammani, Sunaina Taj, ... Atta ullah khan

Article 100163

[Download PDF](#) [Article preview](#)

Abstract

FEEDBACK

Results in Chemistry

Open access

Submit your article

Guide for autho

Menu



Search in this journal

Summarizes the fabrication of graphene by chemical, mechanical, thermal decomposition and chemical vapor deposition. In addition, the characterization methods and applications of graphene in different research fields have been discussed. This article winds up by giving a brief summary, illuminate the problems, and states the prospects of graphene.

supramolecular chemistry

Research article *Open access*

Development of metallosupramolecular phosphatases based on the combinatorial self-assembly of metal complexes and organic building blocks for the catalytic hydrolysis of phosphate monoesters

Shin Aoki, Akib Bin Rahman, Yosuke Hisamatsu, Yuya Miyazawa, ... Tomohiro Tanaka

Article 100133

[Download PDF](#) [Article preview](#)

Abstract

Abstract

FEEDBACK

Results in Chemistry

Open access

Submit your article

Guide for autho

Menu



Search in this journal

presented, then followed by a description of artificial metallosupramolecular complexes formed by the combinatorial self-

VSI:Recent Adv in org chem

Organic Chemistry

Research article *Open access*

Microwave assisted synthesis of phenanthridine derivatives via Suzuki coupling and condensation

Satheesh Kumar Dende, Raghu Babu Korupolu, Raju Doddipalla, Krishnakanth Reddy Leleti

Article 100149

[Download PDF](#) [Article preview](#)

Abstract

Abstract

FEEDBACK

Results in Chemistry

Open access

Submit your article

Guide for autho

Menu



Search in this journal



Page 1 of 2



[< Previous vol/issue](#)

[Next vol/issue >](#)

ISSN: 2211-7156

Copyright © 2022 Elsevier B.V.



Copyright © 2022 Elsevier B.V. or its licensors or contributors.
ScienceDirect® is a registered trademark of Elsevier B.V.

RELX™

FEEDBACK



Biflavonoid as potential 3-chymotrypsin-like protease (3CLpro) inhibitor of SARS-Coronavirus



Yustina Hartini, Bakti Saputra, Bryan Wahono, Zerlinda Auw, Friska Indayani, Lintang Adelya, Gabriel Namba, Maywan Hariono*

Faculty of Pharmacy, Sanata Dharma University, Campus III, Paingan, Maguwoharjo, Depok, Sleman 55282, Yogyakarta, Indonesia

ARTICLE INFO

Keywords:

Biflavonoid
SARS-Coronavirus-2
3CL protease

ABSTRACT

3CL protease is one of the key proteins expressed by SARS-Coronavirus-2 cell, the potential to be targeted in the discovery of antiviral during this COVID-19 pandemic. This protein regulates the proteolysis of viral polypeptide essential in forming RNA virus. 3CL protease (3CLpro) was commonly targeted in the previous SARS-Coronavirus including bat and MERS, hence, by blocking this protein activity, the coronavirus should be eradicated. This study aims to review the potency of biflavonoid as the SARS-Coronavirus-2 3CLpro inhibitor. The review was initiated by describing the chemical structure of biflavonoid and followed by listing its natural source. Instead, the synthetic pathway of biflavonoid was also elaborated. The 3CLpro structure and its function were also illustrated followed by the list of its 3D-crystal structure available in a protein data bank. Lastly, the pharmacophores of biflavonoid have been identified as a protease inhibitor, was also discussed. This review hopefully will help researchers to obtain packed information about biflavonoid which could lead to the study in designing and discovering a novel SARS-Coronavirus-2 drug by targeting the 3CLpro enzyme.

Contents

1. Introduction	1
2. Chemical structure	2
3. Natural sources	3
4. Synthetic sources	3
5. 3-Chymotrypsin-like protease	4
6. Biflavonoid as the protease –Inhibitor	8
7. Perspectives	10
8. Conclusion	11
CRediT authorship contribution statement	11
Declaration of Competing Interest	11
Acknowledgement	11
References	11

1. Introduction

The Covid-19 pandemic has extended for almost 10 months since its outbreak in January 2020 [1]. The present statistic (by 24 October 2020) shows 43 M cases, 29 M recovered and 1.15 M death across the

world. The United States of America is the country with the highest cases reported at 8.5 M approximately [2]. Meanwhile, the cases in Indonesia are still increasing. There are approximately 393,000 cases with 318,000 treated and 13,500 death [3]. This situation has made very huge impacts on all aspects of life including the economy, politics,

* Corresponding author.

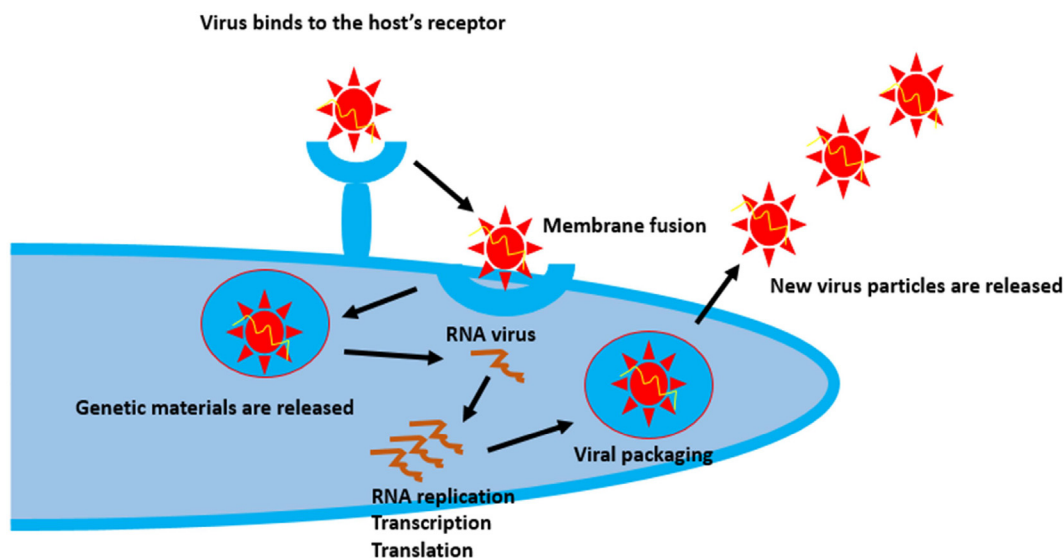


Fig. 1. The life cycle of coronaviruses is initiated by the binding of the viral cell through its protein spike (S) to the host cell's receptor namely angiotensin-converting enzyme 2 (ACE2). Upon membrane fusion (endocytosis), the virus is coated by the endosome. The following endosomal break down releases RNA from the virus into the host cell. The incoming viral genome is translated to produce two large precursor polyproteins 1a (pp1a) and 1ab (pp1ab) which are cleaved by proteases into small products. A series of subgenomic mRNA are transcribed and finally translated into viral proteins. The viral protein along with RNA is packed into virion in the ER and Golgi and then transported via vesicles and released out of the cell [9].

social, culture, health, and education. For example, United Nations Industrial Development Organization (UNIDO) reported that since April 2020, the high-income countries (30 countries) have a 18% average economic losses, whereas upper-middle-income countries (13 countries) suffer a 24% average losses. The lower-middle-income countries (6 countries) are hit by a 22% average loss, confirming the economic crisis unleashed by the pandemic, regardless of the income level [4]. The SARS-Coronavirus-2 viral vector is still a topic for debate. However, either bats or snakes are predicted as the first virus transmitting species to human [5].

Like some other coronaviruses, SARS-Coronavirus-2 is also a family of coronaviridae, which is genomically composed by the structural as well as non-structural proteins. This is an RNA virus in which on one hand, the structural protein contains S protein (spike), M protein (membrane), E protein (envelope), and N protein (nucleocapsid) [6]. On the other hand, the non-structural protein (NSP) is an open reading frame (ORF) consisting of NSP1-16 [7]. Upon entry into the host cell, the incoming viral genome is translated to produce two large precursor polyproteins 1a (pp1a) and 1ab (pp1ab) that are processed by ORF 1a-encoded viral proteinases, papain-like proteinase (PLpro), and 3C-like proteinase (3CLpro) into 16 mature non-structural proteins (NSP1–NSP16, numbered according to their order from the N-terminus to the C-terminus of the ORF 1 polyproteins). Many of the NSPs perform essential functions in viral RNA replication and transcription [8]. The virus life cycle is illustrated in Fig. 1.

One of the common studied NSPs is NSP5, in which chymotrypsin-like protease (3CLpro) is one kind of this non-structural protein [10]. 3CLpro cleaves the polyprotein into viral RNA which is then replicated and packed in the new mature virus. Therefore, by interfering with this proteolytic step, the viral RNA replication will be interrupted leading to the prevention of new viruses for further expansion. 3CLpro is one of the interesting protein targets in combating coronavirus by competitive inhibition with the peptide substrate [11].

Reviews on natural product compounds potential for SARS-Coronavirus have been published by targeting diverse proteins. These includes tanshinones, diarylheptanoids and geranylated flavonoids targeting PLpro [12], quercetine (reverse transcriptase) [13], aloemodin and hesperitin (3CLpro) [14], apigenin (viral internal ribosome entry) [15], isatisindigotica (protease) [16], amentoflavone (biflavonoid;

protease) [17], kaempferol (3a ion channel) [18], glycyrrhizin (protease) [19], tetradrine (viral S and N) [20], silvestrol (cap-dependent viral mRNA translation) [21,22], etc.

Biflavonoid is currently attractive to be proposed as the serine protease inhibitor due to the suitability of its chemical structure with the active site of the protease [23]. Serine proteases are characterized by a distinctive structure, consisting of two beta-barrel domains that converge at the catalytic active site. These enzymes can be further categorized based on their substrate specificity as either trypsin-like, chymotrypsin-like, or elastase-like. Therefore, the dimer form of biflavonoid is such a good inhibitor model that would fully occupy the two beta-barrel domain (main site and prime site) [24].

In this review, we will focus on the biflavonoid as the interesting compound, which is potential for the 3CLpro inhibitor of SARS-Coronavirus-2. The review will start by defining the chemical structure of biflavonoid and its sources from both natural products as well as synthesis. The following section would elaborate the 3CLpro structure and its function as the interesting protein target for biflavonoid. The review also summarizes the existing SARS-Coronavirus-2 3CLpro 3D crystal structure in the protein data bank. Last but not least, the current study on the biflavonoid as a diverse protease inhibitor will be carried out to give the insight mechanism on how the biflavonoid can act as a potential SARS-Coronavirus-2 antiviral agent.

2. Chemical structure

Biflavonoid is a natural product compound bearing a dimer of two sets of flavonoid, linked by either C–C or C–O bond [25,26]. The flavonoid itself is chemically constructed by a 15-C skeleton, which is divided into two aromatic rings (Ring A and Ring B) and connected by a heterocyclic ring having α , β -unsaturated carbonyl chain [27]. In addition to flavonoid being the major form of such compound class, there are two kind of analogs which enrich the flavonoid structural diversity. They are isoflavonoid (derived from 3-phenylchromen-4-one (3-phenyl-1,4-benzopyrone) and neoflavonoid (derived from 4-phenylcoumarin (4-phenyl-1,2-benzopyrone). Other sub-groups of flavonoid including flavan, flavanone, flavanonol, anthocyanidin,

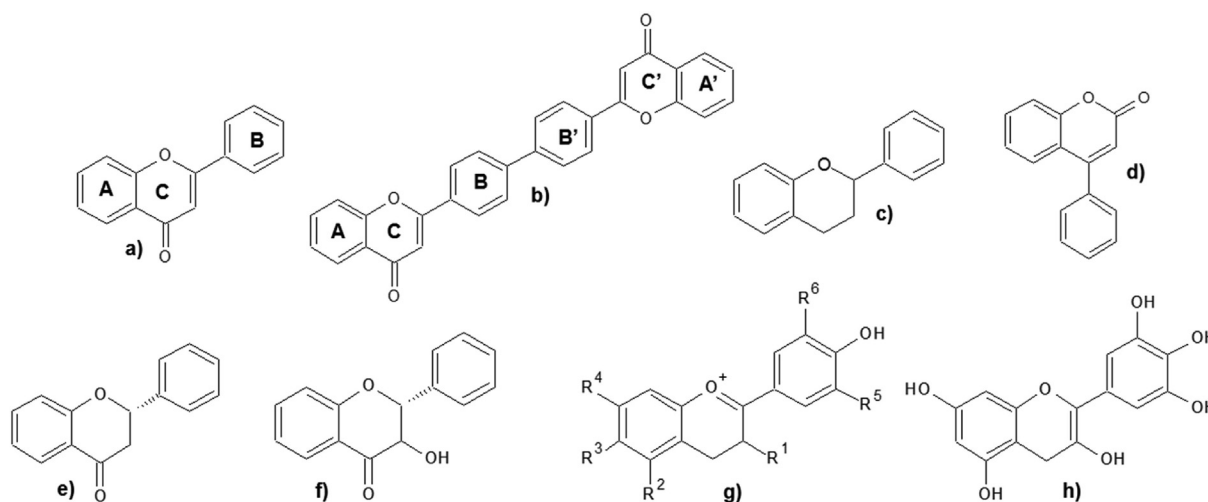


Fig. 2. The structures of a) flavonoid, b) biflavonoid, c) isoflavonoid, d) neoflavonoid, e) flavanone, f) flavanonol, g) anthocyanidin and h) anthoxantin which are naturally occurred in plants.

and anthoxantin are also widely distributed among natural resources [28]. Fig. 2 illustrates the structure of flavonoid and their analogs.

The aromatic rings are often decorated by poly-hydroxy group. Therefore, this compound's class are frequently called polyphenolic compounds. The presence of OH group has also given chance for the flavonoid to be biosynthetically formed in a glycoside. The sugar moiety in the glycosidic form makes the flavonoid more soluble in water than organic solvents due to the polar character of the sugar [29,30].

Spectroscopically, alike to the polyphenolic flavonoid, the yellowish biflavonoid absorbs UV light at 500–600 nm. The colorimetric reaction namely bathochromic shift (redshift) occurs when it reacts with an alkaline solution to prolong the maximum wavelength (650 nm). Similarly, polyvalent ion such as Al^{3+} may shift the wavelength into a hypsochromic shift (blue shift) with a lower wavelength (450 nm) [31]. Using the fourier transform infrared (FTIR) spectroscopy, the carbonyl of chromone group stretching vibration is transmitted at 1600 cm^{-1} . Meanwhile, the vinyl aromatic group appears at 3600 cm^{-1} as a bending vibration [32]. The proton of biflavonoid is indicated as multiplet signals around 6–8 ppm which often overlap in *trans/cis* configuration protons of α, β -unsaturated carbonyl chain as confirmed by nuclear magnetic resonance (NMR) spectroscopy. In conjunction, the carbon signal of the carbonyl chromone group is indicated at 160 ppm, whereas the vinylic aromatic carbon appears at 150 ppm. Using a mass spectroscopy, the origin of the flavonoid skeleton could be the most stable mass/ion (base peak) during the fragmentation due to the electron impact bombardment [33].

3. Natural sources

A naturally occurring biflavonoid is distributed in various plant species. The first isolated natural biflavonoid was from *Ochna squarrosa* Linn. (Ochnaceae) [34] and later was from *Lonicera japonica* (Caprifoliaceae) [35]. *Torreya nucifera* was also identified as the natural source producing four biflavonoids [36]. Amentoflavone is another kind of biflavonoid isolated from abroad family of plants such as selaginellaceae, cupressaceae, euphorbiaceae, podocarpaceae, and calophyllaceae [37]. It was reported that at least 127 biflavonoids are distributed among plants, but the most occurrences are *Ginkgo biloba*, *Lobelia chinensis*, *Polygala sibirica*, *Ranunculus ternatus*, *Selaginella pulvinata*, and *Selagenella tamariscina* [37].

A more recent study had identified the biflavonoid I3' I18-binarigenin in drupes of *Schinus terebinthifolius*, which was indicated by UHPLC-MS [38]. Five biflavonoids were lately found in *Ceratodon*

purpureus presenting a diastereomeric form in the second biflavonoid [39]. In the same year, three biflavonoid types were also discovered in *Selaginella doederleinii* including the amentoflavone type, robustaflavone type, and hinokiflavone type [40]. From the zingiberaceae family, new biflavonoids with flavanone-chalcone type can be found in fingerroot (*Boesenbergia rotunda*) [41]. The pure biflavonoid with aglycones morelloflavone (Mo) type, volkensiflavone (Vo) type, as well as the morelloflavone's glycoside fukugiside (Fu) type was characterized in *Garcinia madruno* [42]. The genus of garcinia again shows its resource of biflavonoid by the discovery of seven compounds including volkensiflavone, fukugetin, fukugeside, GB 1a, GB 1a glucoside, GB 2a, and GB 2a glucoside from *Garcinia xanthochymus* fruits [43]. Fig. 3 illustrates the chemical structure of hinokiflavone, ochnaflavone, amentoflavone, morelloflavone, and volkensiflavone. For more data, Table 1 tabulates the various studies reporting biflavonoid found in a natural source in the last three years.

4. Synthetic sources

Instead of natural sources, biflavonoid is also produced via a synthetic pathway. This usually aims to derivatize the biflavonoid lead compound into a modified diverse functional group that could be responsible for its biological activity. Besides, the synthetic pathway could be more reproducible than isolating the biflavonoid from its genuine natural sources. This will proportionally reduce the cost of production as well as increase the yields [74,75].

Biflavonoid is synthetically formed by two units (monomer) of flavonoid undergoing the Ullmann coupling reaction [76]. This reaction forms a diaryl ether link between two units of flavonoid, which is conditioned by mixing them with an alkaline carbonate solution, *N,N*-dimethylacetamide, and dry toluene solvent under nitrogen exposure, followed by heating the mixture above $100\text{ }^{\circ}\text{C}$ for several hours [77]. The total synthesis of biflavonoid is initiated by reacting *ortho*-hydroxy acetophenone with benzaldehyde under Claisen Smith condensation to form chalcone as the intermediate compound [78]. The next step is the synthesis of flavone (monomer) by iodinating the chalcone using DMSO as the solvent [79]. The detailed total synthesis of biflavonoid is schemed out in Scheme 1.

An interesting biflavonoid was constructed according to the naringenin monomer by reacting to the available phloroglucinol and 4-hydroxy- or 4-methoxybenzaldehyde. Naringenin is the flavanone-skeleton structure attached by three hydroxy groups at the 4', 5, and

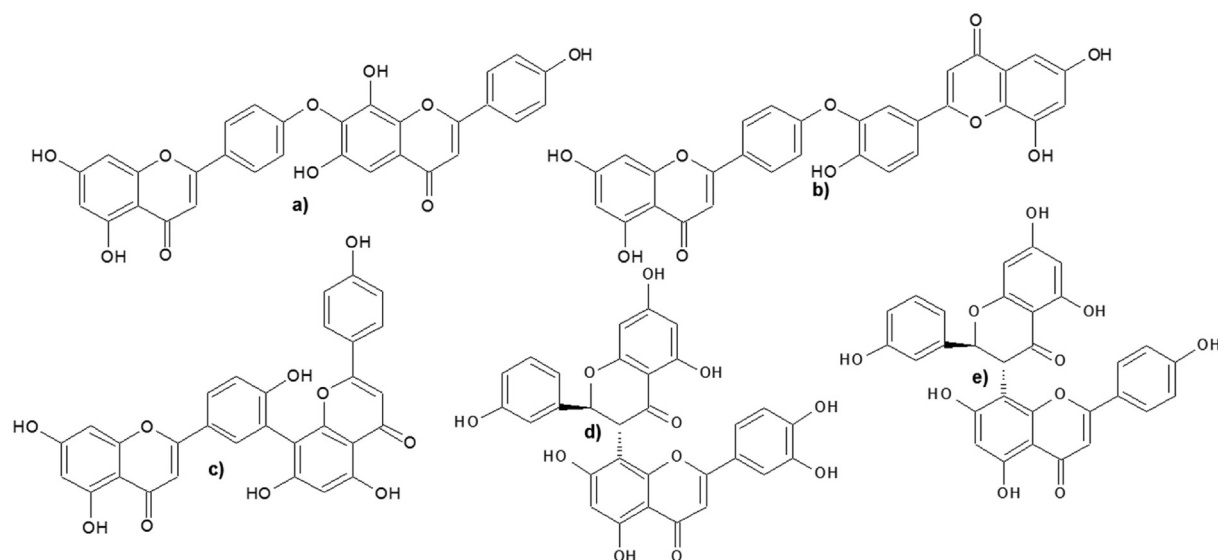


Fig. 3. The chemical structures of earlier biflavonoid found in plants: a) hinokiflavone, b) ochnaflavone, c) amentoflavone, d) morelloflavone, and e) volkensiflavone.

7 carbons. The product was confirmed as 3',3''-binaringenin, and four related biflavonoids with a considerably good yield (15–35%) [81].

Biflavonoid was also prepared electrochemically by reacting to flavonol isorhamnetin, LiClO_4 , and amine in acetonitrile solvent. The mixture was electrolyzed in a diaphragm cell at anodic current density of 5 mA/cm^2 for 3.5 h. Platinum-plated with a working surface of 2 cm^2 was used as the anode. Once the electrolysis was completed, about 90% of the acetonitrile was distilled from the anode compartment. Further purification using chromatography column was applied and followed by recrystallization to obtain the biflavonoid product with a good yield (60–70%) [82].

A step-economical preparation of a very rare biflavonoid has been performed by combining the methylated bioflavone undergoing a modular and divergent synthesis strategy. The divergent synthesis was carried out by using bialdehyde as the building block such as isophthalaldehyde, terephthalaldehyde, and benzene-1,3,5-tricarbaldehyde to produce the chalcone intermediate under Claisen Smith condensation. The following reaction was oxidative cyclization to obtain the biflavonoid as the targeted compound. Interestingly, instead of biflavonoid, the divergent method is also applied in the production of triflavonoid [83].

The synthesis of biflavonoid was further explored by applying the Suzuki-Miyaura cross-coupling reaction followed by alcohol methylation for the synthesis of rare 'hybrid' derivatives. These derivatives belong to different sub-classes of monomers. The second biflavonoid was constructed as homodimeric compounds in which a methylenedioxy group acts as the linker between the two flavonoid monomers. This reaction facilitates the probing of uncharted regions of biologically interesting chemical space [84].

The first stereodivergent synthesis of biflavanone was conducted by exclusively controlling the temperature to produce a stereoselective product. The scaffold of 2,2'-biflavanones was attached by diverse substitution at the phenyl ring and conditioned by $\text{SmI}_2/\text{Methanol}/\text{THF}$, confirmed by a highly selected good yield for both stereoisomers of the expected compounds. On one hand, the (R^*,R^*)-stereoisomer was only formed when the temperature was controlled at -40°C . On the other hand, the reaction generated the (R^*,S^*)-isomer when the mixture was refluxed [85]. The control of regioselective reaction was performed using aromatic prenyltransferase from *Aspergillus terreus* (AtaPT). Prenylation was applied to produce biflavonoids 1–3 dimerized connected by a diphenyl linkage at the hydrogen bond

involving C5''-OH group. This OH is chemically less accessible than other OH groups in the ring. The AtaPT was used as the substrate that successfully yielded the different regio and chemoselective products. This study would be recommended for developing green synthetic reactions for such prenylated biflavonoids [86].

5. 3-Chymotrypsin-like protease

The extensive process of proteolysis releases the functional polypeptides which are mainly achieved by the main proteinase and are also frequently named 3C-like proteinase (3CLpro). This indicates a similar cleavage site with the early picornavirus of 3C proteinases (3Cpro), although further studies showed that the similarity is limited by two families of the protease. 3CLpro cleaves at least 11 conserved amino acid residues includes $\text{GLN} \rightarrow (\text{SER}, \text{ALA}, \text{GLY})$ sequences (the cleavage site is indicated by \rightarrow) [87]. This process is initiated by the autocleavage of its enzyme from two polypeptides (polypeptide A and polypeptide B). There are three non-canonical 3CLpro cleavage sites at the P2 position employing PHE, MET, or VAL residues in SARS-Coronavirus polyproteins. The cleavage site of 3CLpro SARS-Coronavirus is illustrated in Fig. 4 [10,88].

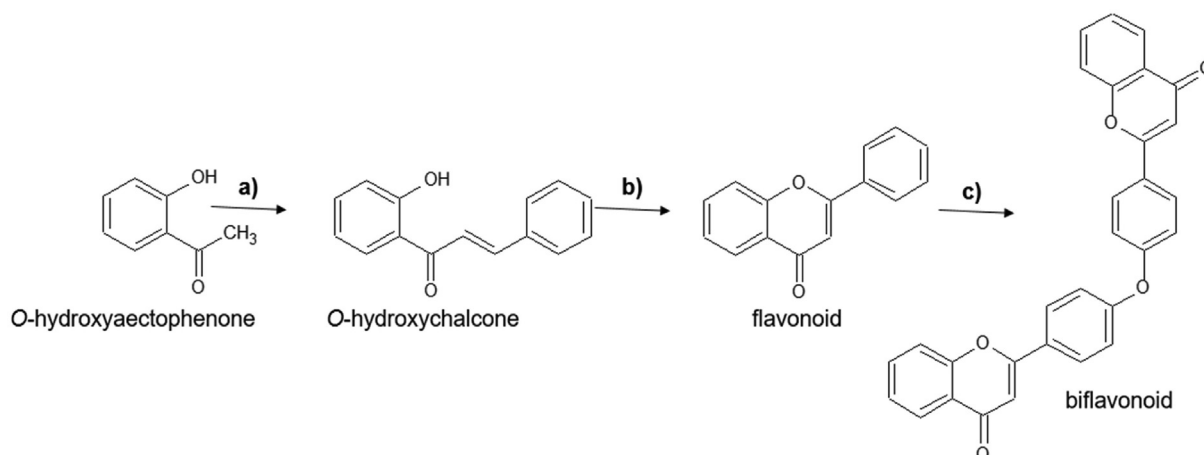
The availability of experimentally determined three-dimensional (3D) structures of the SARS-Coronavirus-2 3CLpro has greatly aided in the design of anti-SARS-Coronavirus-2 drug [91]. Recently, the sudden increase in the number of crystal structures of 3CLpro is deposited in the protein data bank (PDB) [92]. Most of the earlier crystal structures are devoid of inhibitor. Thus, it could not explain the particular binding site of 3CLpro properly [93]. Therefore, many efforts conducted to understand the structure and function of 3CLpro relied mainly on the models developed based on the crystal structures of other betacoronavirus such as SARS-Coronavirus, MERS, Bat Corona, etc [94].

To date, there are more than 100 3D structures of SARS-Coronavirus-2 3CLpro deposited in the protein data bank (PDB) (www.rcsb.org). In general, the crystal structures of 3CLpro reveal the presence of three structural domains in each monomer, in which domains I (position 8–101), II (position 102–184), and III (position 201–303) have a chymotrypsin-like characteristic fold with a catalytic cysteine (CYS145) and histidine (HIS41). This is linked to a third C-terminal domain by a long loop (position 185–200) by orienting the

Table 1

Biflavonoids from natural resources have been reported in the last three years.

No	Biflavonoid	Plants	References
1	dihydrodaphnodorin B	<i>Fumana procumbens</i>	[44]
2	daphnodorin B	<i>Fumana procumbens</i>	[44]
3	volkesiflavone	<i>Garcinia gardneriana</i>	[45]
4	morelloflavone	<i>Garcinia gardneriana</i> , <i>Garcinia madruno</i>	[45]
5	7,7''-di- <i>O</i> -methylchamaejasmin	<i>Ormocarpum kirkii</i>	[46]
6	campylospermone A	<i>Ormocarpum kirkii</i>	[46]
7	a dimeric chromene [diphysin	<i>Ormocarpum kirkii</i>	[46]
8	amentoflavone 7''- <i>O</i> - β - <i>D</i> -glucopyranoside	<i>Ginkgo Biloba</i>	[47]
9	bilobetin	<i>Ginkgo Biloba</i>	[47]
10	isoginkgetin	<i>Ginkgo Biloba</i>	[47]
11	sciadopitysin	<i>Ginkgo Biloba</i>	[48]
12	agathisflavone	<i>Schinus terebinthifolius</i> ; <i>Anacardium occidentale</i>	[49,50]
13	tetrahydroamentoflavone	<i>Schinus terebinthifolius</i>	[49]
14	uncinatabiflavone C 7-methyl ether	<i>Selaginella uncinata</i>	[50]
15	7, 4', 7'', 4''-tetra- <i>O</i> -methyl amentoflavone	<i>Cephalotaxus harringtonia</i>	[51]
16	7, 4', 7''-tri- <i>O</i> -methyl amentoflavone	<i>Cephalotaxus harringtonia</i>	[51]
17	sequoiaflavone	<i>Cephalotaxus harringtonia</i> ; <i>Ouratea ferruginea</i>	[51,52]
18	amentoflavone monomethoxy derivatives	<i>Cunninghamia lanceolata</i>	[53]
19	dihydrochalcone flavanone	<i>Sophora flavescens</i>	[54]
20	2',3'-dihydroochnaflavone	<i>Ochna mauritiana</i>	[55]
21	dulcisbiflavonoid B	<i>Garcinia dulcis</i>	[56]
22	dulcisbiflavonoid C	<i>Garcinia dulcis</i>	[56]
23	umcephabiflovin A	<i>Cephalotaxus oliveri</i>	[57]
24	umcephabiflovin B	<i>Cephalotaxus oliveri</i>	[57]
25	S-taiwanhomoflavone-B	<i>Cephalotaxus oliveri</i>	[57]
26	5, 6, 6'-trihydroxy-[1,1'-biphenyl]-3,3'-dicarboxylic acid	<i>Mesua ferrea</i>	[58]
27	fukugiside	<i>Garcinia madruno</i>	[59]
28	neochamaejasmin B	<i>Stellera chamaejasme</i>	[60]
29	oliveriflavone A, B, and C	<i>Cephalotaxus oliveri</i>	[61]
30	thusflavanone	<i>Mesua ferrea</i>	[62]
31	mesuaferone B	<i>Mesua ferrea</i>	[62]
35	sinodiflavonoids A	<i>Sinopodophyllum emodi</i>	[63]
36	sinodiflavonoids B	<i>Sinopodophyllum emodi</i>	[63]
37	oxytrodiflavanone A	<i>Oxytropis chiliophylla</i>	[64]
38	oxytrochalcovanones A	<i>Oxytropis chiliophylla</i>	[64]
39	oxytrochalcovanones B	<i>Oxytropis chiliophylla</i>	[64]
40	hinokiflavone	<i>Selaginella sinensis</i>	[65]
41	isocampylospermone A	<i>Ochna Serrulata</i>	[66]
42	campylospermone A	<i>Ochna Serrulata</i>	[66]
43	cupressuflavone	<i>Cupressus sempervirens</i>	[67]
44	(8-hydroxy-3'- β - <i>D</i> -galactosyl-isoflavone)-2'-8''-(4''-hydroxy-flavone)-biflavone	<i>Solanum nigrum</i>	[68]
45	2',3',5-trihydroxy-5'-methoxy-3'- <i>O</i> - α -glucosyl-3-4''- <i>O</i> -biflavone	<i>Solanum nigrum</i>	[68]
46	7''- <i>O</i> -methyl hinokiflavone	<i>Selaginella tamariscina</i>	[69]
47	(2 <i>R</i> ,3 <i>S</i>)-volkensiflavone-7- <i>O</i> - β -acetylglucopyranoside	<i>Allanblackia floribunda</i>	[70]
48	(2 <i>S</i> ,3 <i>S</i>)-morelloflavone-7- <i>O</i> - β -acetylglucopyranoside	<i>Allanblackia floribunda</i>	[70]
49	(<i>S</i>)-2'' <i>R</i> ,3'' <i>R</i> - and (<i>R</i>)-2'' <i>S</i> ,3'' <i>S</i> -dihydro-3''-hydroxyamentoflavone-7- methyl ether	<i>Cardiocrinum giganteum</i>	[71]
50	(<i>S</i>)-2'' <i>R</i> ,3'' <i>R</i> - and (<i>R</i>)-2'' <i>S</i> ,3'' <i>S</i> -dihydro-3''-hydroxyamentoflavone	<i>Cardiocrinum giganteum</i>	[71]
51	4,4',7-tri- <i>O</i> -methylisocampylospermone A	<i>Ochna serrulata</i>	[72]
52	4''- <i>de-O</i> -methylafzelone A	<i>Ochna serrulata</i>	[72]
53	serrulone A	<i>Ochna serrulata</i>	[72]
54	sumaflavone	<i>Juniperus phoenicea</i>	[73]

**Scheme 1.** Total synthesis of biflavonoid. Reagents and conditions: a) benzaldehyde, KOH, MeOH, rt, overnight, 70–87%; b) I₂, DMSO, 100 °C, overnight, 75–86%; and c) Ullmann modified coupling reaction, 8–58% [80].

3CLpro Cleavage Site	P6	P5	P4	P3	P2	P1	P1'	P2'	P3'	P4'	P5'	Relative Kcal/Km
nsp4/5	T	S	A	V	L	Q	S	G	F	R	K	100%
nsp5/6	S	G	V	T	F	Q	G	K	F	K	K	41%
nsp6/7	K	V	A	T	V	Q	S	K	M	S	D	3%
nsp7/8	N	R	A	T	L	Q	A	I	A	S	E	5%
nsp8/9	S	A	V	K	L	Q	N	N	E	L	S	2%
nsp9/10	A	T	V	R	L	Q	A	G	N	A	T	22%
nsp10-12	R	E	P	L	M	Q	S	A	D	A	S	0,2%
nsp12/13	P	H	T	V	L	Q	A	V	G	A	C	8%
nsp13/14	N	V	A	T	L	Q	A	E	N	V	T	9%
nsp14/15	T	F	T	R	L	Q	S	L	E	N	V	28%
nsp16/15	F	Y	P	K	L	Q	A	S	Q	A	W	27%

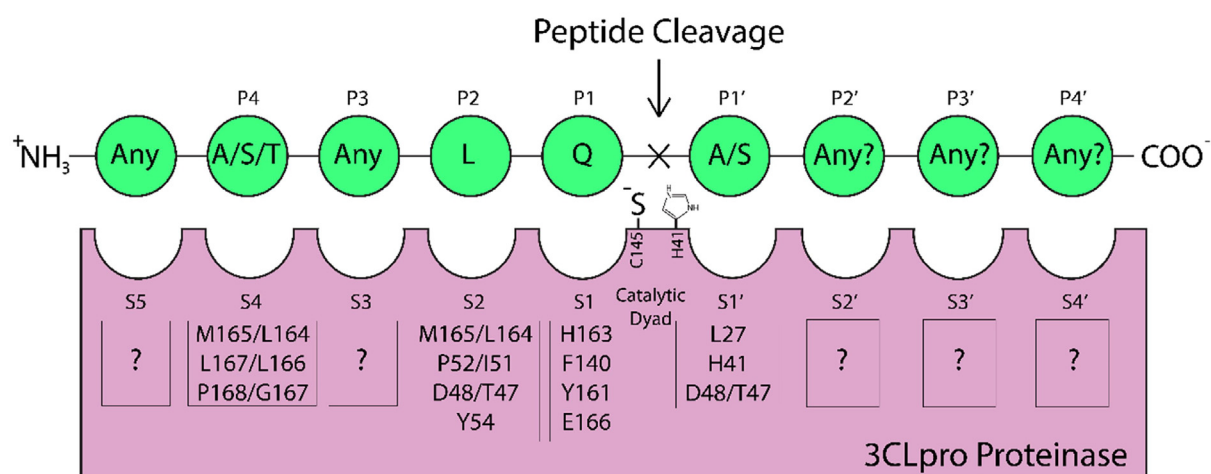


Fig. 4. The 3CLpro cleavage sites of SARS Coronavirus which recognize 11 sequences of peptide substrate with their respective Kcal/Km. These Kcal/Km values reflect the canonical recognition which is supported by the recognition sites of a series of other coronavirus 3C proteases [89,90].

N-terminal residues that are essential for the dimerization [95-98]. Domain I and domain II are decorated in an antiparallel β -barrel structure, whereas domain III is composed of five α -helices arranged in a globular cluster. The helical domains of the two monomers form a dimer through H-bond interactions from the end to end of the N-terminal residues and the key residues from the individual monomers. The catalytic activity is suggested to be contributed by the salt bridge between the N-terminal SER1 of one monomer and GLU166 of the other monomer [97,99]. Table 2 presents the 115 3D-structures of 3CLpro available in the protein data bank.

SARS-Coronavirus-2 3CL pro in complex with a novel inhibitor 5,6,7-trihydroxy-2-phenyl-4H-chromen-4-one solved its 3D-crystal structure in 2.20 Å solution. This flavonoid inhibitor binds the active site of the protease through the hydrogen bond interaction between *ortho*-hydroxyphenyl (ring A) of the ligand with GLY143, and the carbonyl group of ring C with GLU166. The non-bonding interaction was also observed between the phenyl of ring B with HIS41 and CYS44. Fig. 5 illustrates the interaction between 5,6,7-trihydroxy-2-phenyl-4H-chromen-4-one and the active site of SARS-Coronavirus-2 3CLpro (PDB ID 6M2N) [100].

Two peptidomimetic-based inhibitors are complexed with SARS-Coronavirus-2 in different monomer of trimer with 2.15 Å of the crystal resolution (PDB 6WTT) [101]. (1S,2S)-2-((N-[(benzyloxy)carbonyl]-L-leucyl)amino)-1-hydroxy-3-[(3S)-2-oxopyrrolidin-3-yl]pr

opane-1-sulfonic acid binds the active site in monomer A by interacting it with CYS145, GLU166, GLN189, HIS164, and PHE140 at the respective atoms of O (OH), O (C = O), H (NH-amide), H (NH-amide) and H (NH-pyrrolidinone) (Fig. 6). Monomer B demonstrates the same binding mode as monomer A, whereas monomer C is bound by *N* ~ 2 ~ -[(benzyloxy)carbonyl]-*N*-[(1R,2S)-1-hydroxy-3-[(3S)-2-oxopyrrolidin-3-yl]-1-(trimethyl-lambda ~ 4 ~ -sulfanyl)propan-2-yl]-*L*-leucinamide. In monomer C, the ligand interacts with GLU166, HIS164, HIS41, and GLN189 at the respective atoms of O (C = O), N (NH-amide) and N- (NH-pyrrolidinone), O (OH), and N (NH-amide).

A class of imidazole-4-carboxamide compound was also complexed to SARS-Coronavirus-2 3CLpro and the 3D crystal structure was resolved at 1.46 Å (PDB ID 6W79; Fig. 7a) [102]. This inhibitor binds the active site of the protease by interacting it with the residues GLY143 and GLU166 at atom O (C=O-amide) and also the next O (C=O-amide), respectively. The hydrophobic interaction was also performed via the interaction between ASN142- O (C=O-amide), THR26-H-CH-imidazole), CYS145-imidazole ring, and LEU141-ASN142-pyridine.

An inhibitor which was a repurposed drug from antineoplastic, was complexed with SARS-Coronavirus-2 3CLpro in 1.60 Å of 3D-crystal resolution (PDB ID 7BUY; Fig. 7b) [103]. Interestingly, this inhibitor binds covalently (distance 1.8 Å) at its O (C=O) to CYS145 which is one of the catalytic site residues. This inhibitor's name is carmofur,

Table 2

The list of 3CLpro 3D-crystal structure available in protein data bank.

PDB ID	Co-crystallized Ligand	Resolution (Å)	Reference
6M2N	5,6,7-trihydroxy-2-phenyl-4H-chromen-4-one	2.20	[100]
6M2Q	–	1.70	[100]
6WQF	–	2.30	[105]
6XB1	1-ethyl-pyrrolidine-2,5-dione	1.80	[106]
6XB0	dimethyl sulfoxide	1.80	[106]
6XB2	1-ethyl-pyrrolidine-2,5-dione, dimethyl sulfoxide	2.10	[106]
6L00 and 6LNY	(2- <i>S</i>)-4-methyl- <i>N</i> -[(2- <i>S</i>)-1-oxidanylidene-3-[(3- <i>S</i>))-2-oxidanylidene-pyrrolidin-3-yl]propan-2-yl]-2-[[(<i>E</i>))-3-phenylprop-2-enoyl]amino]pentanamide	1.94 and 2.25	[107]
7JFQ	1,2-ethanediol, formic acid	1.55	[108]
6XKF	1,2-ethanediol, chloride ion	1.80	[109]
6XKH	1,2-ethanediol, acetate ion, formic acid	1.28	[110]
6XOA	1,2-ethanediol	2.10	[111]
6LNQ	<i>N</i> -[(2 <i>S</i>)-3-methyl-1-[(2 <i>S</i>)-4-methyl-1-oxidanylidene-1-[(2 <i>S</i>)-1-oxidanylidene-3-[(3 <i>S</i>)-2-oxidanylidene-pyrrolidin-3-yl]propan-2-yl]amino]pentan-2-yl]amino]-1-oxidanylidene-butan-2-yl]-1H-indole-2-carboxamide	2.24	[107]
7JUN	–	2.30	[112]
7JR3	–	1.55	[113]
7JR4	–	1.55	[114]
6XHU	–	1.80	[115]
6XQT	(1 <i>R</i> ,2 <i>S</i> ,5 <i>S</i>)-3-[<i>N</i> -{1-[(<i>tert</i> -butylsulfonyl)methyl]cyclohexyl}carbamoil]-3-methyl- <i>L</i> -valyl]- <i>N</i> -{(1 <i>S</i>)-1-[(1 <i>R</i>)-2-(cyclopropylamino)-1-hydroxy-2-oxoethyl]pentyl]-6,6-dimethyl-3-azabicyclo[3.1.0]hexane-2-carboxamide	2.30	[116]
6XQS	(1 <i>S</i> ,3 <i>aR</i> ,6 <i>aS</i>)-2-[(2 <i>S</i>)-2-[(2 <i>S</i>)-2-cyclohexyl-2-[(pyrazin-2-ylcarbonyl)amino]acetyl]amino]-3,3-dimethylbutanoyl]- <i>N</i> -[(2 <i>R</i> ,3 <i>S</i>)-1-(cyclopropylamino)-2-hydroxy-1-oxohexan-3-yl]octahydrocyclopenta[<i>c</i>]pyrrole-1-carboxamide	1.90	[116]
6XQU	boceprevir (bound form)	2.20	[116]
6W2A	[4,4- <i>bis</i> (fluoranyl)cyclohexyl]methyl- <i>N</i> -[(2- <i>S</i>))-1-[[1- <i>R</i>),2- <i>S</i>))-1- <i>bis</i> (oxidanyl)-oxidanylidene- Γ {5}-sulfanyl]-1-oxidanyl-3-[(3- <i>S</i>))-2-oxidanylidene-pyrrolidin-3-yl]propan-2-yl]amino]-4-methyl-1-oxidanylidene-pentan-2-yl]carbamate, (1 <i>S</i> ,2 <i>S</i>)-2-[(<i>N</i> -{[(4,4-difluorocyclohexyl)methoxy]carbonyl}- <i>L</i> -leucyl)amino]-1-hydroxy-3-[(3 <i>S</i>)-2-oxopyrrolidin-3-yl]propane-1-sulfonic acid	1.65	[117]
6WTK	<i>N</i> ~ 2 ~ -[(benzyloxy)carbonyl]- <i>N</i> -{(2 <i>S</i>)-1-hydroxy-3-[(3 <i>S</i>)-2-oxopyrrolidin-3-yl]propan-2-yl]- <i>L</i> -leucinamide	2.00	[118]
6WTM	–	1.85	[118]
6WTJ	(1 <i>S</i> ,2 <i>S</i>)-2-[(<i>N</i> -[(benzyloxy)carbonyl]- <i>L</i> -leucyl)amino]-1-hydroxy-3-[(3 <i>S</i>)-2-oxopyrrolidin-3-yl]propane-1-sulfonic acid	1.90	[118]
6 W63 and 6 W79	<i>N</i> -(4- <i>tert</i> -butylphenyl)- <i>N</i> -[(1 <i>R</i>)-2-(cyclohexylamino)-2-oxo-1-(pyridin-3-yl)ethyl]-1H-imidazole-4-carboxamide	2.10	[102]
6WCO	<i>N</i> -(4- <i>tert</i> -butylphenyl)- <i>N</i> -[(1 <i>R</i>)-2-(cyclopentylamino)-2-oxo-1-(pyridin-3-yl)ethyl]-1H-imidazole-4-carboxamide	1.48	[102]
6XBH	–	1.60	[119]
6XBG	–	1.45	[120]
6XFN	–	1.70	[121]
7JU7	Masitinib	1.60	[122]
3SZN	ethyl (4 <i>R</i>)-4-[(<i>N</i> -[(benzyloxy)carbonyl]- <i>l</i> -phenylalanyl)amino]-5-[(3 <i>S</i>)-2-oxopyrrolidin-3-yl]pentanoate	1.69	[123]
3SNE	2-(<i>N</i> -morpholino)-ethanesulfonic acid	2.60	[124]
3SNA, 3SNB, and 3SNC	–	3.05, 2.40 and 2.58	[124]
6XBI	–	1.70	[125]
6XHO	ethyl (2 <i>E</i> ,4 <i>S</i>)-4-[[<i>N</i> -(4-methoxy-1H-indole-2-carbonyl)- <i>L</i> -leucyl]amino]-5-[(3 <i>S</i>)-2-oxopyrrolidin-3-yl]pent-2-enoate	1.45	[126]
6XHN	(3 <i>S</i>)-3-[[<i>N</i> -(4-methoxy-1H-indole-2-carbonyl)- <i>L</i> -leucyl]amino]-2-oxo-4-[(3 <i>S</i>)-2-oxopyrrolidin-3-yl]butyl 2-cyanobenzoate	1.38	[126]
6XHL and 6XHM	<i>N</i> -[(2 <i>S</i>)-1-[(2 <i>S</i>)-4-hydroxy-3-oxo-1-[(3 <i>S</i>)-2-oxopyrrolidin-3-yl]butan-2-yl]amino]-4-methyl-1-oxopentan-2-yl]-4-methoxy-1H-indole-2-carboxamide	1.47 and 1.41	[126]
6XA4	–	1.65	[127]
6Y2E	–	1.75	[128]
6Y2G, 6Y2F	~(<i>tert</i>)-butyl- <i>N</i> -[1-[(2- <i>S</i>))-3-cyclopropyl-1-oxidanylidene-1-[[2- <i>S</i>),3- <i>R</i>))-3-oxidanyl-4-oxidanylidene-1-[(3- <i>S</i>))-2-oxidanylidene-pyrrolidin-3-yl]-4-[(phenylmethyl)amino]butan-2-yl]amino]propan-2-yl]-2-oxidanylidene-pyridin-3-yl]carbamate	2.20, and 1.95	[128]
7JKV	<i>N</i> -[(2 <i>S</i>)-1-[(1 <i>S</i> ,2 <i>S</i>)-1-(1,3-benzothiazol-2-yl)-1-hydroxy-3-[(3 <i>S</i>)-2-oxopyrrolidin-3-yl]propan-2-yl]amino]-4-methyl-1-oxopentan-2-yl]-4-methoxy-1H-indole-2-carboxamide	1.25	[129]
5RHF	1-acetyl- <i>N</i> -methyl- <i>N</i> -phenylpiperidine-4-carboxamide	1.76	[104]
5RHE	1-acetyl- <i>N</i> -(6-methoxypyridin-3-yl)piperidine-4-carboxamide	1.56	[104]
5RGG	4-methyl- <i>N</i> -phenylpiperazine-1-carboxamide	2.26	[104]
5RG1	<i>N</i> -alpha-acetyl- <i>N</i> -(3-bromoprop-2-yn-1-yl)- <i>L</i> -tyrosinamide	1.57	[104]
5RGH	5-fluoro-1-[(5-methyl-1,3,4-thiadiazol-2-yl)methyl]-1,2,3,6-tetrahydropyridine	1.70	[104]
5RGR	<i>N</i> ,1-dimethyl- <i>N</i> -(propan-2-yl)-1H-pyrazolo[3,4- <i>d</i>]pyrimidin-4-amine	1.41	[104]
5RG3	<i>N</i> ~ 2 ~ -acetyl- <i>N</i> ~ 1 ~ -prop-2-en-1-yl- <i>L</i> -aspartamide	1.58	[104]
5RG2	<i>N</i> ~ 2 ~ -acetyl- <i>N</i> -prop-2-en-1-yl- <i>D</i> -allothreoninamide	1.63	[104]
5RGS	[(2- <i>R</i>))-4-(phenylmethyl)morpholin-2-yl]methanol	1.72	[104]
5RGK	2-fluoro- <i>N</i> -[2-(pyridin-4-yl)ethyl]benzamide	1.43	[104]
5RGJ	(5 <i>S</i>)-7-(pyrazin-2-yl)-2-oxa-7-azaspiro[4.4]nonane	1.34	[104]
5RGM	<i>N</i> -acetyl-4,5,6,7-tetrahydro-1-benzothiophene-2-carbohydrazide	2.04	[104]
5RGM	<i>N</i> -acetyl-4,5,6,7-tetrahydro-1-benzothiophene-2-carbohydrazide	2.04	[104]
5RGO	1,1'-(piperazine-1,4-diyl)di(ethan-1-one)	1.72	[104]
5RGN	1-{4-[(4-methylphenyl)sulfonyl]piperazin-1-yl}ethan-1-one	1.86	[104]
5RGQ	1-(4-fluoro-2-methylphenyl)methanesulfonamide	2.15	[104]
5RGP	1-{4-[(2,4-dimethylphenyl)sulfonyl]piperazin-1-yl}ethan-1-one	2.07	[104]
5R8T	–	1.27	[104]
5RGZ	2-(3-cyanophenyl)- <i>N</i> -(pyridin-3-yl)acetamide	1.52	[104]
5RHA	1-{4-[(thiophen-2-yl)methyl]piperazin-1-yl}ethan-1-one	1.51	[104]

(continued on next page)

Table 2 (continued)

PDB ID	Co-crystallized Ligand	Resolution (Å)	Reference
5RH3	(2R)-2-(3-chlorophenyl)-N-(4-methylpyridin-3-yl)propanamide	1.69	[104]
5RH4	(2R)-2-(6-chloro-9H-carbazol-2-yl)propanoic acid	1.34	[104]
5RGU	N-(3-((2R)-4-oxoazetidin-2-yl)oxy)phenyl)-2-(pyrimidin-5-yl)acetamide	2.11	[104]
5RH6	N-[(1R)-2-[(2-ethyl-6-methylphenyl)amino]-2-oxo-1-(pyridin-3-yl)ethyl]-N-[6-(propan-2-yl)pyridin-3-yl]propanamide	1.60	[104]
5RGT	N-[(1R)-2-(tert-butylamino)-2-oxo-1-(pyridin-3-yl)ethyl]-N-(5-tert-butyl-1,2-oxazol-3-yl)propanamide	2.22	[104]
5RH5	N-(5-tert-butyl-1,2-oxazol-3-yl)-N-[(1R)-2-[(4-methoxy-2-methylphenyl)amino]-2-oxo-1-(pyridin-3-yl)ethyl]propanamide	1.72	[104]
5RGW	2-(5-cyanopyridin-3-yl)-N-(pyridin-3-yl)acetamide	1.43	[104]
5RH8	2-(cyanomethoxy)-N-[(1,2-thiazol-4-yl)methyl]benzamide	1.81	[104]
5RGV	2-(isoquinolin-4-yl)-N-phenylacetamide	1.82	[104]
5RH7	N-(5-tert-butyl-1H-pyrazol-3-yl)-N-[(1R)-2-[(2-ethyl-6-methylphenyl)amino]-2-oxo-1-(pyridin-3-yl)ethyl]propanamide	1.71	[104]
5RGY	N-(4-methoxypyridin-2-yl)-2-(naphthalen-2-yl)acetamide	1.976	[104]
5RGX	2-(3-cyanophenyl)-N-(4-methylpyridin-3-yl)acetamide	1.69	[104]
5RH9	N-[4-[(1S)-1-methoxyethyl]phenyl]-N-[(1R)-2-[(4-methoxy-2-methylphenyl)amino]-2-oxo-1-(pyridin-3-yl)ethyl]propanamide	1.91	[104]
5RH0	N-(5-methylthiophen-2-yl)-N'-pyridin-3-ylurea	1.92	[104]
5RH2	2-(3-chlorophenyl)-N-(4-methylpyridin-3-yl)acetamide	1.83	[104]
5RH1	2-(5-chlorothiophen-2-yl)-N-(pyridin-3-yl)acetamide	1.96	[104]
5REA	(azepan-1-yl)(2H-1,3-benzodioxol-5-yl)methanone	1.63	[104]
5REB	1-[(thiophen-3-yl)methyl]piperidin-4-ol	1.68	[104]
5REC	2-[[[1H-benzimidazol-2-yl]amino]methyl]phenol	1.73	[104]
5REE	(2R,3R)-1-benzyl-2-methylpiperidin-3-ol	1.77	[104]
7JVZ	–	2.50	[130]
6W9Q	–	2.05	[131]
7BRR	(1S,2S)-2-((N-[(benzyloxy)carbonyl]-L-leucyl)amino)-1-hydroxy-3-[(3S)-2-oxopyrrolidin-3-yl]propane-1-sulfonic acid	1.40	[132]
7BRO	–	2.00	[133]
7BRP	(1R,2S,5S)-n-[(1S)-3-amino-1-(cyclobutylmethyl)-2,3-dioxopropyl]-3-[(2S)-2-((tert-butylamino)carbonyl)amino]-3,3-dimethylbutanoyl]-6,6-dimethyl-3-azabicyclo[3.1.0]hexane-2-carboxamide	1.80	[134]
7C2Q	–	1.93	[135]
7C8T	N-[(benzyloxy)carbonyl]-O-(tert-butyl)-l-threonyl-3-cyclohexyl-N-[(1S)-2-hydroxy-1-[(3S)-2-oxopyrrolidin-3-yl]methyl]ethyl]-l-alaninamide	2.05	[136]
7C8R	Ethyl (4R)-4-[[[(2S)-4-methyl-2-[[[(2S,3R)-3-[(2-methylpropan-2-yl)oxy]-2-(phenylmethoxycarbonylamino)butanoyl]amino]pentanoyl]amino]-5-[(3S)-2-oxidanylidene-pyrrolidin-3-yl]pentanoate	2.30	[136]
6XCH	–	2.20	[137]
6L70	(1S,2S)-2-((N-[(benzyloxy)carbonyl]-L-leucyl)amino)-1-hydroxy-3-[(3S)-2-oxopyrrolidin-3-yl]propane-1-sulfonic acid	1.56	[138]
6FV1	(2- <i>S</i>)-4-methyl- <i>N</i> -[(2- <i>S</i>),3- <i>R</i>]-3-oxidanyl-4-oxidanylidene-1-[(3- <i>S</i>)-2-oxidanylidene-pyrrolidin-3-yl]-4-[(phenylmethyl)amino]butan-2-yl)-2-[[(- <i>E</i>)-3-phenylprop-2-enoyl]amino]pentanamide	2.30	[139]
6FV2	(<i>S</i>)- <i>N</i> -benzyl-3-[(<i>S</i>)-2-cinnamido-3-phenylpropanamido]-2-oxo-4-[(<i>S</i>)-2-oxopyrrolidin-3-yl]butanamide	2.95	[139]
7D31	(3- <i>S</i>),3-(<i>a</i>)- <i>S</i> ,6-(<i>a</i>)- <i>R</i>)-2-[3-[3,5-bis(fluoranyl)phenyl]propanoyl]- <i>N</i> -[(2- <i>S</i>)-1-oxidanylidene-3-[(3- <i>S</i>)-2-oxidanylidene-pyrrolidin-3-yl]propan-2-yl]-3,3-(<i>a</i>),4,5,6,6-(<i>a</i>)-hexahydro-1- <i>H</i> -cyclopenta[<i>c</i>]pyrrole-3-carboxamide 2	2.00	[140]
7D1O	(1R,2S,5S)-3-[<i>N</i> -((1-[(<i>tert</i> -butylsulfonyl)methyl]cyclohexyl)carbonyl)-3-methyl- <i>L</i> -valyl]- <i>N</i> -[(1S)-1-[(1R)-2-(cyclopropylamino)-1-hydroxy-2-oxoethyl]pentyl]-6,6-dimethyl-3-azabicyclo[3.1.0]hexane-2-carboxamide	1.78	[141]
7C7P	(1S,3aR,6aS)-2-[(2S)-2-((2S)-2-cyclohexyl-2-[(pyrazin-2-ylcarbonyl)amino]acetyl)amino]-3,3-dimethylbutanoyl]- <i>N</i> -[(2R,3S)-1-(cyclopropylamino)-2-hydroxy-1-oxohexan-3-yl]octahydrocyclopenta[<i>c</i>]pyrrole-1-carboxamide	1.74	[142]
7COM	boceprevir (bound form)	2.25	[143]
6ZRU	boceprevir (bound form)	2.10	[144]
6ZRT	(1S,3aR,6aS)-2-[(2S)-2-((2S)-2-cyclohexyl-2-[(pyrazin-2-ylcarbonyl)amino]acetyl)amino]-3,3-dimethylbutanoyl]- <i>N</i> -[(2R,3S)-1-(cyclopropylamino)-2-hydroxy-1-oxohexan-3-yl]octahydrocyclopenta[<i>c</i>]pyrrole-1-carboxamide	2.10	[145]
6MOK	–	5.10	[146]
6LZE	~ <i>N</i> -[(2- <i>S</i>)-3-cyclohexyl-1-oxidanylidene-1-[(2- <i>S</i>)-1-oxidanylidene-3-[(3- <i>S</i>)-2-oxidanylidene-pyrrolidin-3-yl]propan-2-yl]amino]propan-2-yl]-1- <i>H</i> -indole-2-carboxamide	1.50	[147]
7C6S	boceprevir (bound form)	1.60	[148]
7CX9	3-iodanyl-1- <i>H</i> -indazole-7-carbaldehyde	1.73	[149]

bearing hexylcarbamide acid structure, in which the fatty acid tail occupies the hydrophobic S2 sub-site. A study reported that carmofur inhibits viral replication in cells ($EC_{50} = 24.30 \mu\text{M}$) and is a promising lead compound to develop a new antiviral treatment for SARS-Coronavirus-2.

A more diverse inhibitor's structure was observed from the 3D-crystal structure with PDB ID 5RGG which was resolved at 2.26 Å of resolution [104]; Fig. 7c). The inhibitor is a carboxamide derivative namely 4-methyl-*N*-phenylpiperazine-1-carboxamide, binds at HIS80 via H-bond interaction. Instead of H-bond, HIS80 was also interacting with the inhibitor via hydrophobic interaction which was co-bound with LYS90. This experiment could give an insight into understanding that even a small molecule is able to bind the protease. However, the potency of such inhibitor could be low due to the larger cavities which need an extending occupation.

6. Biflavonoid as the protease –Inhibitor

There are a few studies of biflavonoid-class compounds reporting their activities as protease inhibitors. Amentoflavone from *Torreya nucifera* was the early biflavonoid studied in its inhibitory activity against SARS-Coronavirus 3CLpro by showing $IC_{50} 8.3 \mu\text{M}$. The results were compared to three types of flavonoid (apigenin, luteolin, and quercetin) which showed less inhibition and therefore, the structure–activity relationships were generated to confirm that the more potent activity of biflavonoid appeared to be associated with the presence of benzene ring moiety at C-3' position of flavones, as biflavone affected 3CLpro inhibitory activity [36].

Based on Ryu et al. findings, a QSAR study of biflavonoid and its analogs was carried out to generate a QSAR model defining the increasing value of the dipole moment along the X-axis that may be

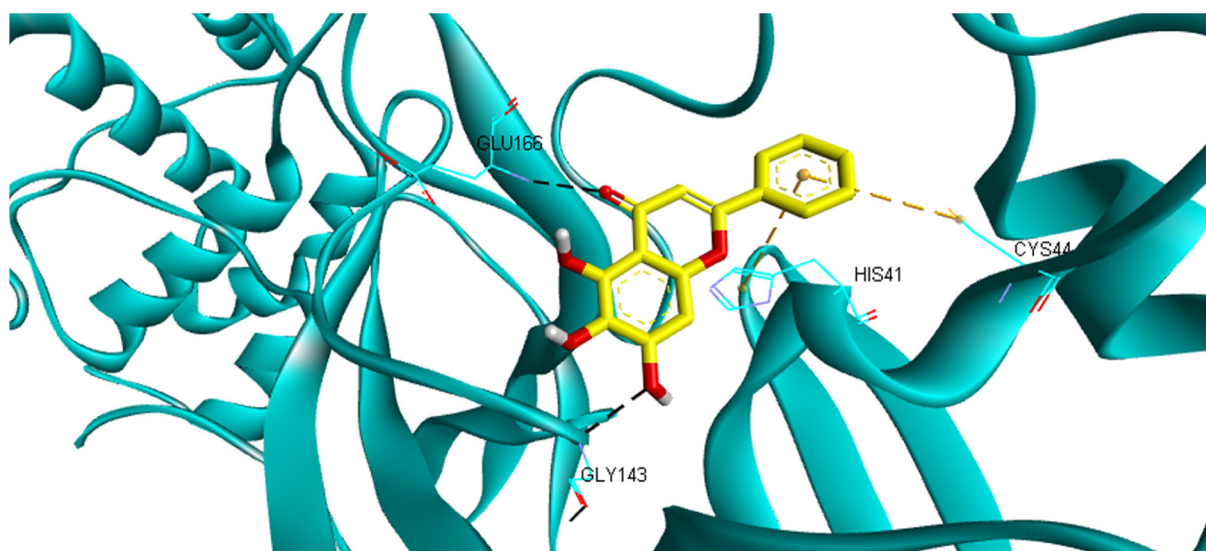


Fig. 5. The interaction between 5,6,7-trihydroxy-2-phenyl-4H-chromen-4-one and the active site of SARS-Coronavirus-2 (PDB ID 6M2N). The 3CLpro is presented in a blue ribbon model, whereas the inhibitor is in a stick model (yellow = C, white = H, and red = O). The H-bond and hydrophobic interactions are presented in black and yellow dot lines, respectively. (For interpretation of the references to colour in this figure legend, the reader is referred to the web version of this article.)

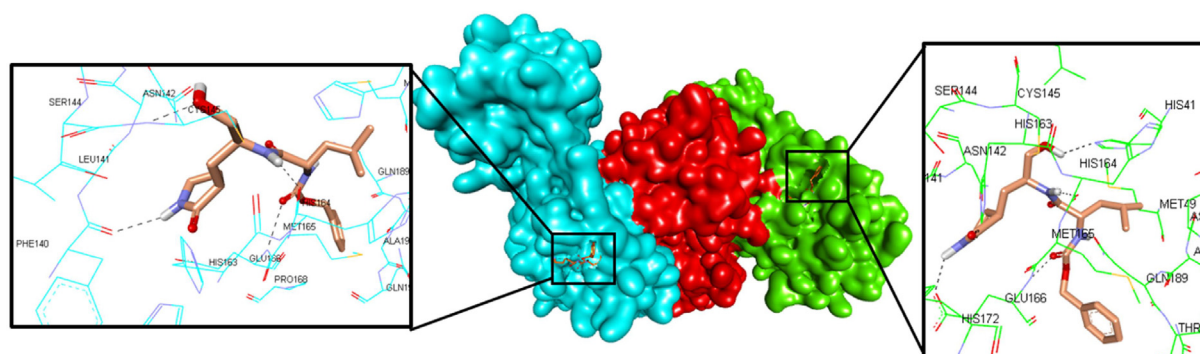


Fig. 6. The trimer structure of 3CLpro as indicated by blue (monomer A), red (monomer B), and green (monomer C) surface models. Inset is the ligand complex to the active site of the enzyme (presented by blue stick and green stick, for monomer A and monomer C, respectively), presented in a stick model (orange = C, white = H, blue = N and red = O). The H-bond is presented in black dot lines, respectively. (For interpretation of the references to colour in this figure legend, the reader is referred to the web version of this article.)

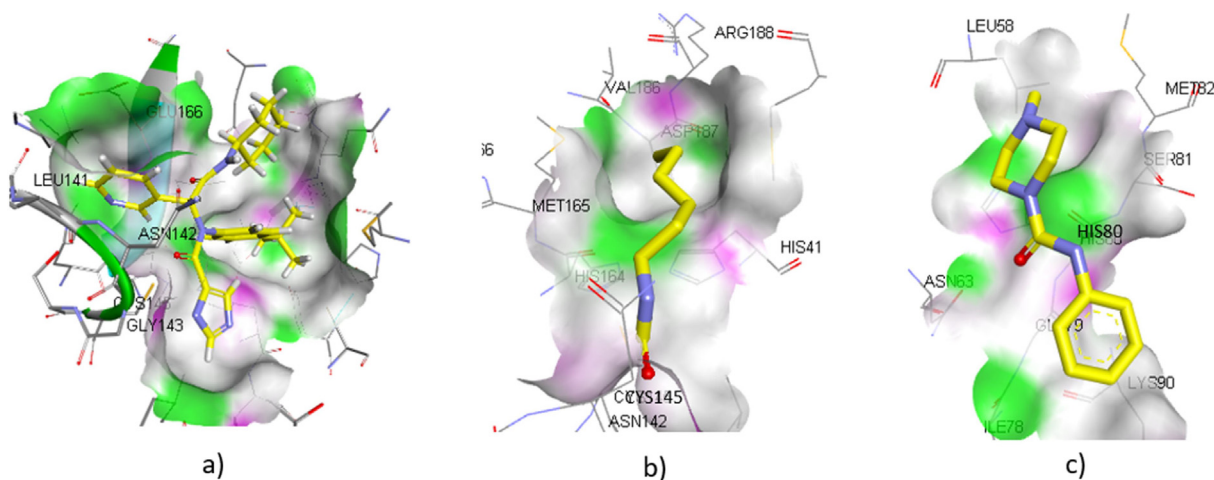


Fig. 7. The presentation of a) imidazole-4-carboxamide, b) carmofur, and c) 4-methyl-N-phenylpiperazine-1-carboxamide bound into the active site of SARS-Coronavirus-2 3CLpro. The protein is visualized in the surface model with the green area = hydrogen bond acceptor residues, white area = neutral residues, and magenta area = hydrogen bond donor residues. The ligands are presented in a stick form with yellow = C, white = H, blue = N, and red = O. (For interpretation of the references to colour in this figure legend, the reader is referred to the web version of this article.)

conductive to the activity. Therefore, the steric character of this part may be favorable for its activity. Compounds having higher dipole moment due to the much bulky aryl groups, therefore, have a higher activity than the compound having less bulky aryl group [23].

The antiproteolytic activity of biflavonoid was determined early on morelloflavone-4''-O- β -D-glycosyl, (\pm)-fukugiside, and morelloflavone. These biflavonoids were isolated from the fruit epocarp of *Garcinia brasiliensis* which were further semi synthesized into three morelloflavone derivatives i.e. morelloflavone-7,4',7'',3''',4''''-penta-O-acetyl, morelloflavone-7,4',7'',3''',4''''-penta-O-methyl, and morelloflavone-7,4',7'',3''',4''''-penta-[-butanoyl. High inhibitory activity was demonstrated by this biflavonoid against r-CPB2.8 and r-CPB3 isoforms which are papain-like protease of *Leishmania mexicana* with IC₅₀ 0.42–1.01 μ M for the four most active compounds. Interestingly, there was no cytotoxic activity towards the normal cell lines as observed from the *in vitro* study [150].

Further study was pursued by the same research group in evaluating those biflavonoid activities against the cysteine protease (papain and cruzain) and serine protease of *Trypanozoma cruzii*. All biflavonoid compounds demonstrated excellent inhibitions toward all protease enzymes (IC₅₀ 0.02–106 μ M). However, morelloflavone-7,4',7'',3''',4''''-penta-O-acetyl showed the best activity which might be due to the carbonyl group in the structure. This functional group could favor a higher nucleophilic attack by serine and cysteine proteases. This is in accordance with morelloflavone-7,4',7'',3''',4''''-penta-O-methyl (IC₅₀ = 15.4 \pm 0.7 μ M for papain), in which the compound having no carbonyl group in structure was less active in the inhibition process. This was confirmed by the structure–activity relationships (SARs) study which had been performed using flexible docking simulations [151].

A study by Assis et al. reported that fukugetin, a biflavone originated from *Garcinia brasiliensis*, demonstrated partial competitive and hyperbolic-mix type inhibitions against the major cysteine protease of *Trypanosoma cruzii* (cruzain and papain), respectively. The potency of such biflavone was expressed in a slowly reversible type of inhibition with Ki 1.1 and 13.4 μ M for cruzain and papain, respectively, describing that the biflavone has 12 times faster inhibition toward cruzain than papain in inhibiting the enzymes. The molecular docking study predicted that this activity is due to the chemical interaction between biflavone at ring C with S3 pocket, whereas the ring C' binds at S2 pocket through hydrogen bonds as well as the hydrophobic interactions [152].

Virtual screening was performed to identify the hits of the tryptase inhibitor followed by *in vitro* experiments to identify the lead compounds. Tryptase is a class of serine protease enzyme released as the allergic response such as skin inflammation and asthma from the mast cells. Out of the 98,000 compounds screened, 2.28% of the library (2503 compounds) were selected as the hits. Interestingly, biflavonoids were one of the most frequently represented in the 200 compounds with the strongest tryptase binding energy. Using fluorescence resonance energy transfer (FRET)-based assay, these 200 compounds were further *in vitro* screened to afford the lead compound, and then the biflavonoid podocarpus flavone A blocks the tryptase activity by 61.6%. The docking study suggested that the biflavonoid is favorably binding at the S4 of tryptase [153].

Biflavonoid was also reported to down-regulate the expression of matrix metalloproteinase-1 (MMP-1) from human skin fibroblasts. MMP is a zymogen (zinc-dependent peptidase) that degrades the extracellular matrix to perform angiogenesis, inflammation, cell migration, and tissue remodeling. The high expression of this enzyme is often associated with cancer and wound diabetic foot ulcers. 2',8''-biapigenin, sumaflavone, taiwaniaflavone, amentoflavone, and robustaflavone which were isolated from *Selaginella tamariscina* showed significant MMP-1 inhibitory activity in primary human dermal fibroblasts after UV irradiation. The IC₅₀ values of sumaflavone, amen-

toflavone, and retinoic acid (used as the positive control) were 0.78, 1.8, and 10 μ M, respectively [154].

7. Perspectives

Two main protein targets in the coronaviral genome are classified into structural and non-structural proteins. Structural protein which is composed of the membrane, envelope and nucleocapsid is formed in the inner viral cell, whereas the spike protein is located in the outer cell [155,156]. It might be difficult to control the activity of such structural protein because they control the virus's life during the viral cell assembly which could be too fast to control. Most likely, the host will be suddenly infected by the virus while there is no time to block the activity of the S protein during viral-host attachment as well as its endocytosis. Therefore, in designing the protein inhibitor for coronavirus, the non-structural protein could be more favorable than the structural protein due to its role in controlling the polypeptide proteolytic, reverse transcription, RNA replication as well as protein translation, which might take more time than the viral assembly.

Among the 16 non-structural proteins, NSP5 is the most attractive target while the others are still elusive [157]. The NSP5 main protease (3CLpro) is the most common targeted protein in coronavirus because it is formed in the host and acts during cleavage and post-translational polyprotein synthesis. Thus, it is relatively easier to control their activities. Two classes of the compound are reported to have these protein activities, including peptide and non-peptide compound. Naturally, the protease has a peptide substrate due to its function to hydrolyze the peptide bond upon proteolysis. Therefore, for a competitive inhibitor, a compound having a peptide-like structure should be suitable to block the enzyme-substrate binding. There are notable peptide (like) compounds demonstrating low micromolar activity towards the protease such as lopinavir and ritonavir [158].

Although peptide is the suitable structure designed for the protease inhibitor, however, the physic-chemical properties of this class of compound often make it fails under clinical trials. The peptide has a number of flexible bonds which makes it energetically unstable either during preparation or the pharmacokinetic stage. The structure is mimicking protein, therefore, it is sensitive towards denaturation and hydrolysis during preparation. At the pharmacokinetic stage especially during absorption, the peptide is less absorbed due to its isoelectric character which makes it very polar in aqueous biological fluids. Thus, it is hard to penetrate the intestinal membrane lipid bilayer [159]. This causes the peptide to become unsuitable for oral preparation which requires the absorption process.

Another alternative is formulated in the parenteral preparation. However, this is costly and not applicable to be administered by the patient. Therefore, the peptide is practically used as the model only and then should be further modified to the more rigid character to improve the stability. One effort has been conducted to formulate the drug delivery system to improve bioavailability such as using liposome technology. However, the use of organic solvents in the liposome dosage form could make it toxic [160,161].

Non-peptide or often called as small molecule inhibitors currently takes more attention used as the molecule target for protease inhibitors. The presence of aromatic rings could make the compound energetically more stable than the peptide due to its rigid character [162]. The rigid character causes less entropy of the compound and thus stabilizes the compound-enzyme affinity upon binding [163]. The non-peptide inhibitor can still be divided into natural and synthetic compounds. Natural compound is a unique structure due to the presence of chiral carbon which could make the ligand–protein binding more specific. A class of biflavonoid showed the *in vitro* competitive inhibition in low micromolar activities towards the protease which agreed with the docking explanation. Amentoflavone is the

early biflavonoid found active against 3CLpro of SARS-Coronavirus underlining the potency of such compounds to be this protease inhibitor. It was postulated that the presence of benzene ring moiety is at position C-3' of flavones, as biflavone affected 3CLpro inhibitory activity. The synthetic (semi-synthetic) biflavonoids are the further strategy to get the product being more feasible to be developed as a protease inhibitor. Compounds bearing more carbonyl groups seem promising to be the protease inhibitor as it is designed to favor a higher nucleophilic attack by serine and cysteine proteases using molecular docking. The complex of 5,6,7-trihydroxy-2-phenyl-4H-chromen-4-one with SARS-Coronavirus-2 3CLpro (PDB ID 6M2N) is one of the proofs that flavonoid is such an important feature for 3CLpro pharmacophore and so does the biflavonoid which could cover more space to interact with the 3CLpro.

3CLpro is still the most recommended protein target in the discovery of anti-SARS coronaviral agents. The availability of crystal structure and its high conserved binding site make the structure-based drug design becomes applicable [164,165]. The structure-based drug design can also be combined with ligand-based drug design since the structure information of the compounds either in peptide or non-peptide has been reported as the protease inhibitors. The non-peptide compound such as biflavonoid provides more promising candidate to enter either pre- or clinical stage due to its more stable physicochemical properties during preparation as well as pharmacokinetics.

8. Conclusion

In conclusion, our review strongly recommends that biflavonoid, either from the natural product or its synthetic is very potential to be used as of SARS-Coronavirus-2 3CLpro inhibitor. Its dimer and big structure are more suitable for a 3CLpro binding site composing two beta barrels than the corresponding flavones. To the best of our knowledge, this is the first review to describe the potential inhibitory effects of biflavonoid against SARS-Coronavirus-2 3CLpro. Thus, we believe that this compound may be a good candidate for development as a natural therapeutic drug against SARS-Coronavirus-2 infection.

CRedit authorship contribution statement

Yustina Hartini: Writing. **Bakti Saputra:** Writing. **Bryan Wahono:** Writing. **Zerlinda Auw:** Writing. **Friska Indayani:** Writing. **Lintang Adelya:** Writing. **Gabriel Namba:** Writing. **Maywan Hari-ono:** Conceptualization, Editing.

Declaration of Competing Interest

The authors declare that they have no known competing financial interests or personal relationships that could have appeared to influence the work reported in this paper.

Acknowledgement

MH show profound gratitude to Lembaga Penelitian dan Pengabdian Masyarakat (LPPM) Sanata Dharma University under special scheme "Covid-19", No. 035/Penel./LPPM-USD/III/2019 for their financial support.

References

- [1] R. Djalante, J. Lassa, D. Setiawati, C. Mahfud, A. Sudjatma, M. Indrawan, L.A. Gunawan, Review and analysis of current responses to COVID-19 in Indonesia: Period of January to March 2020, *Prog Disaster Sci* 6 (2020), <https://doi.org/10.1016/j.pdisas.2020.100091> 100091.
- [2] World Health Organization. WHO coronavirus disease (covid-19) dashboard, <https://covid19.who.int/>; 2020 (accessed 24 October 2020).
- [3] Kompas.com, Data covid-19 di Indonesia, <https://www.kompas.com/covid-19/>; 2020 (accessed 24 October 2020).
- [4] United Nations Industrial Development Organization, Coronavirus, the economic impact-10 July 2020, <https://www.unido.org/stories/coronavirus-economic-impact-10-july-2020>; 2020 (accessed 24 October 2020).
- [5] K. Dhama, S.K. Patel, K. Sharun, M. Pathak, R. Tiwari, M.L. Yattoo, K.P. Singh, SARS-CoV-2 jumping the species barrier: zoonotic lessons from SARS, MERS and recent advances to combat this pandemic virus, *Travel Med. Infect. Dis.* 37 (2020), <https://doi.org/10.1016/j.tmaid.2020.101830> 101830.
- [6] E.S. Hosseini, N.R. Kashani, H. Nikzad, J. Azadbakht, H.H. Bafrani, H.H. Kashani, The novel coronavirus Disease-2019 (COVID-19): Mechanism of action, detection and recent therapeutic strategies, *Virology* 551 (2020) 1–9, <https://doi.org/10.1016/j.virol.2020.08.011>.
- [7] N. Prasad, N. Gopalakrishnan, M. Sahay, A. Gupta, S.K. Agarwal, Epidemiology, genomic structure, the molecular mechanism of injury, diagnosis and clinical manifestations of coronavirus infection: An overview, *Indian J Nephrol* 30 (2020) 143, <https://doi.org/10.4103/ijn.191.20>.
- [8] E.J. Snijder, E. Decroly, J. Ziebuhr, The nonstructural proteins directing coronavirus RNA synthesis and processing, *Adv. Virus Res.* 96 (2016) 59–126, <https://doi.org/10.1016/bs.aivir.2016.08.008>.
- [9] M.A. Shereen, S. Khan, A. Kazmi, N. Bashir, R. Siddique, COVID-19 infection: Origin, transmission, and characteristics of human coronaviruses, *J. Adv. Res.* 24 (2020) 91–98, <https://doi.org/10.1016/j.jare.2020.03.005>.
- [10] V. Grum-Tokars, K. Ratia, A. Begaye, S.C. Baker, A.D. Mesecar, Evaluating the 3C-like protease activity of SARS-Coronavirus: recommendations for standardized assays for drug discovery, *Virus Res.* 133 (2008) 63–73, <https://doi.org/10.1016/j.virusres.2007.02.015>.
- [11] S. Joshi, M. Joshi, M.S. Degani, Tackling SARS-CoV-2: proposed targets and repurposed drugs, *Future Med. Chem.* 12 (2020) 1579–1601, <https://doi.org/10.4155/fmc-2020-0147>.
- [12] Y.M. Báez-Santos, S.E.S. John, A.D. Mesecar, The SARS-coronavirus papain-like protease: structure, function and inhibition by designed antiviral compounds, *Antivir Res* 115 (2015) 21–38, <https://doi.org/10.1016/j.antiviral.2014.12.015>.
- [13] R.M.L. Colunga Biancatelli, M. Berrill, J.D. Catravas, P.E. Marik, Quercetin and vitamin C: an experimental, synergistic therapy for the prevention and treatment of SARS-CoV-2 related disease (COVID-19), *Front. Immunol.* 11 (2020) 1451, <https://doi.org/10.3389/fimmu.2020.01451>.
- [14] K. Chojnacka, A. Witek-Krowiak, D. Skrzypczak, K. Mikula, P. Młynarz, Phytochemicals containing biologically active polyphenols as an effective agent against Covid-19-inducing coronavirus, *J. Funct. Foods* 73 (2020), <https://doi.org/10.1016/j.jff.2020.104146> 104146.
- [15] R. Jain, S. Shukla, N. Nema, A. Panday, H.S. Gour, A systemic review: structural mechanism of SARS-CoV-2A and promising preventive cure by phytochemicals, *Int. J. Immunol. Immunother.* 7 (2020) 051, <https://doi.org/10.23937/2378-3672/1410051>.
- [16] S.Y. Li, C. Chen, H.Q. Zhang, H.Y. Guo, H. Wang, L. Wang, R.S. Li, Identification of natural compounds with antiviral activities against SARS-associated coronavirus, *Antivir. Res.* 67 (2005) 18–23, <https://doi.org/10.1016/j.antiviral.2005.02.007>.
- [17] C.W. Lin, F.J. Tsai, C.H. Tsai, C.C. Lai, L. Wan, T.Y. Ho, P.D.L. Chao, Anti-SARS coronavirus 3C-like protease effects of *Isatis indigotica* root and plant-derived phenolic compounds, *Antivir. Res.* 68 (2005) 36–42, <https://doi.org/10.1016/j.antiviral.2005.07.002>.
- [18] S. Schwarz, D. Sauter, K. Wang, R. Zhang, B. Sun, A. Karioti, W. Schwarz, Kaempferol derivatives as antiviral drugs against the 3a channel protein of coronavirus, *Planta Med.* 80 (2014) 177, [10.1055%2Fs0033-1360277](https://doi.org/10.1055%2Fs0033-1360277).
- [19] J. Cinatl, B. Morgenstern, G. Bauer, P. Chandra, H. Rabenau, H.W. Doerr, Glycyrrhizin, an active component of liquorice roots, and replication of SARS-associated coronavirus, *Lancet* 361 (2003) 2045–2046, [https://doi.org/10.1016/S0140-6736\(03\)13615-X](https://doi.org/10.1016/S0140-6736(03)13615-X).
- [20] D.E. Kim, J.S. Min, M.S. Jang, J.Y. Lee, Y.S. Shin, C.M. Park, S. Kwon, Natural bis-benzylisoquinoline alkaloids-tetrandrine, fangchinoline, and cepharanthine, inhibit human coronavirus OC43 infection of MRC-5 human lung cells, *Biomolecules* 9 (2019) 696, <https://doi.org/10.3390/biom9110696>.
- [21] C. Müller, F.W. Schulte, K. Lange-Grünweller, W. Obermann, R. Madhugiri, S. Pleschka, A. Grünweller, Broad-spectrum antiviral activity of the eIF4A inhibitor silvestrol against corona- and picornaviruses, *Antivir Res* 150 (2018) 123–129, <https://doi.org/10.1016/j.antiviral.2017.12.010>.
- [22] A.T. Jamiu, C.E. Aruwa, I.A. Abdulakeem, A.A. Ajao, S. Sabiu, Phytotherapeutic Evidence Against Coronaviruses and Prospects for COVID-19, *Pharmacogn J* 12 (2020) 1252–1257, <https://doi.org/10.5530/pj.2020.12.174>.
- [23] Adhikari N, Baidya SK, Saha A, Jha T. Structural Insight Into the Viral 3C-Like Protease Inhibitors: Comparative SAR/QSAR Approaches. In *Viral Proteases and Their Inhibitors 2017* (pp. 317–409). Academic Press. <https://doi.org/10.1016/B978-0-12-809712-0.00011-3>
- [24] E. Di Cera, Serine proteases. *IUBMB life* 61 (2009) 510–515, <https://doi.org/10.1002/iub.186>.
- [25] Geiger H, Quinn C. Biflavonoids. In *The flavonoids 1975* (pp. 692–742). Springer, Boston, MA. https://doi.org/10.1007/978-1-4899-2909-9_13
- [26] A.B. GMercader, A. Pomilio, Naturally-occurring dimers of flavonoids as anticarcinogens, *Anti-Cancer Agents Med. Chem.* 13 (2013) 1217–1235, <https://doi.org/10.2174/18715206113139990300>.
- [27] A.N. Panche, A.D. Diwan, S.R. Chandra, Flavonoids: an overview, *J Nutr Sci* 5 (2016) 1–15, <https://doi.org/10.1017/jns.2016.41>.
- [28] J.B. Harborne, H. Marby, T.J. Marby, *The flavonoids*, Springer, 2013. <https://doi.org/10.1007/978-1-4899-2909-9>.
- [29] P.G. Pietta, Flavonoids as antioxidants, *J. Nat. Prod.* 63 (2000) 1035–1042, <https://doi.org/10.1021/np9904509>.

- [30] T.T. Cushnie, A.J. Lamb, Antimicrobial activity of flavonoids, *Int. J. Antimicrob. Agents* 26 (2005) 343–356, <https://doi.org/10.1016/j.ijantimicag.2005.09.002>.
- [31] Mabry T, Markham KR, Thomas, MB. The systematic identification of flavonoids. Springer Science & Business Media. 1st Ed. Berlin-Heidelberg; Springer verlag: 1970. <https://doi.org/10.1007/978-3-642-88458-0>
- [32] R.N. Oliveira, M.C. Mancini, F.C.S.D. Oliveira, T.M. Passos, B. Quilty, R.M.D.S.M. Thiré, G.B. McGuinness, FTIR analysis and quantification of phenols and flavonoids of five commercially available plants extracts used in wound healing, *Matéria* 21 (2016) 767–779, <https://doi.org/10.1590/S1517-707620160003.0072>.
- [33] R. March, J. Brodbelt, Analysis of flavonoids: tandem mass spectrometry, computational methods, and NMR, *J. Mass Spectrom.* 43 (2008) 1581–1617, <https://doi.org/10.1002/jms.1480>.
- [34] M. Okigawa, N. Kawano, The structure of ochnaflavone, a new type of biflavone and the synthesis of its pentamethyl ether, *Tetrahedron Lett* 22 (1973) 2003, [https://doi.org/10.1016/S0040-4039\(01\)96104-0](https://doi.org/10.1016/S0040-4039(01)96104-0).
- [35] K.H. Son, J.O. Park, K.C. Chung, H.W. Chang, H.P. Kim, J.S. Kim, S.S. Kang, Triterpenoid saponins from the aerial parts of *Lonicera japonica*, *Arch Pharm Res* 15 (1994) 365, [https://doi.org/10.1016/S0031-9422\(00\)90656-3](https://doi.org/10.1016/S0031-9422(00)90656-3).
- [36] Y.B. Ryu, H.J. Jeong, J.H. Kim, Y.M. Kim, J.Y. Park, D. Kim, M.C. Rho, Biflavonoids from *Torreya nucifera* displaying SARS-CoV 3CLpro inhibition, *Bioorg. Med. Chem.* 18 (2010) 7940–7947, <https://doi.org/10.1016/j.bmc.2010.09.035>.
- [37] S. Yu, H. Yan, L. Zhang, M. Shan, P. Chen, A. Ding, S.F.Y. Li, A review on the phytochemistry, pharmacology, and pharmacokinetics of amentoflavone, a naturally-occurring biflavonoid, *Molecules* 22 (2017) 299, <https://doi.org/10.3390/molecules22020299>.
- [38] M.M. Feuerisen, M.G. Barraza, B.F. Zimmermann, A. Schieber, N. Schulze-Kaysers, Pressurized liquid extraction of anthocyanins and biflavonoids from *Schinus terebinthifolius* Raddi: A multivariate optimization, *Food Chem.* 214 (2017) 564–571, <https://doi.org/10.1016/j.foodchem.2016.07.002>.
- [39] M.J. Waterman, A.S. Nugraha, R. Hendra, G.E. Ball, S.A. Robinson, P.A. Keller, Antarctic moss biflavonoids show high antioxidant and ultraviolet-screening activity, *J. Nat. Prod.* 80 (2017) 2224–2231, <https://doi.org/10.1021/acs.jnatprod.7b00085>.
- [40] D. Li, Y. Qian, Y.J. Tian, S.M. Yuan, W. Wei, G. Wang, Optimization of ionic liquid-assisted extraction of biflavonoids from *Selaginella doederleinii* and evaluation of its antioxidant and antitumor activity, *Molecules* 22 (2017) 586, <https://doi.org/10.3390/molecules22040586>.
- [41] N. Chatsumpun, B. Sritularak, K. Likhitwitayawuid, New biflavonoids with α -glucosidase and pancreatic lipase inhibitory activities from *Boesenbergia rotunda*, *Molecules* 22 (2017) 1862, <https://doi.org/10.3390/molecules22111862>.
- [42] J.H. Tabares-Guevara, O.J. Lara-Guzmán, J.A. Londoño-Londoño, J.A. Sierra, Y. M. León-Varela, R.M. Álvarez-Quintero, J.R. Ramirez-Pineda, Natural Biflavonoids Modulate Macrophage-Oxidized LDL Interaction In Vitro and Promote Atheroprotection In Vivo, *Front. Immunol.* 8 (2017) 923, <https://doi.org/10.3389/fimmu.2017.00923>.
- [43] P. Li, G.G.L. Yue, H.F. Kwok, C.L. Long, C.B.S. Lau, E.J. Kennelly, Using ultra-performance liquid chromatography quadrupole time of flight mass spectrometry-based chemometrics for the identification of anti-angiogenic biflavonoids from edible *Garcinia* species, *J. Agric. Food Chem.* 65 (2017) 8348–8355, <https://doi.org/10.1021/acs.jafc.7b02867>.
- [44] P. Gürbüz, Ş.D. Doğan, Biflavonoids from *Fumana procumbens* (Dunal), *Gren. & Godr. Biochem Syst Ecol* 74 (2017) 57–59, <https://doi.org/10.1016/j.bse.2017.09.004>.
- [45] Recalde-Gil MA, Klein-Júnior LC, dos Santos Passos C, Salton J, de Loreto Bordignon SA, Monace FD, Henriques AT. Monoamine oxidase inhibitory activity of biflavonoids from branches of *Garcinia gardneriana* (Clusiaceae). *Nat Prod Commun* 2017; 12: 1934578X1701200411. <https://doi.org/10.1177%2F1934578X1701200411>
- [46] F.A. Adem, A.T. Mbangeng, V. Kuete, M. Heydenreich, A. Ndakala, B. Irungu, T. Efferth, Cytotoxicity of isoflavones and biflavonoids from *Ormocarpum kirkii* towards multi-factorial drug resistant cancer, *Phytomedicine* 58 (2019), <https://doi.org/10.1016/j.phymed.2019.152853> 152853.
- [47] M. Li, B. Li, Z.M. Xia, Y. Tian, D. Zhang, W.J. Rui, F.J. Xiao, Anticancer effects of five biflavonoids from *Ginkgo biloba* L. male flowers in vitro, *Molecules* 24 (2019) 1496, <https://doi.org/10.3390/molecules24081496>.
- [48] L.I. Yun-Ying, L.U. Xiao-Yan, S.U.N. Jia-Li, W.A.N.G. Qing-Qing, Y.D. Zhang, J.B. Zhang, F.A.N. Xiao-Hui, Potential hepatic and renal toxicity induced by the biflavonoids from *Ginkgo biloba*, *Chin. J. Nat. Med.* 17 (2019) 672–681, [https://doi.org/10.1016/S1875-5364\(19\)30081-0](https://doi.org/10.1016/S1875-5364(19)30081-0).
- [49] M. Linden, C. Brinckmann, M.M. Feuerisen, A. Schieber, Effects of structural differences on the antibacterial activity of biflavonoids from fruits of the Brazilian peppertree (*Schinus terebinthifolius* Raddi), *Food Res. Int.* 133 (2020), <https://doi.org/10.1016/j.foodres.2020.109134> 109134.
- [50] J. Xu, L. Yang, R. Wang, K. Zeng, B. Fan, Z. Zhao, The biflavonoids as protein tyrosine phosphatase 1B inhibitors from *Selaginella uncinata* and their antihyperglycemic action, *Fitoterapia* 137 (2019), <https://doi.org/10.1016/j.fito.2019.104255> 104255.
- [51] Mendiratta A, Dayal R, Bartley JP, Smith G. A Phenylpropanoid and Biflavonoids from the Needles of *Cephalotaxus harringtonia* var. *harringtonia*. *Nat Prod Commun* 2017; 12: 1934578X1701201132. <https://doi.org/10.1177%2F1934578X1701201132>
- [52] Oliveira PDA, Fidelis QC, Fernandes TFDC, Souza MCD, Coutinho DM, Prudêncio ER, Marinho BG. Evaluation In Vivo and In Vitro of the Antioxidant, Antinociceptive, and Anti-Inflammatory Activities of Biflavonoids From *Ouratea hexasperma* and *O. ferruginea*. *Nat Prod Commun* 2019; 14: 1934578X19856802. <https://doi.org/10.1177%2F1934578X19856802>
- [53] N. Sirimangkalakitti, L.D. Juliawaty, E.H. Hakim, I. Waliiana, N. Saito, K. Koyama, K. Kinoshita, Naturally occurring biflavonoids with amyloid β aggregation inhibitory activity for development of anti-Alzheimer agents, *Bioorg. Med. Chem. Lett.* 29 (2019) 1994–1997, <https://doi.org/10.1016/j.bmcl.2019.05.020>.
- [54] H.W. Yan, H. Zhu, X. Yuan, Y.N. Yang, Z.M. Feng, J.S. Jiang, P.C. Zhang, Eight new biflavonoids with lavandulyl units from the roots of *Sophora flavescens* and their inhibitory effect on PTP1B, *Bioorg. Chem.* 86 (2019) 679–685, <https://doi.org/10.1016/j.bioorg.2019.01.058>.
- [55] G.A. Dziwormu, N.R. Toorabally, M.G. Bhowon, S. Jhaumeer-Laulloo, S. Sunassee, A. Moser, D. Argyropoulos, Computer Assisted Structure Elucidation of Two Biflavonoids from the Leaves of *Ochna mauritiana*, *Plant Med. Int. Open* 4 (2017) Mo-PO, <https://doi.org/10.1055/s-0037-1608237>.
- [56] I. Abdullah, S. Phongpaichit, S.P. Voravuthikunchai, W. Mahabusarakam, Prenylated biflavonoids from the green branches of *Garcinia dulcis*, *Phytochem. Lett.* 23 (2018) 176–179, <https://doi.org/10.1016/j.phytol.2017.12.004>.
- [57] D. Ren, F.C. Meng, H. Liu, T. Xiao, J.J. Lu, L.G. Lin, Q.W. Zhang, Novel biflavonoids from *Cephalotaxus oliveri* Mast, *Phytochem. Lett.* 24 (2018) 150–153, <https://doi.org/10.1016/j.phytol.2018.02.005>.
- [58] X. Zhang, R. Gao, Y. Liu, Y. Cong, D. Zhang, Y. Zhang, C. Lu, Anti-virulence activities of biflavonoids from *Mesua ferrea* L. flower, *Drug Discov. Ther.* 13 (2019) 222–227, <https://doi.org/10.5582/ddt.2019.01053>.
- [59] L. Carrillo-Hormaza, A.M. Ramírez, C. Quintero-Ortiz, M. Cossio, S. Medina, F. Ferreres, E. Osorio, Comprehensive characterization and antioxidant activities of the main biflavonoids of *Garcinia madruno*: A novel tropical species for developing functional products, *J Funct Food* 27 (2016) 503–516, <https://doi.org/10.1016/j.jff.2016.10.001>.
- [60] H. Jin, H. Cui, X. Yang, L. Xu, X. Li, R. Liu, X. Song, Nematicidal activity against *Aphelenchoides besseyi* and *Ditylenchus destructor* of three biflavonoids, isolated from roots of *Stellera chamaejasme*, *J. Asia Pac. Entomol.* 21 (2018) 1473–1478, <https://doi.org/10.1016/j.aspen.2018.11.013>.
- [61] S. Xiao, Z.Q. Mu, C.R. Cheng, J. Ding, Three new biflavonoids from the branches and leaves of *Cephalotaxus oliveri* and their antioxidant activity, *Nat. Prod. Res.* 33 (2019) 321–327, <https://doi.org/10.1080/14786419.2018.1448817>.
- [62] K. Zar Wynn Myint, T. Kido, K. Kusakari, H. Prasad Devkota, T. Kawahara, T. Watanabe, Rhusflavanone and mesuaferone B: tyrosinase and elastase inhibitory biflavonoids extracted from the stamens of *Mesua ferrea* L, *Nat. Prod. Res.* (2019) 1–5, <https://doi.org/10.1080/14786419.2019.1613395>.
- [63] Y. Sun, B. Shi, M. Gao, L. Fu, H. Chen, Z. Hao, W. Feng, Two New Biflavonoids from the Roots and Rhizomes of *Sinopodophyllum emodi*, *Chem. Nat. Compd.* 54 (2018) 649–653, <https://doi.org/10.1007/s10600-018-2438-4>.
- [64] Y. Liu, N. Kelsang, J. Lu, Y. Zhang, H. Liang, P. Tu, Q. Zhang, Oxytrodidiflavone A and Oxytrochalcoflavanones A, B: New Biflavonoids from *Oxytropis chiliophylla*, *Molecules* 24 (2019) 1468, <https://doi.org/10.3390/molecules24081468>.
- [65] D. Li, C. Sun, J. Yang, X. Ma, Y. Jiang, S. Qiu, G. Wang, Ionic liquid-microwave-based extraction of biflavonoids from *Selaginella sinensis*, *Molecules* 24 (2019) 2507, <https://doi.org/10.3390/molecules24132507>.
- [66] M. Ndoile, F. Van Heerden, Cytotoxic and antimalarial biflavonoids isolated from the aerial parts of *Ochna serrulata* (Hochst.) Walp, *Tanzania J. Sci.* 44 (2018) 152–162.
- [67] E.A. Ibrahim, S.Y. Desoukey, G.M. Hadad, R.A. Salam, A.K. Ibrahim, S.A. Ahmed, M.A. ElSohly, Analysis of cupressuflavone and amentoflavone from *Cupressus sempervirens* L. and its tissue cultured callus using HPLC-DAD method, *Pharm. Pharmacol. Int. J.* 5 (2017) 174–180.
- [68] T. Sabudak, M. Ozturk, E. Alpaly, New Bioflavonoids from *Solanum nigrum* L. by anticholinesterase and anti-tyrosinase activities-guided fractionation, *Rec. Nat. Prod.* 1 (2017) 130–140.
- [69] S.Y. Shim, S.G. Lee, M. Lee, Biflavonoids isolated from *Selaginella tamariscina* and their anti-inflammatory activities via ERK 1/2 signaling, *Molecules* 23 (2018) 926, <https://doi.org/10.3390/molecules23040926>.
- [70] B.Y.G. Mountessou, J. Tchamgoue, J.P. Dzoyem, R.T. Tchuenguem, F. Surup, M.I. Choudhary, S.F. Kouam, Two xanthenes and two rotameric (3 \rightarrow 8) biflavonoids from the Cameroonian medicinal plant *Allanblackia floribunda* Oliv. (Guttiferae), *Tetrahedron Lett.* 59 (2018) 4545–4550, <https://doi.org/10.1016/j.tetlet.2018.11.035>.
- [71] J.W. Shou, R.R. Zhang, H.Y. Wu, X. Xia, H. Nie, R.W. Jiang, P.C. Shaw, Isolation of novel biflavonoids from *Cardiocrinum giganteum* seeds and characterization of their antitussive activities, *J. Ethnopharmacol.* 222 (2018) 171–176, <https://doi.org/10.1016/j.jep.2018.05.003>.
- [72] M.M. Ndoile, F.R. Van Heerden, Antimalarial biflavonoids from the roots of *Ochna serrulata* (Hochst.) Walp, *Int. Res. J. Pure Appl. Chem.* 16 (2018) 1–9, <https://doi.org/10.9734/IRJPAC/2018/42440>.
- [73] A. Al Groshi, H.A. Jasim, A.R. Evans, F.M. Ismail, N.M. Dempster, L. Nahar, S.D. Sarker, Growth inhibitory activity of biflavonoids and diterpenoids from the leaves of the Libyan *Juniperus phoenicea* against human cancer cells, *Phytother. Res.* 33 (2019) 2075–2082, <https://doi.org/10.1002/ptr.6397>.
- [74] H. Wagner, L. Farkas, Synthesis of flavonoids, *The Flavonoids*, Springer, Boston-MA, 1975. https://doi.org/10.1007/978-1-4899-2909-9_4.
- [75] D. Muller, J.P. Fleury, A new strategy for the synthesis of biflavonoids via arylboronic acids, *Tetrahedron Lett.* 32 (1991) 2229–2232, [https://doi.org/10.1016/S0040-4039\(00\)79688-2](https://doi.org/10.1016/S0040-4039(00)79688-2).
- [76] S.M. Ali, M. Ilyas, Biomimetic approach to biflavonoids: Oxidative coupling of 2'-hydroxychalcones with iodine in alkaline methanol, *J. Org. Chem.* 51 (1986) 5415–5417, <https://doi.org/10.1021/jo00376a069>.

- [77] Y.M. Lin, M.T. Flavin, C.S. Cassidy, A. Mar, F.C. Chen, Biflavonoids as novel antituberculosis agents, *Bioorg. Med. Chem.* 11 (2001) 2101–2104, [https://doi.org/10.1016/S0960-894X\(01\)00382-1](https://doi.org/10.1016/S0960-894X(01)00382-1).
- [78] F.D. Riswanto, M.S. Rawat, V. Murgaiyah, N.H. Salin, E.P. Istyastono, M. Hariono, H.A. Wahab, Anti-cholinesterase activity of chalcone derivatives: synthesis, in vitro assay and molecular docking study, *Med. Chem.* 16 (2019) 1–11, <https://doi.org/10.2174/1573406415666191206095032>.
- [79] S. Imran, M. Taha, N.H. Ismail, S.M. Kashif, F. Rahim, W. Jamil, H. Wahab, Synthesis of novel flavone hydrazone: In-vitro evaluation of α -glucosidase inhibition, QSAR analysis and docking studies, *Eur. J. Med. Chem.* 105 (2015) 156–170, <https://doi.org/10.1016/j.ejmech.2015.10.017>.
- [80] S.S. Kim, V.A. Vo, H. Park, Synthesis of Ochnaflavone and Its Inhibitory Activity on PGE 2 Production, *Bull. Korean Chem. Soc.* 35 (2014) 3219–3223, <https://doi.org/10.5012/bkcs.2014.35.11.3219>.
- [81] G. Sagraera, G. Seoane, Total Synthesis of 3', 3'''-Binarigenin and Related Biflavonoids, *Synthesis* 2010 (2010) 2776–2786, <https://doi.org/10.1055/s-0030-1258140>.
- [82] R.K. Nadirov, K.S. Nadirov, A.M. Esimova, Z.K. Nadirova, Electrochemical synthesis of amino derivatives of biflavonoids, *Chem. Nat. Compd.* 50 (2014) 735–736, <https://doi.org/10.1007/s10600-014-1067-9>.
- [83] T.H. Sum, T.J. Sum, S. Collins, W.R. Galloway, D.G. Twigg, F. Hollfelder, D.R. Spring, Divergent synthesis of biflavonoids yields novel inhibitors of the aggregation of amyloid β (1–42), *Org. Biomol. Chem.* 15 (2017) 4554–4570, <https://doi.org/10.1039/C7OB00804J>.
- [84] T.J. Sum, T.H. Sum, W.R. Galloway, D.G. Twigg, J.J. Ciardello, D.R. Spring, Synthesis of structurally diverse biflavonoids, *Tetrahedron* 74 (2018) 5089–5101, <https://doi.org/10.1016/j.tet.2018.05.003>.
- [85] M. Soto, R.G. Soengas, A.M. Silva, V. Gotor-Fernández, H. Rodríguez-Solla, Temperature-controlled stereodivergent synthesis of 2, 2'-biflavanones promoted by samarium diiodide, *Chem. Eur. J.* 25 (2019) 13104–13108, <https://doi.org/10.1002/chem.201902927>.
- [86] K. Xu, C. Yang, Y. Xu, D. Li, S. Bao, Z. Zou, X. Yu, Selective geranylation of biflavonoids by *Aspergillus terreus* aromatic prenyltransferase (AtaPT), *Org. Biomol. Chem.* 18 (2020) 28–31, <https://doi.org/10.1039/C9OB02296A>.
- [87] K. Anand, J. Ziebuhr, P. Wadhvani, J.R. Mesters, R. Hilgenfeld, Coronavirus main proteinase (3CLpro) structure: basis for design of anti-SARS drugs, *Science* 300 (2003) 1763–1767, <https://doi.org/10.1126/science.1085658>.
- [88] X. Tian, G. Lu, F. Gao, H. Peng, Y. Feng, G. Ma, G.F. Gao, Structure and cleavage specificity of the chymotrypsin-like serine protease (3CLSP/nsp4) of porcine reproductive and respiratory syndrome virus (PRRSV), *J. Mol. Biol.* 392 (2009) 977–993, <https://doi.org/10.1016/j.jmb.2009.07.062>.
- [89] L. Kiemer, O. Lund, S. Brunak, N. Blom, Coronavirus 3CL pro proteinase cleavage sites: Possible relevance to SARS virus pathology, *BMC Bioinf.* 5 (2004) 72, <https://doi.org/10.1186/1471-2105-5-72>.
- [90] V. Thiel, K.A. Ivanov, A. Putics, T. Hertzog, B. Schelle, S. Bayer, A.E. Gorbalenya, Mechanisms and enzymes involved in SARS coronavirus genome expression, *J. Gen. Virol.* 84 (2003) 2305–2315, <https://doi.org/10.1099/vir.0.19424-0>.
- [91] M.A. Alamri, M. Tahir Ul Qamar, M.U. Mirza, R. Bhadane, S.M. Alqahtani, I. Muneer, O.M. Salo-Ahen, Pharmacoinformatics and molecular dynamics simulation studies reveal potential covalent and FDA-approved inhibitors of SARS-CoV-2 main protease 3CLpro, *J. Biomol. Struct. Dyn.* (2020) 1–13, <https://doi.org/10.1080/07391102.2020.1782768>.
- [92] A.K. Ghosh, M. Brindisi, D. Shahabi, M.E. Chapman, A.D. Mesecar, Drug development and medicinal chemistry efforts toward SARS-coronavirus and Covid-19 therapeutics, *ChemMedChem* (2020), <https://doi.org/10.1002/cmdc.202000223> [Epub ahead of print].
- [93] Mesecar AD. A taxonomically-driven approach to development of potent, broad-spectrum inhibitors of coronavirus main protease including SARS-CoV-2 (COVID-19), <http://www.rcsb.org/structure/6W63>; 2020 (accessed 24 October 2020).
- [94] M. Stoermer, Homology models of coronavirus 2019-nCoV 3CLpro protease, *ChemRxiv* (2020).
- [95] Z. Jin, X. Du, Y. Xu, Y. Deng, M. Liu, Y. Zhao, Y. Duan, Structure of M pro from SARS-CoV-2 and discovery of its inhibitors, *Nature* 582 (2020) 289–293, <https://doi.org/10.1038/s41586-020-2223-y>.
- [96] L. Zhang, D. Lin, X. Sun, U. Curth, C. Drosten, L. Sauerhering, R. Hilgenfeld, Crystal structure of SARS-CoV-2 main protease provides a basis for design of improved α -ketoamide inhibitors, *Science* 368 (2020) 409–412, <https://doi.org/10.1126/science.abb3405>.
- [97] H. Yang, M. Yang, Y. Ding, Y. Liu, Z. Lou, Z. Zhou, G.F. Gao, The crystal structures of severe acute respiratory syndrome virus main protease and its complex with an inhibitor, *Proc. Natl. Acad. Sci.* 100 (2003) 13190–13195, <https://doi.org/10.1073/pnas.1835675100>.
- [98] F. Wang, C. Chen, W. Tan, K. Yang, H. Yang, Structure of main protease from human coronavirus NL63: insights for wide spectrum anti-coronavirus drug design, *Sci. Rep.* 6 (2016) 22677, <https://doi.org/10.1038/srep22677>.
- [99] A. Acharya, R. Agarwal, M. Baker, J. Baudry, D. Bhowmik, S. Boehm, O. Demerdash, Supercomputer-based ensemble docking drug discovery pipeline with application to Covid-19, *ChemRxiv* (2020). Preprint. 10.26434/chemrxiv.12725465.v1.
- [100] H.X. Su, S. Yao, W.F. Zhao, M.J. Li, L.K. Zhang, Y. Ye, Y.C. Xu, Identification of a novel inhibitor of SARS-CoV-2 3CLpro, *Acta Pharmacol. Sin.* 41 (2020) 1167–1177, <https://doi.org/10.1038/s41401-020-0483-6>.
- [101] C. Ma, M.D. Sacco, B. Hurst, J.A. Townsend, Y. Hu, T. Szeto, J. Wang, Boceprevir, GC-376, and calpain inhibitors II, XII inhibit SARS-CoV-2 viral replication by targeting the viral main protease, *Cell Res.* 30 (2020) 678–692, <https://doi.org/10.1038/s41422-020-0356-z>.
- [102] Mesecar AD. A taxonomically-driven approach to development of potent, broad-spectrum inhibitors of coronavirus main protease including SARS-CoV-2 (COVID-19), <http://www.rcsb.org/structure/6W63>; 2020 (accessed 24 October 2020).
- [103] Z. Jin, Y. Zhao, Y. Sun, B. Zhang, H. Wang, Y. Wu, Y. Duan, Structural basis for the inhibition of SARS-CoV-2 main protease by antineoplastic drug carmofur, *Nat. Struct. Mol. Biol.* 27 (2020) 529–532, <https://doi.org/10.1038/s41594-020-0440-6>.
- [104] Fearon, D., Owen, C.D., Douangamath, A., Lukacik, P., Powell, A.J., Strain-Damerell, C.M., & von Delft, F., PanDDA analysis group deposition SARS-CoV-2 main protease fragment screen, <http://www.rcsb.org/structure/5RHF>; 2020 (accessed 24 October 2020).
- [105] Kneller DW, Phillips G, O'Neill HM, Jedrzejczak R, Stols L, Langan P, Kovalevsky A. Structural plasticity of SARS-CoV-2 3CL Mproactive site cavity revealed by room temperature X-ray crystallography <http://www.rcsb.org/structure/6WQF>; 2020 (accessed 24 October 2020).
- [106] Kneller DW, Phillips G, O'Neill HM, Tan K, Joachimiak A, Coates L, Kovalevsky A, Room temperature X-ray crystallography reveals catalytic cysteine in the SARS-CoV-2 3CL Mpro is highly reactive: Insights for enzyme mechanism and drug design, <http://www.rcsb.org/structure/6XBI>; 2020 (accessed 24 October 2020).
- [107] Wang H, He S, Deng W, Zhang Y, Li G, Sun J, Zhao W, Shang L. Comprehensive Insights into the Catalytic Mechanism of Middle East Respiratory Syndrome 3C-Like Protease and Severe Acute Respiratory Syndrome 3C-Like Protease, <http://www.rcsb.org/structure/6LOO>; 2020 (accessed 24 October 2020).
- [108] Tan K, Maltseva NI, Welk LF, Jedrzejczak RP, Joachimiak A, The crystal structure of 3CL MainPro of SARS-CoV-2 with de-oxidized C145, <http://www.rcsb.org/structure/7JFQ>; 2020 (accessed 24 October 2020).
- [109] Tan K, Maltseva NI, Welk LF, Jedrzejczak RP, Coates L, Kovalevsky AY, Joachimiak A. The crystal structure of 3CL MainPro of SARS-CoV-2 with oxidized Cys145 (Sulfenic acid cysteine), <http://www.rcsb.org/structure/6XKF>; 2020 (accessed 24 October 2020).
- [110] Tan K, Maltseva NI, Welk LF, Jedrzejczak RP, Coates L, Kovalevsky A, Joachimiak A. The 1.28 Å crystal structure of 3cl mainpro of sars-cov-2 with oxidized c145 (sulfenic acid cysteine), <http://www.rcsb.org/structure/6XKH>; 2020 (accessed 24 October 2020).
- [111] Tan K, Maltseva NI, Welk LF, Jedrzejczak RP, Joachimiak A. The crystal structure of 3CL MainPro of SARS-CoV-2 with C145S mutation, <http://www.rcsb.org/structure/6XOA>; 2020 (accessed 24 October 2020).
- [112] Kneller DW, Phillips G, Weiss KL, Pant S, Zhang Q, O'Neill H. Kovalevsky A, Protonation states in SARS-CoV-2 main protease mapped by neutron crystallography <http://www.rcsb.org/structure/7JUN>; 2020 (accessed 24 October 2020).
- [113] de Oliveira RR, Nascimento AFZ, Zeri ACM, Trivella DBB, SARS-CoV-2 3CL protease crystallized under reducing conditions, <https://www.rcsb.org/structure/7JR3>; 2020 (accessed 24 October 2020).
- [114] Nascimento AFZ, de Oliveira RR, Zeri ACM, Trivella DBB. SARS-CoV-2 3CL protease with alternative conformation of the active site promoted by methylene-bridged cysteine and lysine residues, <http://www.rcsb.org/structure/7JRA>; 2020 (accessed 24 October 2020).
- [115] Kneller DW, Phillips G, O'Neill HM, Tan K, Joachimiak A, Coates L, Kovalevsky, A. Room temperature X-ray crystallography reveals oxidation and reactivity of cysteine residues in SARS-CoV-2 3CL Mpro: Insights for enzyme mechanism and drug design, <http://www.rcsb.org/structure/6XHU>; 2020 (accessed 24 October 2020).
- [116] Kneller DW, Galanie S, Phillips G, O'Neill HM, Coates L, Kovalevsky A. Extreme malleability of the SARS-CoV-2 3CL Mpro active site cavity facilitates binding of clinical antivirals: Prospects for repurposing existing drugs and ramifications for inhibitor design, <http://www.rcsb.org/structure/6XQT>; 2020 (accessed 24 October 2020).
- [117] Rathnayake AD, Zheng J, Kim Y, Perera KD, Mackin S, Meyerholz DK, Kashipathy MM, Chang KO, 3C-like protease inhibitors block coronavirus replication in vitro and improve survival in MERS-CoV-infected mice, <http://www.rcsb.org/structure/6W2A>; 2020 (accessed 24 October 2020).
- [118] Vuong W, Khan MB, Fischer C, Arutyunova E, Lamer T, Shields J, McKay RT, Lemieux MJ, Feline coronavirus drug inhibits the main protease of SARS-CoV-2 and blocks virus replication, <http://www.rcsb.org/structure/6WTK>; 2020 (accessed 24 October 2020).
- [119] Ma C, Sacco M, Chen Y, Wang J. Crystal structure of the SARS-CoV-2 (COVID-19) main protease in complex with inhibitor UAW247, <http://www.rcsb.org/structure/6XBH>; 2020 (accessed 24 October 2020).
- [120] Ma C, Sacco M, Chen Y, Wang J. Crystal structure of the SARS-CoV-2 (COVID-19) main protease in complex with inhibitor, <http://www.rcsb.org/structure/6XBG>; 2020 (accessed 24 October 2020).
- [121] Sacco M, Chen Y, Ma C. Crystal structure of the SARS-CoV-2 (COVID-19) main protease in complex with UAW243, <http://www.rcsb.org/structure/6XFN>; 2020 (accessed 24 October 2020).
- [122] Tan K, Maltseva NI, Welk LF, Jedrzejczak RP, Joachimiak A. The crystal structure of SARS-CoV-2 Main Protease in complex with masitinib, <http://www.rcsb.org/structure/7JU7>; 2020 (accessed 24 October 2020).
- [123] Zhu L, Hilgenfeld R. Crystal structures of SARS-Cov main protease complexed with a series of unsaturated esters, <http://www.rcsb.org/structure/3SZN>; 2020 (accessed 24 October 2020).
- [124] Zhu L, George S, Schmidt MF, Al-Gharabi SI, Rademann J, Hilgenfeld R. Peptide aldehyde inhibitors challenge the substrate specificity of the SARS-coronavirus main protease, <http://www.rcsb.org/structure/3SNE>; 2020 (accessed 24 October 2020).

- [125] Ma C, Sacco M, Chen Y, Wang J, Crystal structure of the SARS-CoV-2 (COVID-19) main protease in complex with inhibitor UAW248, <http://www.rcsb.org/structure/6XBI>; 2020 (accessed 24 October 2020).
- [126] Hoffman RL, Kania RS, Brothers MA, Davies JF, Ferre RA, Gajiwala KS, He M, Taggart B. The Discovery of Ketone-Based Covalent Inhibitors of Coronavirus 3CL Proteases for the Potential Therapeutic Treatment of COVID-19, <http://www.rcsb.org/structure/6XHO>; 2020 (accessed 24 October 2020).
- [127] Sacco M, Chen Y, Ma C. Crystal structure of the SARS-CoV-2 (COVID-19) main protease in complex with UAW241, <http://www.rcsb.org/structure/6XA4>; 2020 (accessed 24 October 2020).
- [128] Zhang L, Lin D, Sun, X, Curth U, Drosten C, Sauerhering L, Becker S, Hilgenfeld R. Crystal structure of SARS-CoV-2 main protease provides a basis for design of improved alpha-ketoamide inhibitors, <http://www.rcsb.org/structure/6Y2E>; 2020 (accessed 24 October 2020).
- [129] Hattori SI, Higashi-Kuwata N, Hayashi H, Allu RS, Das D, Takamune N, Kishimoto N, Mitsuya H. A SARS-CoV-2's Main Protease-targeting Small-Compound GRL-2420 Completely Blocks the Infectivity and Cytotoxicity of SARS-CoV-2, <http://www.rcsb.org/structure/7JKV>; 2020 (accessed 24 October 2020).
- [130] Schmidt M, Malla, T. SARS cov-2 main protease 3clpro, room temperature, damage free xfel monoclinic structure, <http://www.rcsb.org/structure/7JVZ>; 2020 (accessed 24 October 2020).
- [131] Littler DR, Gully B, Colson RN, Rossjohn, J. Crystal Structure of the SARS-CoV-2 Non-structural Protein 9, Nsp9, <http://www.rcsb.org/structure/6W9Q>; 2020 (accessed 24 October 2020).
- [132] Fu LF. Crystal structure of the 2019-nCoV main protease complexed with GC376, <http://www.rcsb.org/structure/7BRR>; 2020 (accessed 24 October 2020).
- [133] Fu LF. Crystal structure of the 2019-nCoV main protease, <http://www.rcsb.org/structure/7BRO>; 2020 (accessed 24 October 2020).
- [134] Fu LF. Crystal structure of the 2019-nCoV main protease complexed with Boceprevir, <http://www.rcsb.org/structure/7BRP>; 2020 (accessed 24 October 2020).
- [135] Zhou XL, Zhong FL, Lin C, Hu XH, Zhou H, Wang QS, Li J, Zhang, J. The crystal structure of COVID-19 main protease in the apo state, <http://www.rcsb.org/structure/7C2Q>; 2020 (accessed 24 October 2020).
- [136] Kuo CJ, Shie JJ, Lin CH, Lin YL, Hsieh MC, Lee CC, Chang SY, Liang PH. Complex Structures and Cellular Activities of the Potent SARS-CoV-2 3CLpro Inhibitors Guiding Drug Discovery Against COVID-19, <http://www.rcsb.org/structure/7C8T>; 2020 (accessed 24 October 2020).
- [137] Kneller DW, Coates L, Kovalevsky, A. Structure of the complex between the SARS-CoV-2 Main Protease and Leupeptin, <http://www.rcsb.org/structure/6XCH>; 2020 (accessed 24 October 2020).
- [138] Ye G, Wang X, Tong X, Shi Y, Fu ZF, Peng G. Structural Basis for Inhibiting Porcine Epidemic Diarrhea Virus Replication with the 3C-Like Protease Inhibitor GC376, <http://www.rcsb.org/structure/6L70>; 2020 (accessed 24 October 2020).
- [139] Zhang L, Lin D, Kusov Y, Nian Y, Ma Q, Wang J, von Brunn A, Hilgenfeld, R., Alpha-ketoamides as broad-spectrum inhibitors of coronavirus and enterovirus replication Structure-based design, synthesis, and activity assessment, <http://www.rcsb.org/structure/6FV1>; 2020 (accessed 24 October 2020).
- [140] Qiao JX, Zeng R, Li YS, Wang YF, Lei J, Yang SY. Crystal structure of SARS-CoV-2 main protease in complex with MI-23, <http://www.rcsb.org/structure/7D3I>; 2020 (accessed 24 October 2020).
- [141] Fu LF, Feng Y, Qi JX, Crystal structure of SARS-Cov-2 main protease with nrlaprevir, <http://www.rcsb.org/structure/7D10>; 2020 (accessed 24 October 2020).
- [142] Qiao JX, Zeng R, Wang YF, Li YS, Yao R, Zhou YL, Chen P, Yang SY. Crystal structure of the SARS-CoV-2 main protease in complex with Telaprevir, <http://www.rcsb.org/structure/7C7P>; 2020 (accessed 24 October 2020).
- [143] Qiao JX, Zeng R, Wang YF, Li YS, Yao R, Liu JM, Zhou YL, Yang SY. Crystal structure of the SARS-CoV-2 main protease in complex with Boceprevir (space group P212121), <http://www.rcsb.org/structure/7COM>; 2020 (accessed 24 October 2020).
- [144] Oerlemans R, Wang W, Lunev S, Domling A, Groves MR. Crystal structure of SARS CoV2 main protease in complex with inhibitor Boceprevir, <http://www.rcsb.org/structure/6ZRU>; 2020 (accessed 24 October 2020).
- [145] Oerlemans R, Wang W, Lunev S, Domling A, Groves, M.R., Crystal structure of SARS CoV2 main protease in complex with inhibitor Telaprevir, <http://www.rcsb.org/structure/6ZRT>; 2020 (accessed 24 October 2020).
- [146] Mohan K, Ueda G, Kim AR, Jude KM, Fallas JA, Guo Y, Hafer M, Garcia KC. Topological control of cytokine receptor signaling induces differential effects in hematopoiesis, <http://www.rcsb.org/structure/6MOK>; 2020 (accessed 24 October 2020).
- [147] Dai W, Zhang B, Jiang XM, Su H, Li J, Zhao Y, Xie X, Liu H. Structure-based design of antiviral drug candidates targeting the SARS-CoV-2 main protease, <http://www.rcsb.org/structure/6LZE>; 2020 (accessed 24 October 2020).
- [148] Fu L, Feng Y. Crystal structure of the SARS-CoV-2 main protease complexed with Boceprevir, <http://www.rcsb.org/structure/7C6S>; 2020 (accessed 24 October 2020).
- [149] Qiao JX, Zeng R, Liu XL, Nan JS, Wang YF, Li YS, Lei J, Yang SY. Crystal structure of the SARS-CoV-2 main protease in complex with INZ-1, <http://www.rcsb.org/structure/7CX9>; 2020 (accessed 24 October 2020).
- [150] V.S. Gontijo, W.A. Judice, B. Codonho, I.O. Pereira, D.M. Assis, J.P. Januário, C. V. Junior, Leishmanicidal, antiproteolytic and antioxidant evaluation of natural biflavonoids isolated from *Garcinia brasiliensis* and their semisynthetic derivatives, *Eur. J. Med. Chem.* 58 (2012) 613–623, <https://doi.org/10.1016/j.ejmech.2012.06.021>.
- [151] V.S. Gontijo, J.P. Januário, W.A. de Souza Júde, A.A. Antunes, I.R. Cabral, D.M. Assis, M.H. dos Santos, Morelloflavone and its semisynthetic derivatives as potential novel inhibitors of cysteine proteases and serine proteases, *J Med Plants Res* 9 (2015) 426–434, <https://doi.org/10.5897/JMPR2014.5641>.
- [152] D.M. Assis, V.S. Gontijo, Pereira I de Oliveira, J.A.N. Santos, I. Camps, T.J. Nagem, A.C. Doriguetto, Inhibition of cysteine proteases by a natural flavonone: behavioral evaluation of fukugetin as papain and cruzain inhibitor, *J. Enzyme Inhib. Med. Chem.* 28 (2013) 661–670, <https://doi.org/10.3109/14756366.2012.668539>.
- [153] N.F. Fazio, M.H. Russell, S.M. Flinders, C.J. Gardner, J.B. Webster, M.D. Hansen, A natural product biflavonoid scaffold with anti-tryptase activity, *Naunyn-Schmiedeberg's Arch. Pharmacol.* (2020) 1–9, <https://doi.org/10.1007/s00210-020-01959-2>.
- [154] C.W. Lee, H.J. Choi, H.S. Kim, D.H. Kim, I.S. Chang, H.T. Moon, E.R. Woo, Biflavonoids isolated from *Selaginella tamariscina* regulate the expression of matrix metalloproteinase in human skin fibroblasts, *Bioorg. Med. Chem.* 16 (2008) 732–738, <https://doi.org/10.1016/j.bmc.2007.10.036>.
- [155] B.K. Yap, C.Y. Lee, S.B. Choi, E.E. Kamarulzaman, M. Hariono, H.A. Wahab, In silico identification of novel inhibitors, *Ref Module Life Sci* 3 (2019) 761–779, <https://doi.org/10.1016/B978-0-12-809633-8.20158-1>.
- [156] S.N. Sulaiman, M. Hariono, H.M. Salleh, S.L. Chong, L.S. Yee, A. Zahari, K. Awang, Chemical constituents From *Endiandra kingiana* (Lauraceae) as potential inhibitors for dengue type 2 NS2B/NS3 serine protease and its molecular docking, *Nat. Prod. Commun.* 14 (2019). <https://doi.org/10.1177%2F1934578X19861014>.
- [157] A. El Sahili, J. Lescar, Dengue virus non-structural protein 5, *Viruses* 9 (2017) 91, <https://doi.org/10.3390/v9040091>.
- [158] A.R. Sahin, A. Erdogan, P.M. Agaoglu, Y. Dineri, A.Y. Cakirci, M.E. Senel, A.M. Tasdogan, 2019 novel coronavirus (COVID-19) outbreak: A review of the current literature, *EJMO* 4 (2020) 1–7, <https://doi.org/10.14744/ejmo.2020.12220>.
- [159] L. Di, Strategic approaches to optimizing peptide ADME properties, *AAPS J.* 17 (2015) 134–143, <https://doi.org/10.1208/s12248-014-9687-3>.
- [160] J. Swaminathan, C. Ehrhardt, Liposomal delivery of proteins and peptides, *Expert Opin Drug Deliv* 9 (2012) 1489–1503, <https://doi.org/10.1517/17425247.2012.735658>.
- [161] M.R. Mozafari, Liposomes: an overview of manufacturing techniques, *Cell. Mol. Biol. Lett.* 10 (2005) 711.
- [162] F.M. Tajabadi, M.R. Campitelli, R.J. Quinn, Scaffold Flatness: Reversing the Trend, *Springer Sci Rev* 1 (2013) 141–151, <https://doi.org/10.1007/s40362-013-0014-7>.
- [163] A. Karshikoff, L. Nilsson, R. Ladenstein, Rigidity versus flexibility: the dilemma of understanding protein thermal stability, *FEBS J.* 2015 (282) (2015) 3899–3917.
- [164] M. Hariono, S.H. Yuliani, E.P. Istyastono, F.D. Riswanto, C.F. Adhipandito, Matrix metalloproteinase 9 (MMP9) in wound healing of diabetic foot ulcer: Molecular target and structure-based drug design, *Wound Med* 22 (2018) 1–13, <https://doi.org/10.1016/j.wndm.2018.05.003>.
- [165] E.P. Istyastono, N. Yuniarti, M. Hariono, S.H. Yuliani, F.D.O. Riswanto, Binary quantitative structure-activity relationship analysis in retrospective structure based virtual screening campaigns targeting estrogen receptor alpha, *Asian J. Pharm. Clin. Res.* 10 (2017) 206–211, <https://doi.org/10.22159/ajpcr.2017.v10i12.20667>.